Master Thesis, Department of Geosciences

Weathering of Precambrian basement and formation of sedimentary particles in Scania

Syed Asmar Aal-E-Muhammad Naqvi

UNIVERSITY OF OSLO

FACULTY OF MATHEMATICS AND NATURAL SCIENCES

Weathering of Precambrian basement and formation of sedimentary particles in Scania

Syed Asmar Aal-E-Muhammad Naqvi

Master Thesis in Geosciences

Discipline: Petroleum Geology and Petroleum Geophysics

Department of Geosciences

Faculty of Mathematics and Natural Sciences

University of Oslo

June 3rd, 2013

Tutor(s): Henning Dypvik and Lars Riber, UiO

This work is published digitally through DUO – Digitale Utgivelser ved UiO

http://www.duo.uio.no

It is also catalogued in BIBSYS (http://www.bibsys.no/english)

Abstract

This study describes weathering pattern in saprolites of the Vånga Granite along various profiles at Ivö Klack, Scania (southern Sweden) and provides a model against which paleo-chemical weathering of ancient profiles (e.g. Utsira High) can be compared. These weathering profiles have been analyzed combining field data with XRD, thin sections and SEM analyses. Special emphasis has been on secondary minerals formation associated with paleoclimate, composition of primary minerals and its distribution in parent rock.

Intrusive origin is attributed to the Vånga Granite which has composition between monzogranite and syenogranite (plotted on Streckeisen diagram). Sericite needles identified on plagioclase grains approve post-magmatic alteration of fresh granite. Two weathering profiles namely; profile-1 and profile-2, have been investigated in detail to give a representative overview on weathering processes prevailed at the locality. Two weathering stages (initial and advanced stage of weathering) have been designated to weathering profiles based on XRD% of three minerals (kaolinite, plagioclase and K-feldspar). Chemical weathering reactions largely include transformation of feldspars and phyllosilicates to kaolinite, smectite, illite and vermiculite.

Plagioclase, especially anorthite content, and biotite are readily affected by weathering whereas K-feldspar stands out as more resistant mineral phase. During initial stage of weathering, pore waters achieve equilibrium with K-feldspar, kaolinite and illite. As weathering proceeds (upon total consumption of plagioclase) formation of kaolinite increases greatly due to dissolution of potassic phases. Three clay mineral phases (smectite, illite and kaolinite) are observed in both weathering profiles. In most weathered samples from both weathering profiles kaolinite>> illite > smectite.

Deep kaolinite weathering and argillization at the study area started in humid tropical climate of the Rhaetian. Weathering of bedrock continued in humid tropical to sub-tropical climate from the Late Triassic to Late Cretaceous until Campanian Sea transgressed the area. Further, saprolites were covered and preserved with Late Cretaceous carbonates until quarrying of limestone and kaolinite in late 19th century.

Keywords: Scania, Ivö Klack, weathering profiles, weathering stages, chemical weathering, secondary minerals, kaolinite weathering, XRD, clay mineralogy.

Contents

1. Introduction:

1.1. Introduction:

The thesis is a part of the Lundin AS supported Utsira Project 'Petrography and porosity developments in reservoir formations on the Utsira High - Importance of provenance weathering vs. diagenesis. The project aims to study the formation of sedimentary particles and deposition in petroleum basins in order to understand particle provenance and particle distribution. These processes include weathering, transportation and deposition of material derived from basement rocks. Parallel research work on this project constitutes one PhD student (Lars Riber) who further is co-supervising three master students (Kamran Javed, Nikolas Oberhardt and the writer). Figure 1 shows the working area of the Utsira Project (Utsira High, Åsta graben, Bornholm and Ivö Klack). This master thesis analyses a possible analogue for the Utsira High setting and describes the weathering pattern along various profiles in Ivö Klack (Figure 1b). The result will be compared with parallel analyses from the Utsira High and the Rønne sections of Bornholm.

The Ivö Klack is located in northeast Scania, (southern Sweden) on the margin of the East European Platform, in a complex block-faulted zone involving the Precambrian basement and overlying Early Palaeozoic, Mesozoic and Palaeogene sediments (Norling and Bergström, 1987). The aim of the study will be to better understand processes of weathering and particle formation in Scania. The methods applied are field observation, thin section, microprobe, SEM and X-ray diffraction analysis.

1.2. Study Area:

At Ivö Klack (Figures 1), the solid Precambrian basement passes upwards and outwards into kaolinized saprolite which finally passes further into kaolin (Surlyk and Sørensen, 2010). Above is 5 m of muddy quartz sand overlain by 25 m of carbonate skeletals encrusted in granite boulders, the top 6 m are carbonates free from boulders (Surlyk and Sørensen, 2010). Before quarrying, the kaolin cover above weathered Precambrian bedrock was nearly 40 m (Lidmar-Bergström, 1983).

After discovery of Cretaceous limestone at Blaksudden (northern part of Ivö) in 1884, it was quarried and later kaolinite deposits were found underneath limestone in 1886 (Bergström and

Shaikh, 1980). The kaolin quarry of Ivö Klack located in northern part of Ivö Island (Sørensen and Sulyk, 2010) was abandoned in 1950's (Bergström and Shaikh, 1980).

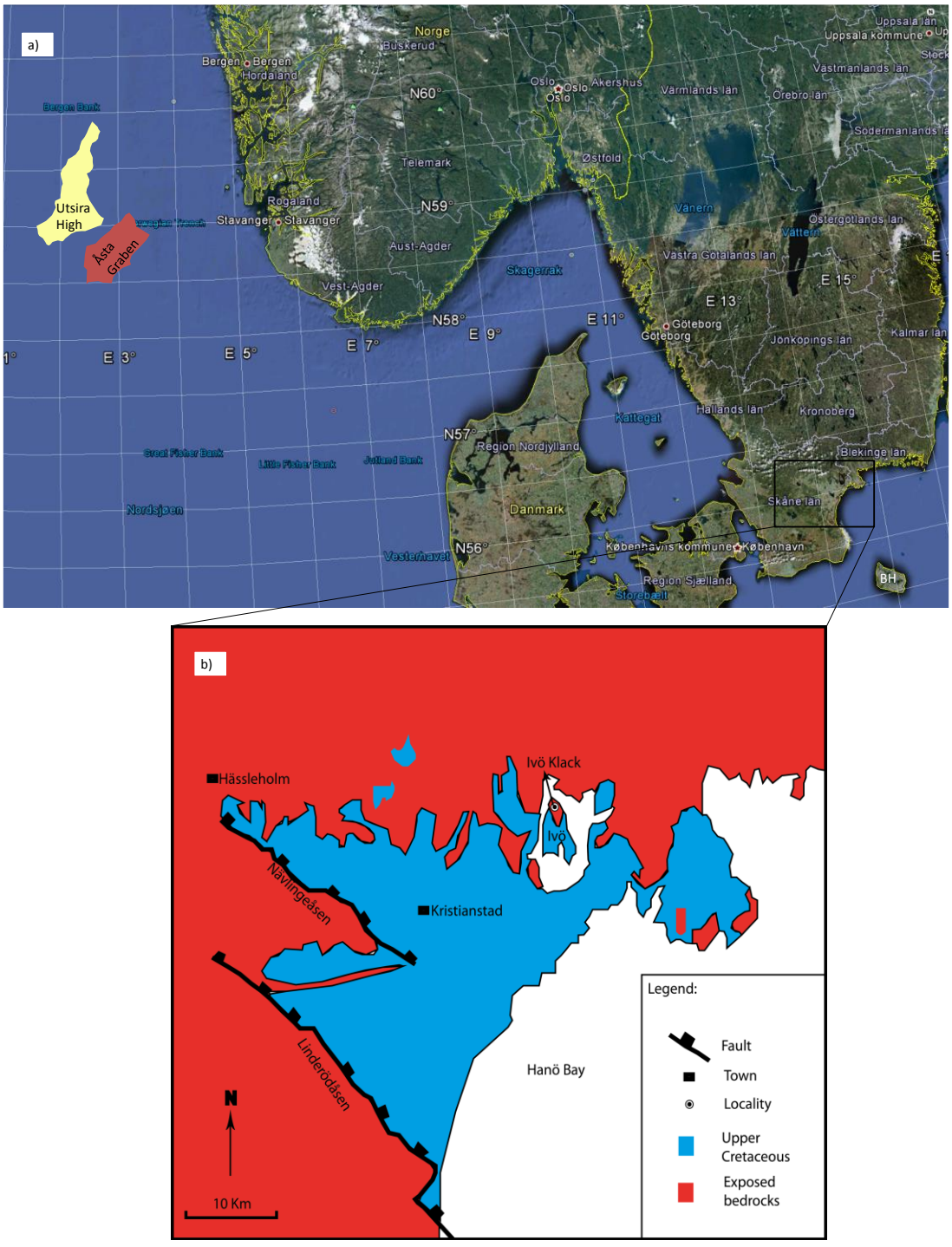

Figure 1: a) Map of southern Sweden and Norway, showing sites of work for Utsira Project (Utsira High, Åsta Graben and BH-Bornholm). b) Map of locality Ivö Klack (modified from Surlyk and Sørensen, 2010).

2. Granites and granite weathering:

2.1. Granite composition:

About ¼ of the exposed crystalline rocks on the Earth are granites (Nesbitt and Young, 1984), with the three main mineral constituents quartz, feldspars and micas (Nockolds et al., 1978). The feldspars are composed of three end members (Figure 2) consisting of albite ($NaAlSi_3O_8$), anorthite ($CaAlSi_3O_8$) and one of the potassium feldspars (microcline, orthoclase or sanidine), where albite takes part in the formation of both plagioclase and alkali feldspar (Johannes, 1979). Micas represent two minerals biotite ($K(Mg,Fe)_3(AlSi_3)O_{10}(OH)_4$) and muscovite ($KAl_2(AlSi_2O_{10})(OH)_2$).

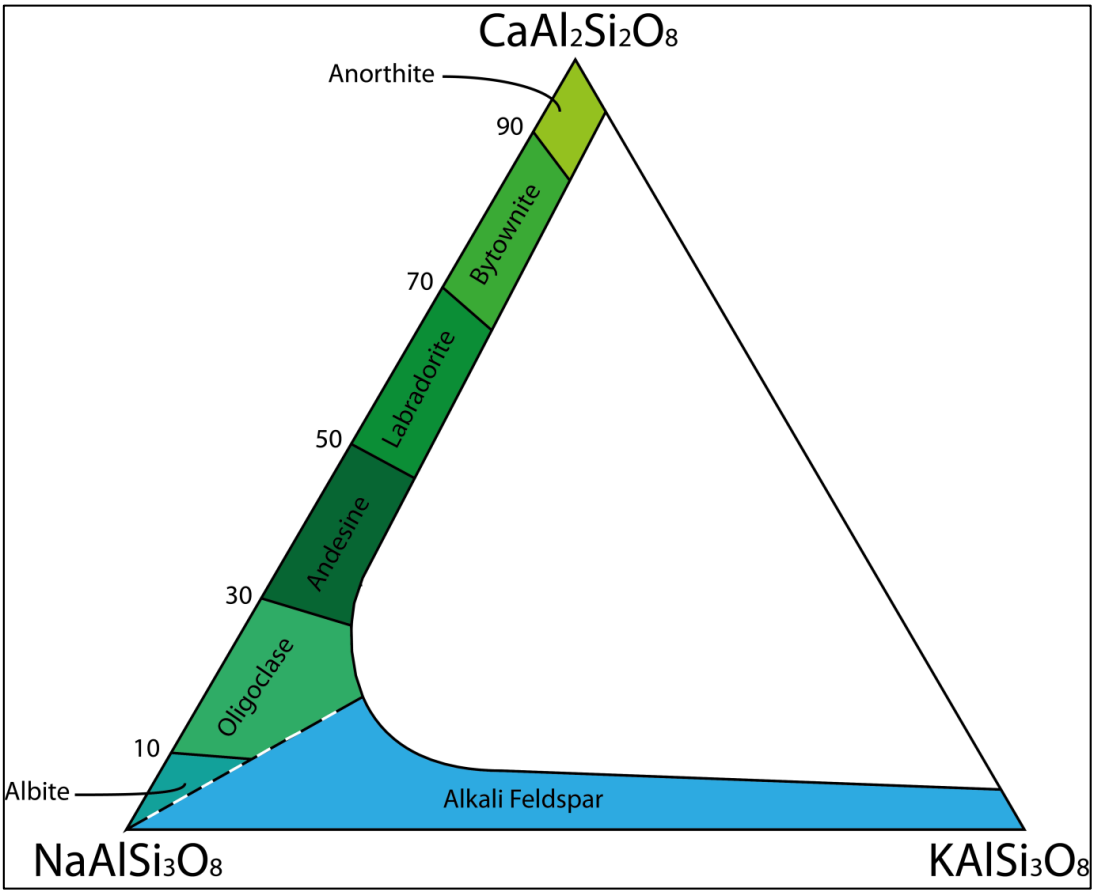

Figure 2: Composition of common feldspar end members (modified from Nesse, 2009).

2.2. Granite weathering and weathering sequence:

Available studies, especially by Lidmar Bergström (1983), Surlyk and Sørensen (2010) and Sørensen and Surlyk (2010) have described the area mainly in reference to geomorphological

evolution and paleontology. Whereas the main theme of this master thesis is to look more closely on the processes and mechanisms of weathering and their end products. In granites, feldspars (plagioclase and alkali-feldspar) and micas are more prone to weathering than quartz (Nesbitt et. al., 1984). Weathering is a combination of processes caused by mechanical, chemical and biological disintegration of a rock upon its interaction with the atmosphere (Dearman, 1975). The physical weathering of the rock creates fracturing while chemical weathering changes mineral composition of the rock (Dearman, 1975) and biological weathering is responsible for both effects (Taylor et al., 2009). The order in which minerals in a rock are altered reflect the stability of the minerals, which mirror the crystallization temperature (Figure 3, red arrow shows order of crystallization and blue arrow shows decreasing trend of stability). For example there is a general increase in chemical stability from olivine via-pyroxene via-plagioclase via-biotite via-muscovite to-quartz (Fairbridge, 1968).

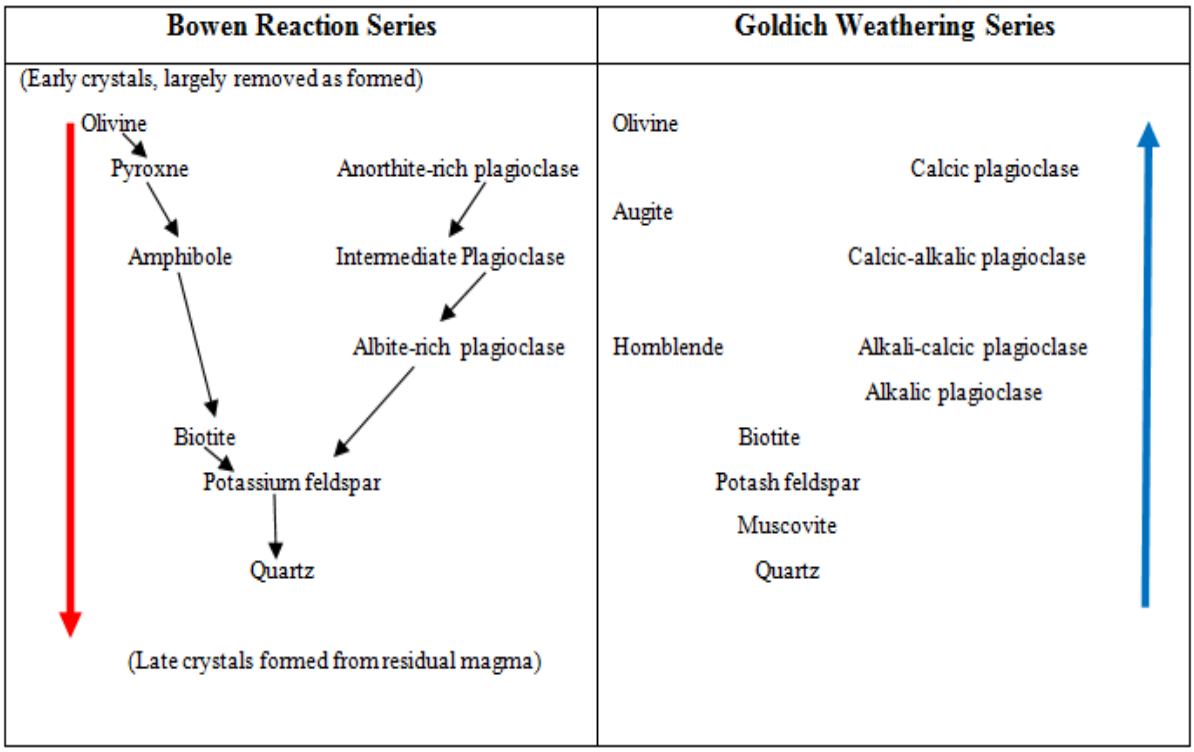

Figure 3: Weathering sequence in minerals versus Bowen's reaction series (modified from Ollier and Pain, 1996).

Tardy et al. (1973) realized that the weathering of primary minerals of basement rocks occurs at different rates and secondary minerals evolve from these in well-established sequences. Primary alumino-silicate minerals found in crystalline rocks decomposes to more stable secondary minerals when come in contact with water, oxygen and carbon dioxide (Steinmann

et al., 1994). The progressive weathering of plagioclase, K-feldspar and biotite (primary minerals) to secondary minerals is shown in Figure 4. The secondary minerals appear, as primary mineral becomes more weathered and their order of appearance remains same irrespective of the nature of the climate (Tardy et al., 1973). Chlorite [$(Mg,Fe)_5Al_2Si_3O_{10}(OH)_8$] in this sequence is a mesonorm (Nesbitt and Young, 1984) and sericite [$(K,Na)_2(Al,Fe,Mg)_3(Si,Al)_8O_{20}(OH)_4$] is formed by the hydrothermal activity (or by alteration of feldspars after magmatism) on feldspars (Que and Allen, 1996; Braga et al., 2002). Sericite and chlorite in the sequence are the result of retrodiagenesis of granites rather than the secondary weathering products (Tardy et al., 1973).

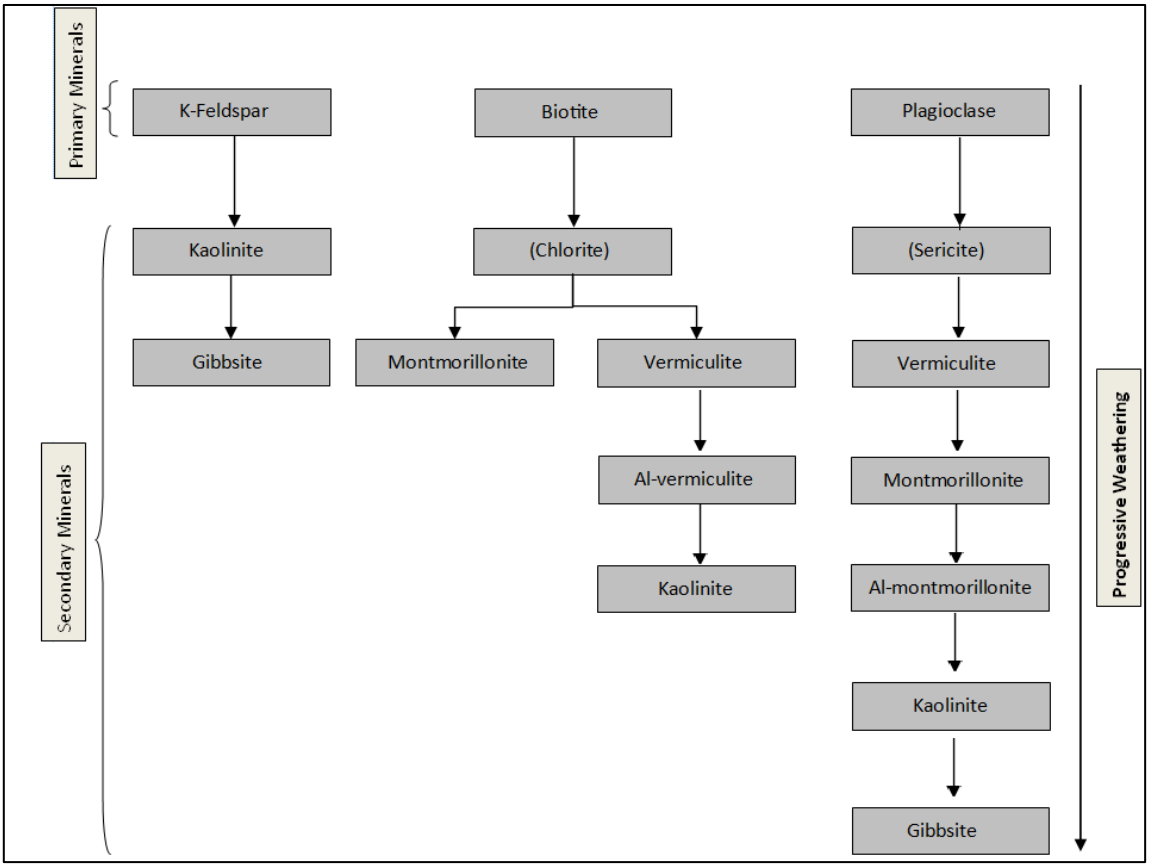

Figure 4: Progressive weathering of primary minerals to secondary minerals in crystalline rocks (modified from Tardy, et al., 1973).

Kaolinite and montmorillonite represent advanced stage of weathering. Montmorillonite forms from products of weakly leached hydrolysis which are rich in silicic acid and bases. In contrast kaolinite is formed from strongly leached acid hydrolysis products (Gjems, 1967). In simple words arid, alkaline and poorly drained environment favours the formation of

montmorillonite whereas humid, acidic and well drained environment favours the formation of kaolinite (Ahlberg et al., 2003a).

2.2.1. Micas:

The depletion of potassium ion in the micas is a diffusion-controlled mechanism and K^+ release rate from biotite is approximately two orders of magnitude faster than from muscovite (Leonard and Weed, 1970). Depending on the nature of environment, weathering product of biotite result in kaolinite or halloysite (acidic environment), vermiculite or smectite (nonacidic environment). However scientists believe that in environments in which biotite transforms to kaolinite, an intermediate alteration product (vermiculite) may form occasionally (Murphy et al., 1998). A brief overview of biotite weathering mechanism is given by Murphy et al. 1998, and an overall biotite weathering reaction in acidic environment can be given as:

$$K_2(Fe_3,Mg_3)(Al_2,Si_6)O_{20}(OH)_4 + 4Al(OH)_2 + 10H^+ = 1.5Al_4Si_4O_{10}(OH)_8 + 2K^+ + 3Fe^{2+} + 3Mg^{2+} + 5H_2O$$

(Biotite) (Kaolinite)……...eq. (1)

Above reaction is dependent on pH, temperature, pressure, plant and biological conditions of the soil solution (Murphy et al., 1998). The normal weathering of muscovite to illite involves a 50-90% loss of potassium content of rock forming mica. Chemically it can be shown as in the form of equation-2 (Roseqvist, 1961):

$$K_2Si_6Al_6O_{20}(OH)_4 + XH_2O = [K(H_3O)]_2Si_6Al_6O_{20}(OH)_4 + XKOH \quad \text{……eq. (2)}$$

(Muscovite) (Illite)

If potassium content in illite drops below 30% of that in parent mica mixed-layered illite-montmorillonite can be formed. Formation of montmorillonite from mica needs replacement of aluminium by silicon and univalent cations are removed to balance the chemical process (Roseqvist, 1961).

The chemical equation (eq. 3) shows this transformation:

$$K_2Si_6Al_6O_{20}(OH)_4 + 5H_2O + {}_{1/2}O_2 = Si_8Al_4O_{16}(OH)_{12} + 2KOH \quad \text{……..eq. (3)}$$

(Muscovite) (Montmorillonite)

A change from trivalent to tetravalent ion in above equation shows the process of oxidation has taken place, to continue making products on the right side of equation we need oxidizing environment (Roseqvist, 1961).

Biotite loses its potassium content during early stages of weathering, in muscovite potassium is replaced by hydronium ion (H_3O^+) and white mica (sericite) loses its potassium as early as biotite (Gjems, 1967). Coarse grained muscovite is more resistant to weathering than biotite. The replacement of potassium by other cations or by water in micas is a process not only confined to crystal surface but affects its interior as well. This cationic exchange in micas is possible due to their structure (Gjems, 1967).

Igneous biotite can be transformed to chlorite by autometamorphism after magmatism, during cooling of magma (Murphy et al., 1998). The chemical equation (eq. 4) below shows transformation of biotite to chlorite (Nesbitt and Young, 1984).

$5K(Mg, Fe)_3Al_3Si_3O_{10}(OH)_2 + 3KA1_3Si_3O_{10}(OH)_2 + 9SiO_2 + 4H_2O = 3(Mg, Fe)_5A1_2Si_3O_{10}(OH)_8$

(Biotite) (Muscovite) (Chlorite) $+8KAlSi_3O_8$ (K-feldspar)...eq. (4)

Mafic chlorites are highly unstable and weather at a rate of 2-3 orders of magnitude faster than biotite (Murphy et al., 1998).

2.2.2. Feldspar:

Dissolution of feldspars involves two steps: 1) dissolution of feldspars in solution, and 2) formation of kaolinite or other secondary minerals. In acidic soils, alteration of the feldspars occurs by selective attack on the Al-sites in tetrahedral position whereas, in non-acidic regimes the role of cation and Al/Si ratios are uncertain (Blum, 1994). Chemically feldspar dissolution can be presented by (Blum, 1994):

$2NaAlSi_3O_8 + 9H_2O = Al_2Si_2O_5(OH)_4 + 4H_4SiO_4 + 2Na^+$ ……eq. (5)

(Albite) (Kaolinite) (Silicic acid)

Comparable reaction will occur for K-feldspar, if we replace K^+ ion in albite. Under acidic environment associated with continuous flux of meteoric water, K-feldspar converts to kaolinite and chemical equation for this reaction can be given as (Blum, 1994):

$2KAlSi_3O_8 + 9H_2O = Al_2Si_2O_5(OH)_4 + 4H_4SiO_4 + 2K^+$…….eq. (6)

(K-feldspar) (Kaolinite)

Advanced leaching of cations results in the formation of kaolin minerals which is initiated by conversion of low stability clay minerals and/or plagioclase. Their occurrence is associated to humid tropical climates but kaolinite formation is in no way limited to tropical climates (Lidmar-Bergström et al., 1997). Further kaolinite converts to gibbsite upon interaction with water even in the absence of carbon dioxide (Lasaga et al., 1994).

$Al_2Si_2O_5(OH)_4 + 5\ H_2O = 2Al(OH)_3 + 2H_4SiO_4$…….……eq. (7)

(Kaolinite) (Gibbsite)

Illite is an intermediate weathering product which can be formed from either feldspar or muscovite (Gjems, 1967). During initial stages of granite weathering, illite forms at the edges of muscovite and feldspar grains. As weathering persists in fractures where movement of water prevails minerals from kaolin group starts to form (Lidmar-Bergström et al., 1997).

Geochemists have used various stability diagrams to discuss the evolution of the composition of solutions in weathering processes. Lasaga et al. (1994) and Steinmann et al. (1994) gave a stability diagram showing relationship between different coexisting mineral phases (Figure 5). Their results showed the evolution of a solution interacting with granite, and the results acquired were based on three assumptions:

1. There is partial equilibrium between different coexisting mineral phases.
2. Dissolution of primary mineral (K-feldspar) is slow.
3. The reaction is irreversible (no aluminium transfer from rock to solution and vice versa).

Steinmann et al. (1994) discussed dissolution of feldspar in both open and closed systems (Figure 5). For closed systems different acidity (pH=4, 5, and 7) of the solution is chosen and reaction is progressed that illustrates different reaction path. Due to third assumption, solution (pH=4) is saturated with gibbsite which precipitates first along reaction path ‘AB’ (Figure 5a).

$KAlSi_3O_8 + H^+ + 7H_2O = Al(OH)_3 + K^+ + 3H_4SiO_4$……..eq. (8)

(K-feldspar) (Gibbsite) (Silicic acid)

By continued dissolution of feldspar, kaolinite starts to precipitate while gibbsite becomes unstable. All the gibbsite will convert to kaolinite along reaction path 'BC'. Along this line silicic acid remains unchanged while potassium ion concentration (K^+) will increase (Steinman et al., 1994).

$KAlSi_3O_8 + 2Al(OH)_3 + H^+ = 1.5Al_2Si_2O_5(OH)_4 + K^+ + 0.5H_2O$……eq. (9)

(K-feldspar) (Gibbsite) (Kaolinite)

When all the gibbsite is consumed, silicic acid as well as K^+ ion concentration starts to increase upon further dissolution of feldspar and kaolinite precipitates along 'CD'.

$KAlSi_3O_8 + H^+ + 4.5H_2O = 0.5Al_2Si_2O_5(OH)_4 + K^+ + 2H_4SiO_4$……..…eq. (10)

(K-feldspar) (Kaolinite) (Silicic acid)

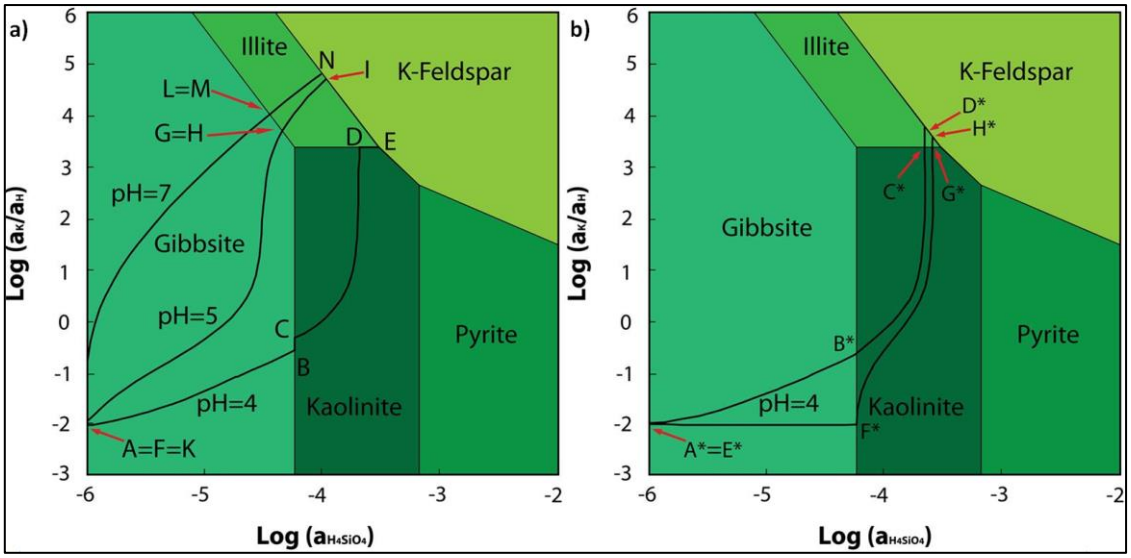

Figure 5: a) Reaction paths in a closed system for K-feldspar dissolution in solutions with different pH (reaction path ABCD for solution with pH=4, reaction path FGHI for solution with pH=5 and KLMN is reaction path for solution of pH=7). b) Reaction paths for K-feldspar dissolution in an open system (A*B*C*D* reaction path for initial stages of chemical weathering and E*F*G*H* reaction path during later stages of chemical weathering) (modified from Steinmann, 1994).

At 'D' kaolinite starts to dissolve and muscovite or illite precipitates and the reaction follows straight line 'DE' unless all the kaolinite is consumed.

$KAlSi_3O_8 + Al_2Si_2O_5(OH)_4 + 3H_2O = KAl_3Si_3O_{10}(OH)_2 + 2H_4SiO_4$……..…eq. (11)

(K-feldspar) (Kaolinite) (Illite) (Silicic acid)

'E' is the equilibrium point solution for three minerals (feldspar, illite and kaolinite). By changing the pH of the solution different stability trends can be achieved in closed sytems as indicated in Figure 5a for solutions with pH= 5 & 7 (Lasaga et al., 1994; Steinman et al., 1994).

However, to describe weathering phenomena in nature where most systems are open, another scheme of reaction paths have to be considered. For simplicity Steinmann et al. (1994) uses a solution with pH= 4 flowing in rock with composition entirely of K-feldspar. The reaction paths for both initial and late stages of weathering are shown in Figure 5b. During the initial stages of chemical weathering gibbsite will precipitate first along A*B* reaction path (Figure 5b), making a gibbsite rich zone (Figure 6). The fluid then flows down making a kaolinite rich zone along reaction path B*C*, and at last a thin illite rich zone which is quantitatively unimportant is developed along reaction path C*D* (Steinmann et al., 1994).

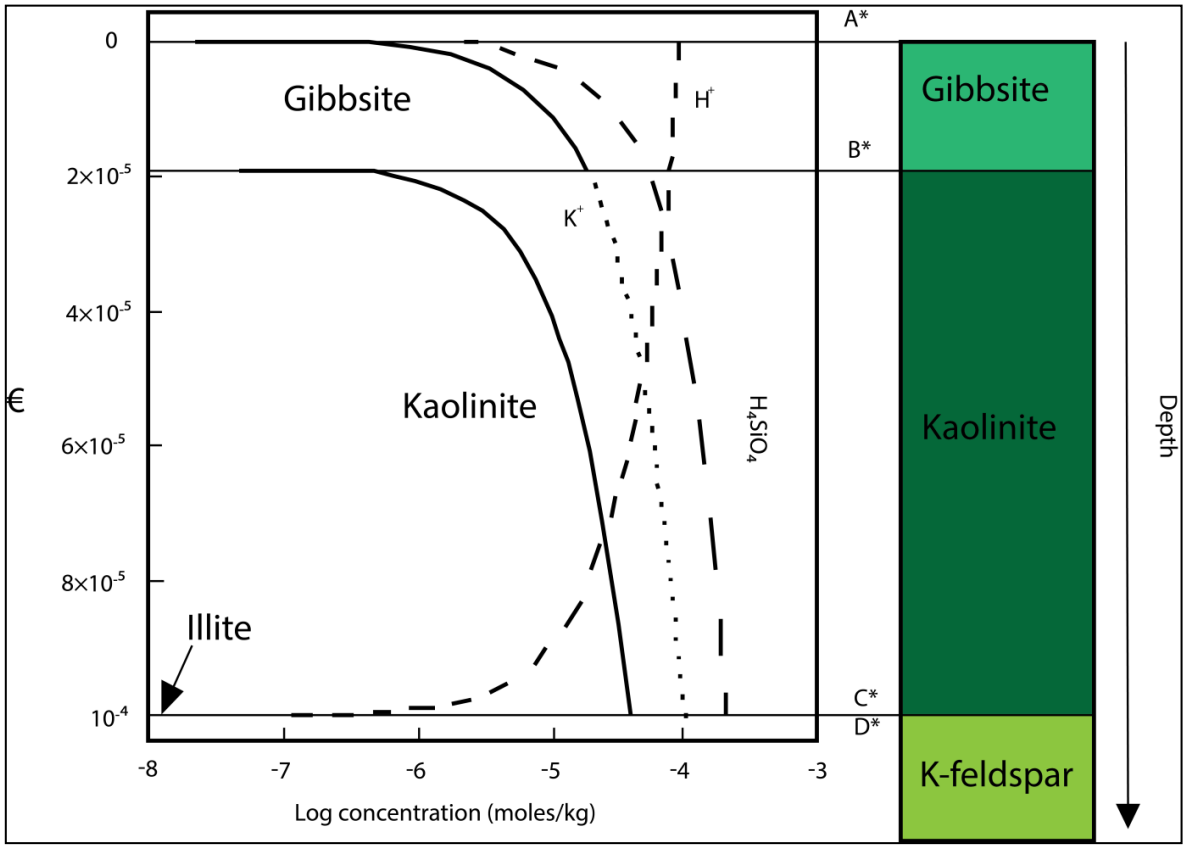

Figure 6: Amount of minerals in moles/kg (solid lines) and concentration of aqueous varieties (dashed lines) for open system along reaction path A*B*C*D* of Figure 5b. Formation of secondary minerals rich zones, illite rich zone along reaction path C*D* is quantitatively unimportant (modified from Steinman et al., 1994).

During later stages of weathering upon further fluid infiltration, no reaction will occur in gibbsite rich zone because of the assumption of no aluminium transfer. However in kaolinite zone, gibbsite will precipitate on the dissolution of kaolinite along E*F* (Figure 5b).

$Al_2Si_2O_5(OH)_4 + 5H_2O = 2Al(OH)_3 + 2H_4SiO_4$……...……eq. (12)

(Kaolinite) (Gibbsite) (Silicic acid)

When solution becomes saturated with kaolinite the reaction will stop, the solution then flows through tiny zone of illite and comes in contact with K-feldspar. Here kaolinite will precipitate upon dissolution of K-feldspar along F*G* (Figure 5b). This is then followed by the precipitation of illite along G*H*. In this later stage of weathering mineral sequence will remain the same but each mineral zone will extend downwards. The reaction path E*F*G*H* is followed in this later stage of K-feldspar dissolution (Lasaga et al., 1994; Steinman et al., 1994). After this chemical reaction seizes fluid comes in equilibrium with the K-feldspar (Steinman et al., 1994).

2.3. Diagenetic effects:

Nesbitt and Young (1989) proposed two types of diagenetic effects that can affect mineral composition of a weathering profile namely;

1) Early diagenetic effects and

2) Late diagenetic effects.

These two possible diagenetic effects are related to either prior burial (early diagenetic effects) or during and after burial (late diagenetic effects) of the weathering profiles (Nesbitt and Young, 1989).

Effects produced due to early diagenetic reactions involve further alteration of secondary weathering products upon reacting with groundwaters (Nesbitt and Young, 1989). Consequently formation of clay minerals (specially smectites) and carbonates occur as a result of accumulation of Si, carbon dioxide, Ca and Mg. Accumulations of these clay minerals and carbonates indicate ancient water tables (Nesbitt and Young, 1989).

Late diagenetic effects are produced due to interaction of basin water or trapped seawaters with the secondary minerals in the weathering profile during or after burial (Nesbitt and

Young, 1989). Metasomatism is the process associated with late diagenetic reactions and comprises formation of illites, smectites and chlorites at the cost of kaolinite and restructuring of moderately weathered feldspars to plagioclase and K-feldspar. Na-metasomatism is favoured in subsiding oceanic sedimentary basin while K-metasomatism is preferred in subsiding continental sedimentary basins. The reason of this contrast is difference in composition of seawaters (high Na/K) and continental ground waters (low Na/K).

2.4. Weathering grade:

Weathering grade for bedrocks has been assigned by various scientists using different techniques, especially for engineering purposes (Dearman, 1975; Thomas, 1994). Weathering intensity or grade refers to the mineralogical and chemical transformation of primary minerals to secondary minerals (White et al., 1998). Table 1 illustrates five weathering grades based on the studies of ISRM (1978) and Begonha and Braga (2002).

Table 1: Weathering classification based on mechanical properties of rock (modified from ISRM, 1978; Begonha and Braga 2002).

Weathering Grade	Bedrock Condition
Grade-I	Bedrock completely intact.
Grade-II	Slightly weathered with color change along fractures.
Grade-III	Less than half of bedrock weathered and decomposed.
Grade-IV	More than half of bedrock converted to clays and soil.
Grade-V	All rock mass converted to secondary minerals.

3. Geological setting and tectonic evolution:

3.1. Geological setting:

The northern part of the East European Craton comprises three crustal segments (Figure 7) Fennoscandia (Baltic Shield and its buried extension) in the northwest, Volgo-Uralia in the east and Sarmatia in the south (Gorbatschev and Bogdanova, 1993). The continental crust of the Baltic Shield was formed through Paleoarchean to Paleoproterozoic during four orogenic activities viz, Lopian orogeny (2.9-2.6 Ga), Svecofennian orogeny (2.0-1.75 Ga), Gothian orogeny (1.75-1.5 Ga) and Sveconorwegian-Grenvillian and Caledonian Orogenies (1.25-0.9 & 0.6-0.4), the latter is associated more with the reworking of the Precambrian continental crust of Baltic Shield (Gaál et al., 1987; Gorbatschev, 1980, 1985; Gorbatschev et al., 1993). From the northeast to southwest the Precambrian of the Baltic Shield is geochronologically divided in three domains, namely the Archean Domain, the Svecofennian Domain and the Southwest Scandinavian Domain (Gaál et al., 1987).

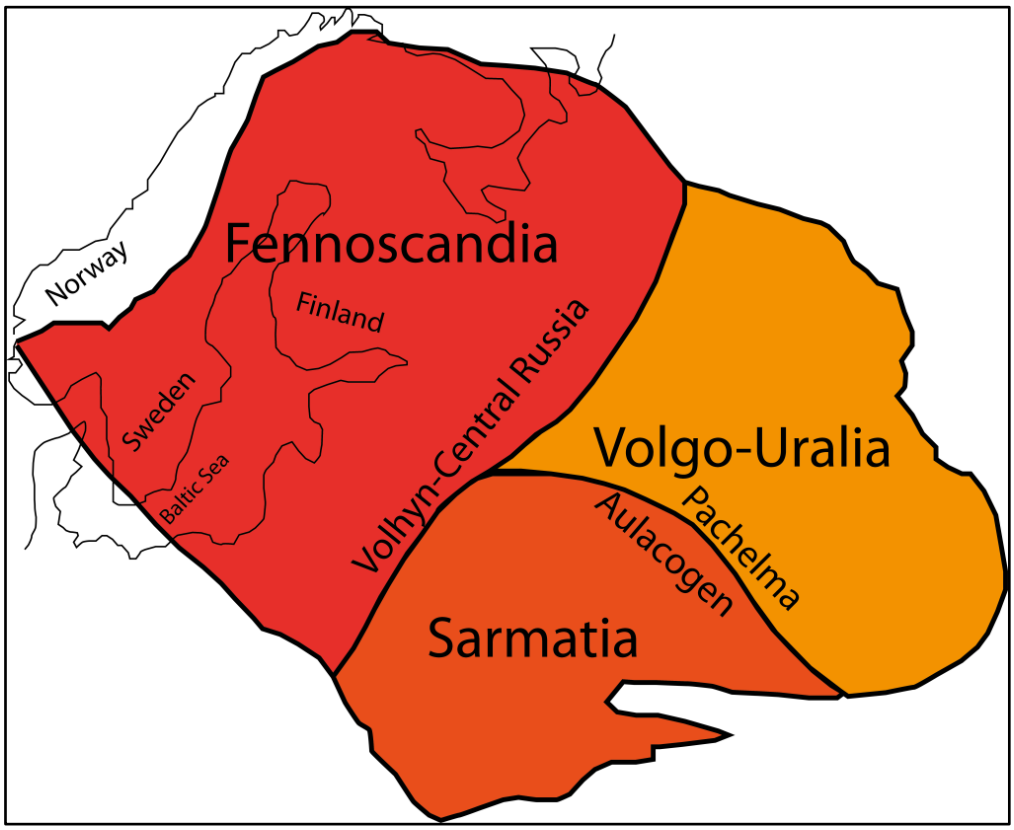

Figure 7: Crustal divisions of the East European Craton (modified from Gorbatschev and Bogdanova, 1993).

Scania is defined by three main structural features (Figure 8) including Baltic (Fennoscandian) Shield, Fennoscandian Border Zone (FBZ) and Danish Basin (Ahlberg et al., 2003a). It forms the transition zone between the chalk-dominated basinal areas (Danish Basin) in the southwest and weathered highs of Baltic Shield to the northeast (Ahlberg et al., 2003a and 2003b; McCann, 2008). The area is a series of horsts with grabens in between, NW-SE oriented Linderödåsen and Nävlingåasen horsts are situated southwest to the Ivö Klack and northeast to the Colonus Shale Trough (Erlström et al., 1997; Surlyk and Sørensen, 2010). Ivö Klack along with Linderödåsen horst, Nävlingåasen horst and some other small islands forms a protected archipelago (Surlyk and Sørensen, 2010).

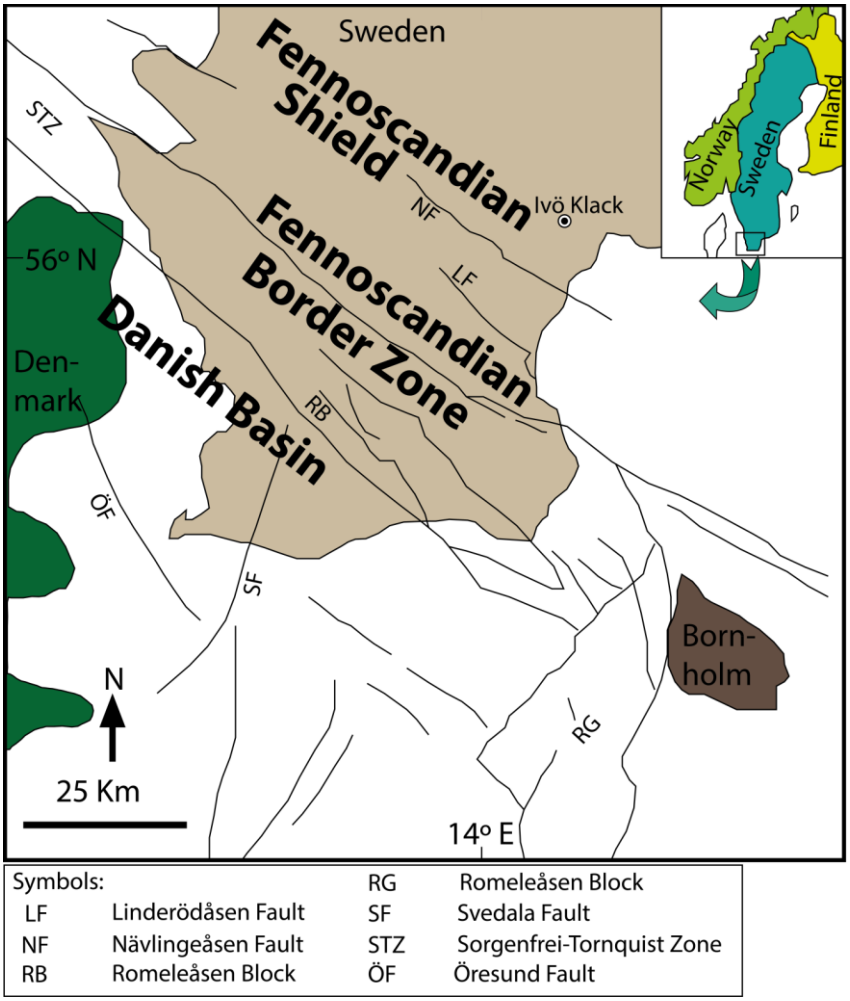

Figure 8: Structural map of Scania showing three main and some minor features (modified from Erlström et al., 1997; Ahlberg et al., 2003).

The Tornquist zone consists of WNW-widening splay faults (Figure 9) of Carboniferous age and the zone was tectonically evolutionized by Mesozoic extensional tectonics and Cretaceous-Tertiary inversion (Thybo, 1997). The zone extends from the North Sea towards

Scania into Poland with NW-SE trending faults (Erlström et al., 1997). This zone consists of the northwest Sorgenfrei-Tornquist Zone (STZ) and southeast Teisseyre-Tornquist Zone (TTZ) separated by Rønne Graben and is the longest tectonic lineament of the Europe (Thybo, 1997).

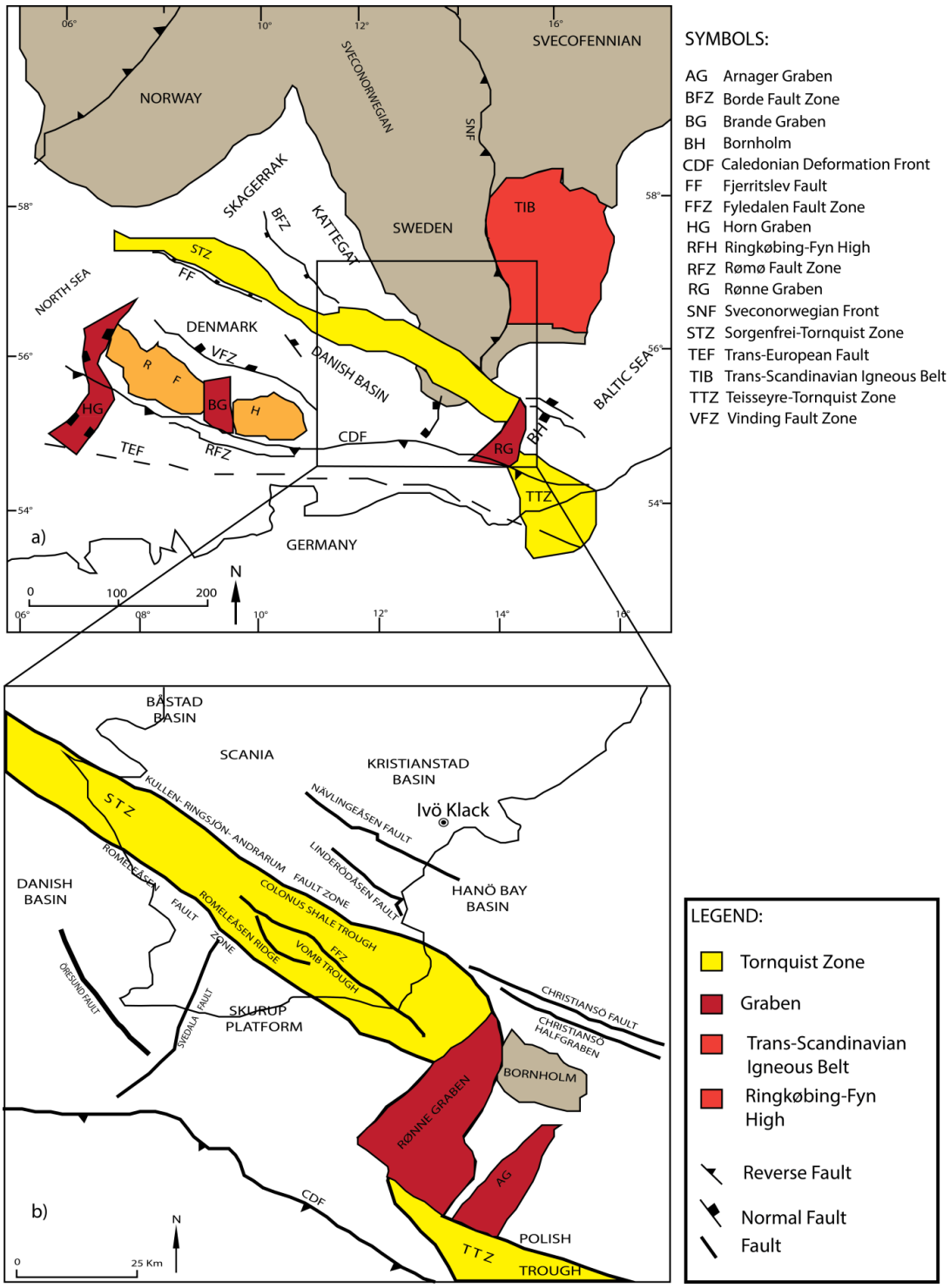

Figure 9: Upper) Geological map of Fennoscandian Border Zone and surrounding areas (modified from Thybo, 1997), lower) Structural elements of southern Sweden (modified from Erlström et al., 1997).

The Trans-European Fault Zone defines the southernmost margin of Precambrian crust of the Baltic Shield (Thybo, 1997) and to the north the Sorgenfrei-Tornquist Line separates old, thick, cold crust of northeastern Europe from the hotter, thinner crust of central and western Europe (Gorbatschev and Bogdanova, 1993), which together with Skagerrak Kattegat Platform is referred to as Fennoscandian Border Zone (Baartmen and Christensen, 1975; Liboriussen et al., 1987; Group, 1988; Erlström et al., 1997). The Sorgenfrei-Tornquist Zone runs from Bornholm, Scania, Kattegat, and Northern Jutland to the North Sea (Group, 1988) and has a width of 20-50 Km (Group, 1988; Erlström et al., 1997). The northern and southern extent of STZ is delineated by Kullen-Ringsjön-Andrarum Fault Zone (KRAFZ) and Fjerritslev Fault respectively (Erlström et al., 1997; Thybo, 1997), and in the southwest the Romeleåsen Fault Zone (RFZ) and the Rønne Graben marks its limit (Erlström et al., 1997). This tectonic zone consists of a number of structural units in Scania, e.g. the Romeleåsen Block (consisting of Romeleåsen Ridge, Vomb Trough and the Ystad-Rønne high) and the Colonus Shale Trough (Erlström et al., 1997). The Romeleåsen Block is demarcated in the southwest by RFZ and in the northeast by Fyledalen Fault Zone (FFZ) which also defines the southern margin of Colonus Shale Trough (Erlström et al., 1997).

3.2. Tectonic evolution:

A detailed note on the Mesozoic and Cenozoic tectonic evolution of Scania is given by Norling and Bergström in 1987. Three main deformation events (Figure 10) have been identified in Scania:

1. The Permian-Carboniferous,
2. The Late Triassic-Jurassic and
3. The Cretaceous-Paleogene (Norling and Bergström, 1987).

Lack of Devonian series in the area makes it difficult to judge the possibility of deformation caused by the Caledonian Orogeny (Norling and Bergström, 1987). During the Caledonian orgeny in earliest Paleozoic Scania was a part of shelf area facing the rising orogen ((Norling and Bergström, 1987; McCann, 2008). After the two major orogenies (Caledonian and Variscan Orogenies) Scania mostly acted as an intermediate zone between tectonically active Central European platform and Baltic shield since late Paleozoic (Liboriussen et al., 1987; Erlström et al., 1997).

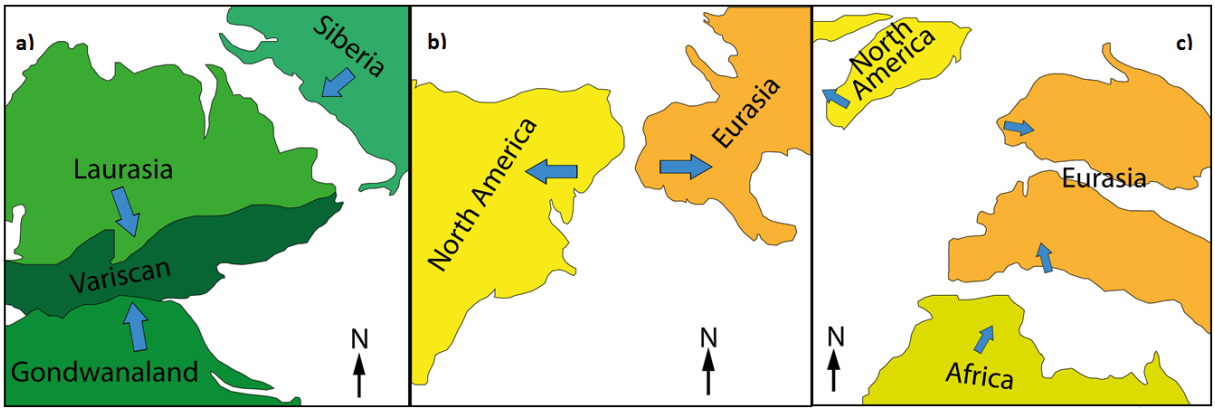

Figure 10: Plate movement during three deformation zone. a) Permo-Carboniferous, b) Triassic-Jurassic and c) Tertiary (modified from epgeology.com).

3.2.1. Phase-I:

The Variscan Orogeny (Figure 10a) resulted by the collision of Laurasia with Gondwana-derived microplates during Late Carboniferous through Early Permian (Warr, 2012; Zeigler and Kent, 1982). The strike–slip movement in the Permo-Carboniferous resulted in the uplift of southern Sweden and erosion of the Early Paleozoic strata. Besides, it is associated with the development of Oslo Graben (Norling and Bergström, 1987). The area was covered with products of volcanic activity during Permian and extensive erosion of these products took place before the Mesozoic transgressions (Norling and Bergström, 1987). The supercontinent Pangea was created at the end of this phase (Warr, 2012).

3.2.2. Phase-II:

In Scania, the second deformation phase affected the rift tectonics (Arctic and North Atlantic) accompanied by the climate change from arid to humid conditions (Lidmar-Bergström, 1983; Norling and Bergström, 1987; Lidmar-Bergström et al., 1997). In this phase rifting and wrench tectonics occurred and the basin formed during Permian continued subsiding in northwestern Europe (Zeigler and Kent, 1982; Norling and Bergström, 1987). In Early Jurassic uplifting of Baltic shield preceded the period of continental erosion and deposition (Norling and Bergström, 1987).

The Scania experienced volcanic activity from Early to Middle Jurassic, dolerite dikes aligned in NW and WNW directions in Scania (Lidmar-Bergström, 1983). Based on the Triassic and Jurassic sediments in northwestern Scania it is concluded that the horst movements started by Variscan tectonics with the main tectonic activity related to the Late Jurassic (Lidmar-

Bergström, 1983; Ahlberg et al., 2003b). Absence of similar sediments in the Båstad and Kristianstad Basins may indicate that these areas were situated on a high during Triassic and Jurassic (Lidmar-Bergström, 1983). Scania and Blekinge were uplifted even before the formation of other highs in the area and the Kristianstad Basin slanted to the southeast during formation of Nävlingeåsen and Linderödåsen horsts (Bergström et al., 1973). Northeastern Scania remained uplifted until Cretaceous sea transgression and Precambrian crystalline basement stayed exposed to subaerial conditions (Norling and Bergström, 1987; Lidmar-Bergström et al., 1997).

3.2.3. Phase-III:

During the third deformation phase rifting continued in the Arctic and North Atlantic domain during Early Cretaceous referred to as the Late Cimmerian tectonism (Lidmar-Bergström, 1983; Zeigler, 1978; Zeigler and Kent, 1982). The Central European marginal basins experienced inversion during Subhercynian tectonic phase (early Late Cretaceous) but the effect of this inversion tectonics did not reach Scania (Zeigler, 1978; Lidmar-Bergström, 1983). In the Late Cretaceous, Romeleås Fault originated due to compressional tectonics and separated Scania from Romeleås-Vomb block (Norling and Bergström, 1987). During the same period in northeast Scania, the Hanö Bay-Kristianstad Basin experienced subsidence along the Christiansö, the Linderödsåsen and the Nävlingeåsen faults coeval with the uplift of STZ (Norling and Bergström, 1987; Erlström et al., 1997). The sea transgressed in parts of Scania during Cretaceous resulted in deposition of carbonates and flints were formed by subaerial weathering of carbonates upon regression of the sea (Lidmar-Bergström, 1983). Central north Scania underwent a slight tectonic uplift during Tertiary (Norling and Bergström, 1987).

3.3. Paleogeography and paleoclimate:

Lidmar-Bergström (1983) discussed the geomorphological evolution in southern Scandinavia and made a comprehensive reconstruction of the paleogeography and paleoclimate of the area. Large parts of Sweden were flooded by the sea during Cambrian and Silurian periods. Through Devonian the climate was arid and the south Sweden was located on equator. During middle Carboniferous the continental blocks started moving northwards and warm humid climate prevailed across the Europe (Lidmar-Bergström, 1983). No sedimentation occurred throughout the Devonian, Carboniferous and Permian times in Sweden and land surface was

exposed to weathering and denudation. In middle Permian south Sweden was located at 15° N and climate was arid as inferred from the sediments deposited (Lidmar-Bergström, 1983).

Lidmar-Bergström et al. (1997) gave a detailed note on the correlation of palaeotopography, saprolite formation, sedimentation and climate change in southern Fennoscandia from Permian to Pleistocene (Figure 11). In this section it is the intention to give a brief overview of the correspondence between climate and correlative sediments formed in the area along with the paleogeography.

During Triassic-Jurassic times south Sweden was situated at 35° N, dry and arid climate of Permian continued in Triassic which changed into humid condition in Late Triassic as depicted by Figure 11 (Lidmar-Bergström, 1983). In latest Triassic the climate was humid tropical as indicated by fossil flora and the formation of a 50 m thick saprolite in Central Scania (Lidmar-Bergström et al., 1997). This climate change is associated with the early breaking up of Pangea in Late Triassic which was accompanied by enhanced humidity on land. The southern Sweden moved from 33° N to 43° N through Late Triassic to Early Jurassic (Ahlberg et al., 2002; Ahlberg et al., 2003a). In early Late Triassic Scania was located in the continental part of Pangea with long arid season and extreme rain seasons which resulted in formation of haematite cement in the pores of arkosic red beds. The atmosphere and hydrosphere during Mesozoic era was carbondioxide rich (Ahlberg et al., 2002; Ahlberg et al., 2003b).

The transition from arid environment of Triassic to the humid climate in Rhaetian (Late Triassic) is reflected changes from clay mineralogy of smectite dominated composition to kaolinite dominated. The Late Rhaetian deposits are dominated by kaolinitic clays and pure quartz sand. Warmer temperature prevailed throughout Cretaceous apart from in Aptian and Cenomanian (Lidmar-Bergström, 1983; Lidmar-Bergström et al., 1997). Formation of carbonates is associated with the Campanian transgression (Late Cretaceous) and its dissolution in Tertiary period resulted in the formation of flints as residue (Lidmar-Bergström, 1983).

Warm and humid environment prevailed throughout Early-Middle Jurassic and average sea temperature of Europe was 10° C higher as compared with today (Lidmar-Bergström, 1983). The basement rocks in northeast Scania and Halland (southern Sweden) remained uplifted and sub-aerially exposed for a long time until the transgression by the sea in Cretaceous time.

Fresh water and brackish water deposits were associated with the early Cretaceous resulted from the first transgression in the Late Neocomian.

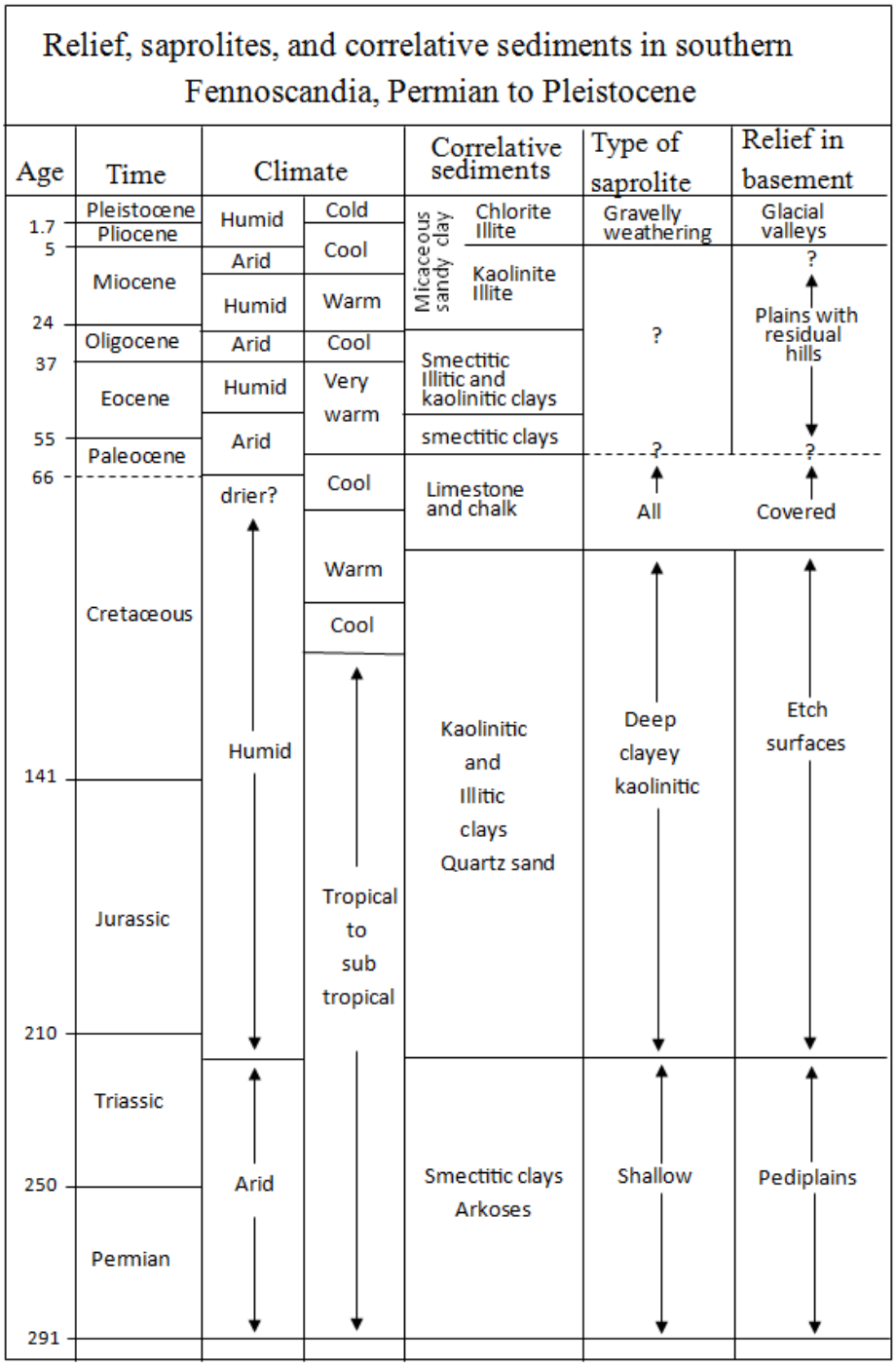

Figure 11: Linking evolution in relief, saprolitization, sedimentation and climate change in southern Fennoscandia through Permian to Pleistocene (modified from Lidmar-Bergström et al., 2011).

A basic difference in Scania is observed between the Early Cretaceous and Late Cretaceous deposits. Early Cretaceous sedimentation seems to be the continuation of Jurassic sedimentation while the Late Cretaceous deposits consist of limestone and chalk facies. In the

Kristianstad and Båstad basins late Cretaceous is attributed to an alternative pattern of regressions and transgressions. The Early Cenomanian, Santonian, Campanian and the Early Maastrichtian represent ages of transgressions while the Turonian, Coniacian and the Late Cenomanian represent ages of regressions. The subsidence rate increased during middle Late Cretaceous in the southwest Scania (Lidmar-Bergström, 1983). The location of south Sweden remained in between 35°-45° N in the Cretaceous with tropical to subtropical climate.

Throughout Tertiary episodes of arid and humid climate prevailed in the area with warm-cool-cold environments (Lidmar-Bergström, 1983; Norling and Bergström, 1987; Lidmar-Bergström et al., 1997). The regression of the sea occurred in the Paleocene over the whole world, and in Early Eocene the transgression protected the erosional surface produced during earlier regressions. Warm and humid climate prevailed in Eocene but it became arid and cooler during Oligocene. The etching processes prevailed in Eocene and stripping occurred in the Oligocene.

During Miocene-Pliocene epochs uplifting of Fennoscandia and marine regression caused formation of two erosional surfaces. Intense stripping and dissolution of Cretaceous limestone occurred in cool and humid climate of Pliocene. Intensified river incision of unweathered bedrock occurred in the Late Pliocene and in the Pleistocene in a colder humid environment. In southwestern Scania Tertiary strata are represented mainly by Lower Paleocene, and sedimentation is controlled by the formation of bioherms or mounds of bryozoans and occasional coral reefs (Lidmar-Bergström, 1983).

The Tertiary period is characterized by alternative arid and humid climate which is also reflected in clay minerals found in the saprolites of southern Sweden. The reliefs in basement rocks are mainly dependent on the climate and etch processes prevailed during its formation. One of the main features of Quaternary saprolites is their gravel content. Saprolitization occurred in Pleistocene but continued through Holocene and formed a ‘new relief’ (Lidmar-Bergström et al., 1997). Sceintists claim that these gravelly saprolites are more or less similar to the saprolites found in other parts of Fennoscandia. The glaciation has little effect of stripping on the saprolites protected by the cover rocks of Jurassic and Cretaceous (Lidmar-Bergström, 1983; Lidmar-Bergström et al., 1997). The relative relief of northeast Scania reaches up to 200 m in some area, this is not only due to deep weathering and erosion. In addition tectonic movements have also affected the relative relief of the area (Lidmar-Bergström, 1983).

4. Materials and methods:

4.1. Sedimentological site logging:

During September, 2012 a field trip to Scania and Bornholm was organized for this master thesis project. Under supervision of Professor Henning Dypvik and Lars Riber, sedimentological site logging was conducted.

With reference to the site at Ivö Klack, logging was done along six different profiles. The scree on the location was removed using shovel before inspecting and sample collection. The scale was different for almost all the logs and shown in appendices.

Besides site logging and sample collection, pictures were taken for all the profiles by Lars Riber, Nikolas Oberhardt and the writer.

4.1.1. Sample collection:

Samples of unweathered and weathered Precambrian basement were collected for further analyses. A total of 70 samples were acquired from the six profiles and one sample of fresh basement was provided by Mr. Lars Riber. Sampling interval and number of samples was different for all the profiles, 20 samples from profile-1, 8 from profile-2, 4 from profile-3, 16 from profile-4, 11 from profile-5, 9 from profile-6 and one sample each from the uppermost veneer of reworked material and transported sand were collected, details are given in Appendix 5. The nomenclature of the samples is devised by Professor Henning Dypvik (locality name, profile number, sample number and year). The logging and sampling is mainly performed by Nikolas Oberhardt and the writer.

4.2. Mineralogical and petrographical analysis:

These analyses have been done using both thin sections and XRD data.

4.2.1. Thin Sections:

Out of above mentioned 70 samples, 36 samples are selected to give a representative image of the site. Thin sections have been prepared at Institute of Geosciences, University of Oslo. Thin sections of rock were cut and glued (with blue epoxy) to a glass slide of 26 mm x 46 mm dimension.

Description:

The main purpose to study thin sections is to get a detailed idea about rock texture and mineralogy. All the samples from profile 1 & 2, one from profile-4 (along fracture), two from profile six, one of fresh granite, one sample of thin layer of sediments (kaolinite cover) above the saprolite and one sample of transported sand near profile-1 were chosen for thin section preparation.

Mineral counting:

A total 12 thin sections are mineral counted to 400 points by employing a Nikon Optiphot-Pol petrographic microscope both with plane polarized and cross polarized light. Table-3 gives detail of samples prepared for thin section analysis and sample names with bold font have been point counted. The procedure of counting minerals is done in sedimentology lab at University of Oslo using a swift automatic counter.

Table 2: Thin section analysis. Point counted thin sections are shown in bold.

Sample name	Location	Depth above base (cm)	Sample name	Location	Depth above base (cm)
Ivö-Extra 1-12	Random	Base	Ivö-1-18-12	Profile-1	255
Ivö-1-1-12	Profile-1	5	Ivö-1-19-12	Profile-1	265
Ivö-1-2-12	Profile-1	15	**Ivö-1-20-12**	Profile-1	275
Ivö-1-3-12	Profile-1	45	**Ivö-2-1-12**	Profile-2	02
Ivö-1-4-12	Profile-1	55	Ivö-2-2-12	Profile-2	11
Ivö-1-5-12	Profile-1	70	Ivö-2-3-12	Profile-2	32
Ivö-1-6-12	Profile-1	75	Ivö-2-4-12	Profile-2	42
Ivö-1-7-12	Profile-1	85	Ivö-2-5-12	Profile-2	43
Ivö-1-8-12	Profile-1	95	Ivö-2-6-12	Profile-2	44
Ivö-1-9-12	Profile-1	115	Ivö-2-7-12	Profile-2	46
Ivö-1-10-12	Profile-1	125	**Ivö-2-8-12**	Profile-2	47
Ivö-1-11-12	Profile-1	135	Ivö-4-5-12	Profile-4	65
Ivö-1-12-12	Profile-1	145	Ivö-6-2-12	Profile-6	35
Ivö-1-13-12	Profile-1	155	Ivö-6-9-12	Profile-6	825
Ivö-1-14-12	Profile-1	185	Ivö-A-6-12	Random	NA
Ivö-1-15-12	Profile-1	205	Ivö-B-6-12	Random	NA
Ivö-1-16-12	Profile-1	225	**Ivö-K1-12**	Saprolite top	NA
Ivö-1-17-12	Profile-1	235	**Ivö-Sand-12**	Random	NA

Michel-Lévy method:

This method is used to determine plagioclase composition in thin section of fresh granite. The Michel-Lévy method relies on the observation of the extinction angle measured to (010) plane of albite twins which vary in an ordered way with composition. Detailed procedure for the method is given by Nesse (2009).

4.2.2. Scanning electron microscopy (SEM):

SEM analysis has been done on both carbon coated thin sections and gold coated samples mounted on stubs using JEO2 JSM-6460LV Scanning electron microscope. Cathodoluminescence analysis has also been carried out using cathodoluminescence detector attached to scanning electron microscope. Different samples (carbon coated thin sections and gold coated stubs) have been studied in detail under electron microscope during several sessions with help of Berit Løken.

4.2.3. X-Ray diffraction analysis:

Qualitative and semi-quantitative analysis has been performed using XRD analyses technique. To get an agreement in results a portion of same the 36 samples as used for thin sections were chosen for XRD analyses.

Bulk analysis:

Samples are first micronized and then filled in glass holders to run in X-Ray diffractometer for bulk analyses. All the methods and techniques have been performed in sedimentology and X-Ray diffraction lab at University of Oslo.

Clay separation and analysis:

20 clay samples from of the above mentioned samples were separated. Table-4 gives detail of the samples prepared for bulk and clay separated XRD analysis. 10 grams of each micronized sample was put in a beaker with 400 ml distilled water and stand in Bandelin Sonorex RK 102 transistor for a 10 min ultrasound treatment. Samples were then put in a flask of 80 cm and upper 70 cm was sucked after 24 hours. Filtering was performed using inverted millipore (after treating with 0,1M Magnesium chloride and washed with distilled water) to get and

place the clay fraction on glass slides which is then ready for the XRD analysis. For identifying different clays four treatments were applied.

1) Air-dried samples were analyzed.

2) Samples exposed to ethylene glycol vapors were analyzed to check for any swelling clays.

3) Samples were heated to 350 ºC for half an hour and analyzed.

4) Samples were heated to 550 ºC for around 45 minutes and analyzed. At this temperature X-rays are unable to identify kaolinite, so by comparing Ethylene glycol treated diffractograms with the diffractograms acquired by 550 ºC heating it is possible to identify kaolinite.

Table 3: Bulk XRD samples, clay separated samples are shown bold.

Sample name	Location	Depth above base (cm)	Sample name	Location	Depth above base (cm)
Ivö-Extra 1-12	Random	Base	**Ivö-1-18-12**	Profile-1	255
Ivö-1-1-12	Profile-1	5	**Ivö-1-19-12**	Profile-1	265
Ivö-1-2-12	Profile-1	15	**Ivö-1-20-12**	Profile-1	275
Ivö-1-3-12	Profile-1	45	**Ivö-2-1-12**	Profile-2	02
Ivö-1-4-12	Profile-1	55	**Ivö-2-2-12**	Profile-2	11
Ivö-1-5-12	Profile-1	70	Ivö-2-3-12	Profile-2	32
Ivö-1-6-12	Profile-1	75	Ivö-2-4-12	Profile-2	42
Ivö-1-7-12	Profile-1	85	**Ivö-2-5-12**	Profile-2	43
Ivö-1-8-12	Profile-1	95	Ivö-2-6-12	Profile-2	44
Ivö-1-9-12	Profile-1	115	**Ivö-2-7-12**	Profile-2	46
Ivö-1-10-12	Profile-1	125	**Ivö-2-8-12**	Profile-2	47
Ivö-1-11-12	Profile-1	135	**Ivö-4-5-12**	Profile-4	65
Ivö-1-12-12	Profile-1	145	Ivö-6-2-12	Profile-6	35
Ivö-1-13-12	Profile-1	155	Ivö-6-9-12	Profile-6	825
Ivö-1-14-12	Profile-1	185	**Ivö-A-6-12**	Random	NA
Ivö-1-15-12	Profile-1	205	**Ivö-B-6-12**	Random	NA
Ivö-1-16-12	Profile-1	225	**Ivö-K1-12**	Saprolite top	NA
Ivö-1-17-12	Profile-1	235	**Ivö-Sand-12**	Random	NA

Quantitative analysis:

For the identification and semi-quantification of different minerals methods suggested by Thorez (1976), Moore and Reynolds (1997) and Bergaya (2006) have been used.

Bulk:

- *Clay minerals:*

  Illite: Peak identified at 10 Å.

  Kaolinite: Peak identified at 7.15 Å (001) and at 3.58 Å (002).

- *Quartz:*

  The reflection at 002 of 4.26 Å.

- *Feldspars:*

  K-feldspar: Peak at 3.24 Å.

  Plagioclase: Peak at 3.19 Å or 3.18 Å.

- *Carbonates:*

  Calcite: 3.03 Å peak was used.

  Dolomite: 2.89 Å peak was used.

  Siderite: 2.79 Å peak was used.

No pyrite (2.71 Å) is observed.

Clay separated samples:

- *Clay minerals:*

  Illite: No change on 10 Å peak after three treatments.

  Kaolinite: Distinguished same as in bulk analysis, peak vanished in diffractogram acquired from 550 ºC heated sample.

  Mixed-layered clay minerals: The area between 10-13 Å has been inspected closely for the presence of mixed-layered clay minerals

Figure 17 shows method of peak identification from diffractograms for both bulk and clay samples. Different colored lines in the figure represent different treatment that samples have undergone.

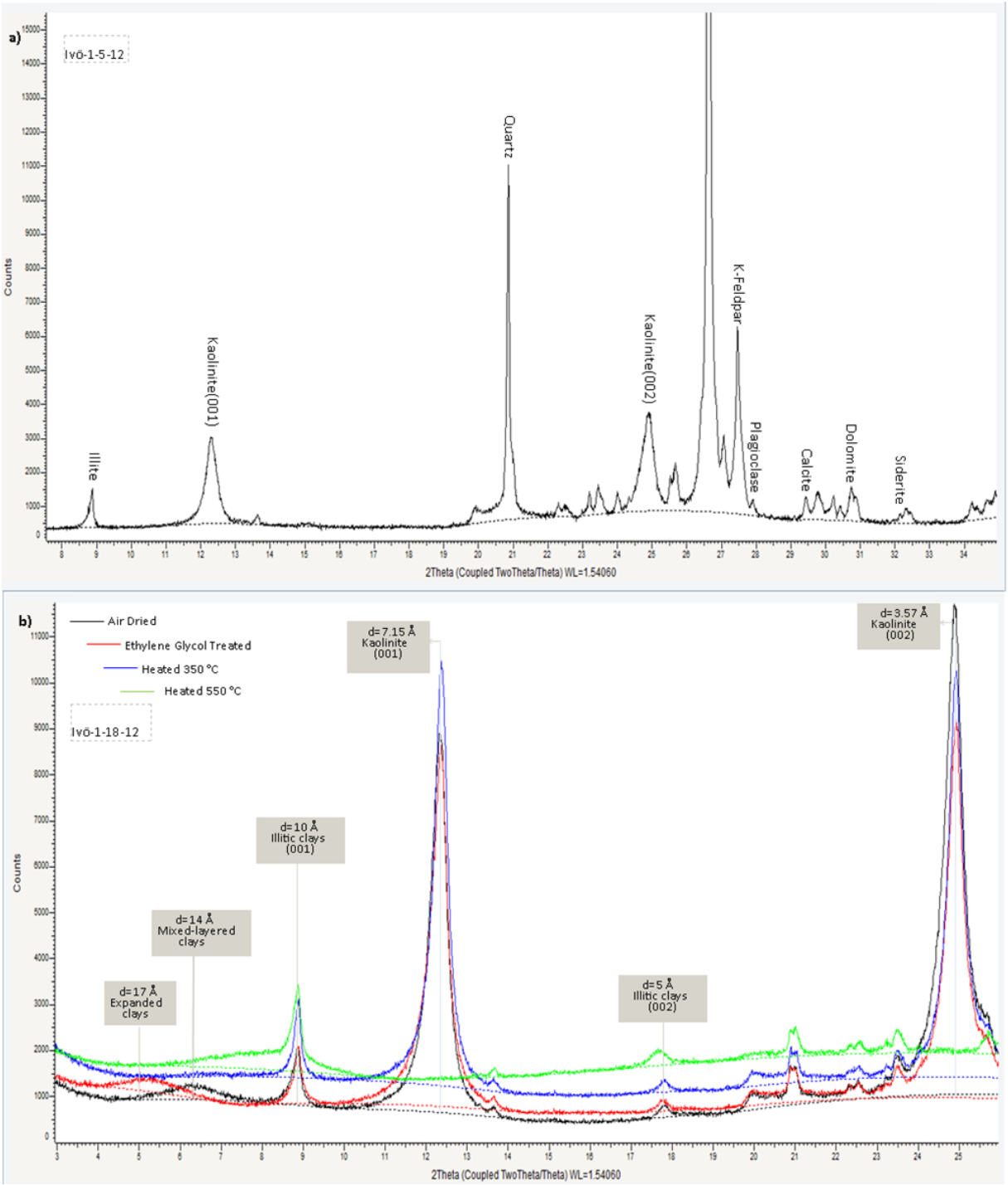

Figure 12: Diffractograms acquired from software (Diffrac.Eva), a) shows identification of clay minerals from diffractogram of sample Ivö-1-5-12 and b) shows identification of clay minerals from diffractogram of clay separated sample Ivö-1-18-12.

Semi quantitative analysis:

The XRD-analysis has been performed on Diffrac.Eva software. Both for the quantification of bulk analysis and clay minerals the observation of maximum intensities (counts) for respective mineral reflection has been carried out. Then percentages for every mineral have been calculated using simple mathematical relations as.

Percentage mineral = (mineral counts/sum of counts) ×100……eq. (13)

Various ratios using simple mathematical formulae have also been calculated including quartz/feldspar, plagioclase/feldspar, kaolinite/feldspar and percentage changes of plagioclase mineral in weathered profile compared to the fresh granite.

A scheme to observe the percentage change of a chemically unstable mineral in comparison with a more stable mineral across the weathering profile is devised by Nesbitt (1979). He used zircon as resistant mineral while quartz is used as resistant mineral by the writer. Quartz stability to chemical weathering is the result of its low solubility in aqueous solution and strong bonding between Si and O_2 molecules.

The mathematical formula can be written as:

Percentage change in feldspar= $\{(F^w/Q^w)/ (F^f/Q^f)-1\}*100$……eq. (14)

Where,

F= feldspar XRD%

Q= quartz XRD%

w= weathered sample

f= fresh granite

5. Results

5.1. Field description:

The landscape of the area is characterized by the presence of well-rounded boulders, weathered basement rocks, vegetation and transported sand sized material. In a total of five profiles, it was possible to distinguish relatively fresh corestones and their weathering rinds within the saprolite. However, corestones of variable length and width are seen in some of the profiles. A sketch map of the locality is illustrated in the Figure 13, location of six profiles, Cretaceous carbonate cover, detached boulders and reworked material of sand sized particles are displayed. The locality is intensely vegetated and weather was dry and sunny during sample collection from the weathering profiles. Different weathering grades (II to IV) are assigned to profiles depending on intensity of weathering experienced by each of it. Sampling of carbonate cover was done in the field along profile-6 (Appendix 6) to see the effect of carbonate sedimentation on weathering of crystalline basement. Detached boulders and bedrock clasts are scattered in thick carbonate cover. Sampling detail for all the profiles is given in Appendix-5.

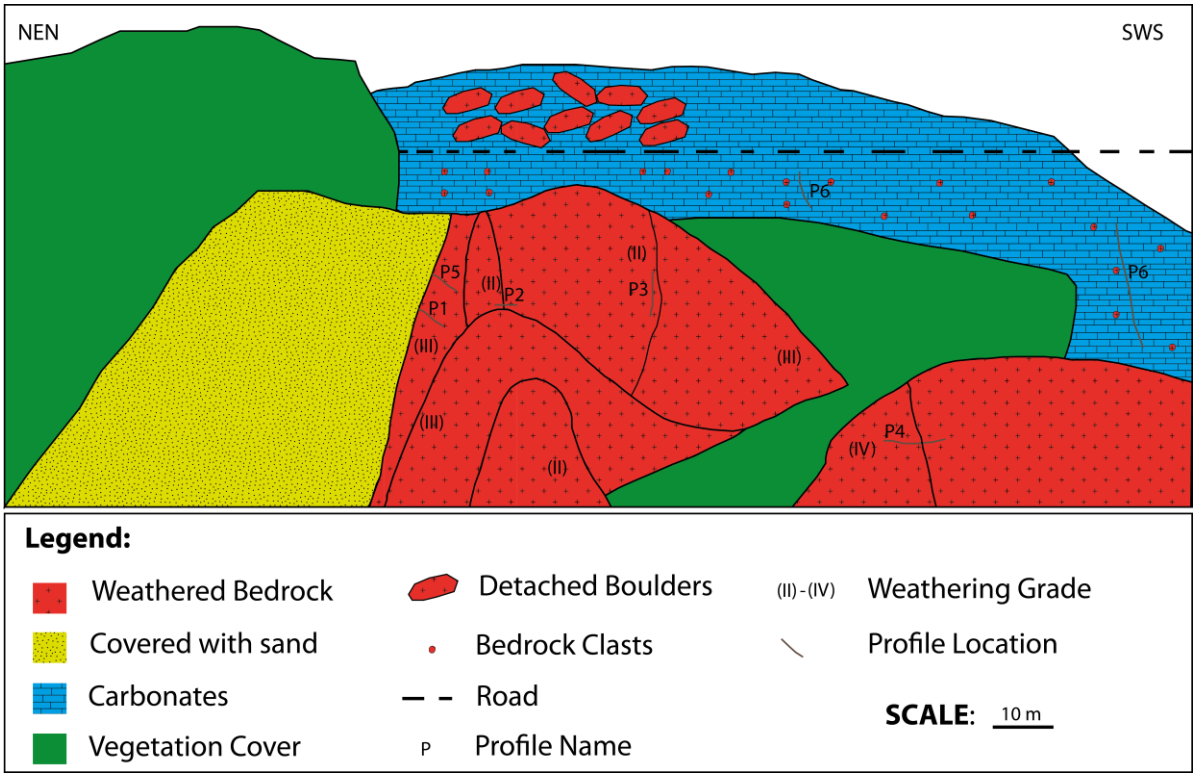

Figure 13: Sketch map of locality. Profile location, weathered bedrock, weathering grade, carbonate cover and detached boulders are visible.

Figure 14 shows satellite image of the area and two photographs of the locality taken side by side, this was done to get the maximum resolution. The transition between the reworked material (sand sized) and the weathered basement can be clearly seen on left photograph. The area above the outcrop is populated with vegetation in contrast with the area in front of it. Location of five weathering profiles is indicated with different colors.

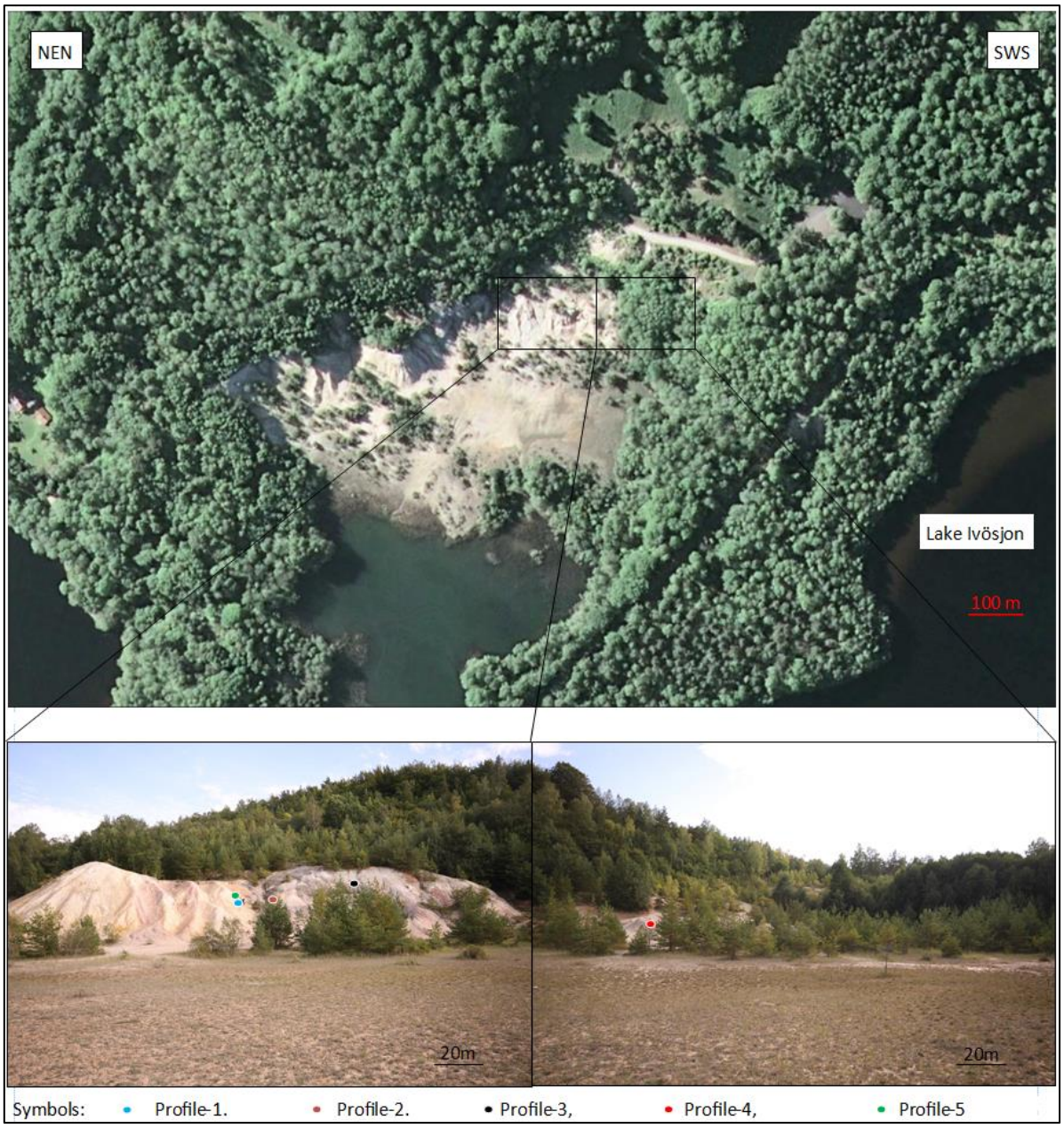

Figure 14: Satellite image of the locality and two photographs of the outcrop taken adjacent to each other, describing profile location at the locality. Location of the profiles is also marked with colored dots (courtesy Lars Riber).

The relief between the highest point of Ivö Klack and Lake Ivösjön is 177m (Lidmar-Bergström, 1983). The study area is characterized by an annual temperature between -1

(winter) and 16.5 °C (summer) and mean precipitation of 850 mm (Yr, 2013). The present study describes the weathering pattern along various profiles (1-5) of the weathered crystalline basement at Ivö Klack (Figure 13 and 14). The weathered basement under discussion is the Vånga granite (mesoproterozoic). Vångaberget, Oppmannaberget and hills of Ivö Klack are wholly dominated by the Vånga granite (Lundegårdh, 1978). It is a medium to coarse grained foliated and afterwards migmatized granite (Lundegårdh, 1978). The Vånga granite has a quite uniform mineral and chemical composition with main mineral constituents potash feldspar, quartz and plagioclase (Åberg et al., 1985). Accessory minerals (less than 5%) include biotite, muscovite, fluorite, chlorite, epidote, allanite, zircon, topaz, sphene and opaque minerals (Åberg et al., 1985).

Figure 15 was taken along a road cut in which carbonates can be seen encrusted on the boulders transported during Pleistocene Ice Age. The boulders in Figure 15 are well-rounded,

Figure 15: Carbonates encrusted on the granite boulders. Root penetration through softer parts (carbonates) is visible (courtesy Lars Riber).

interpreted as till deposit forming the bottom of kaolinized granite and had moved a short distance before deposition (Lidmar-Bergström, 1983). The tree roots have penetrated through

the softer parts of the carbonates, showing an active example of biological weathering. Lidmar-Bergström et al. (1997) termed this stratum as Cretaceous conglomerate consisting of boulders of unweathered granite and matrix of calcarenite. These boulders were accumulated after the erosion of saprolite but before the Late Cretaceous transgression (Lidmar-Bergström et al., 1997). According to Lidmar-Bergström (1983) 50 km^3 of altered Precambrian crystalline rocks were eroded and transported to Kristianstad basin during Devonian to pre-Cretaceous times, the material includes quartz sand, boulders and detrital kaolin minerals. In 1884 it started as Late Cretaceous limestone quarry Ivö Klack, and residual kaolin was lying underneath it. Further up-slope Precambrian bedrock was underlying the Late Cretaceous limestone and quarrying of limestone there uncovered Precambrian surface (Lidmar-Bergström, 1983).

Figure 16 is a photograph taken at the locality, showing the water seepage (dark gray) from a fracture in the saprolite (light gray color above fracture).

Figure 16: Water seeping from a fracture in the saprolite (dark color from centre to bottom).

The photo was taken close to profile-4. The fracturing in granites is rough and may occur due to exfoliation (Ollier and Pain, 1996), also termed as sheeting. There are different theories

describing the development of exfoliation in rocks. According to Bahat et al. 1999, the geomorphologist Grove Karl Gilbert in 1904 proposed that the erosion of overlying rocks and exposure of previously compressed basement rocks to the surface results in radial expansion that creates tensile stress and fracture the rock in layers parallel to the surface. Bahat et al. (1999) has attributed various causes responsible for exfoliation including insulation, earth surface variation in temperature, varied weathering rate, cooling and frost and vegetation. This illustrates that fracturing is the onset of chemical weathering. It is due to the joint and fracture system that forms weathering rinds that ultimately converts to the granitic saprolites (Braga et al., 2002).

5.1.1. Weathering profiles:

Out of a total five weathering profiles, two weathering profiles; profile-1 and profile-2 (Figure 17) are chosen to give a representative overview on the weathering processes active at the locality. Main intention was to start analyzing these two profiles and later add up other profiles if needed.

Figure 17: Location of the two profiles, profile-1 (red line) and profile-2 (blue line). Transition between transported material (left) and weathered bedrock (right) (courtesy Lars Riber).

The red line in Figure 17 represents profile-1 location and blue line shows the position of profile-2 at the locality. Boulders that have been eroded from the top of the saprolite are visible in the photograph.

5.1.1.1. Profile-1:

Figure 18 depicts the sketch log compared with a photograph of profile-1, illustrating the position of corestones in saprolite, position of samples collected and different fracture that are visible.

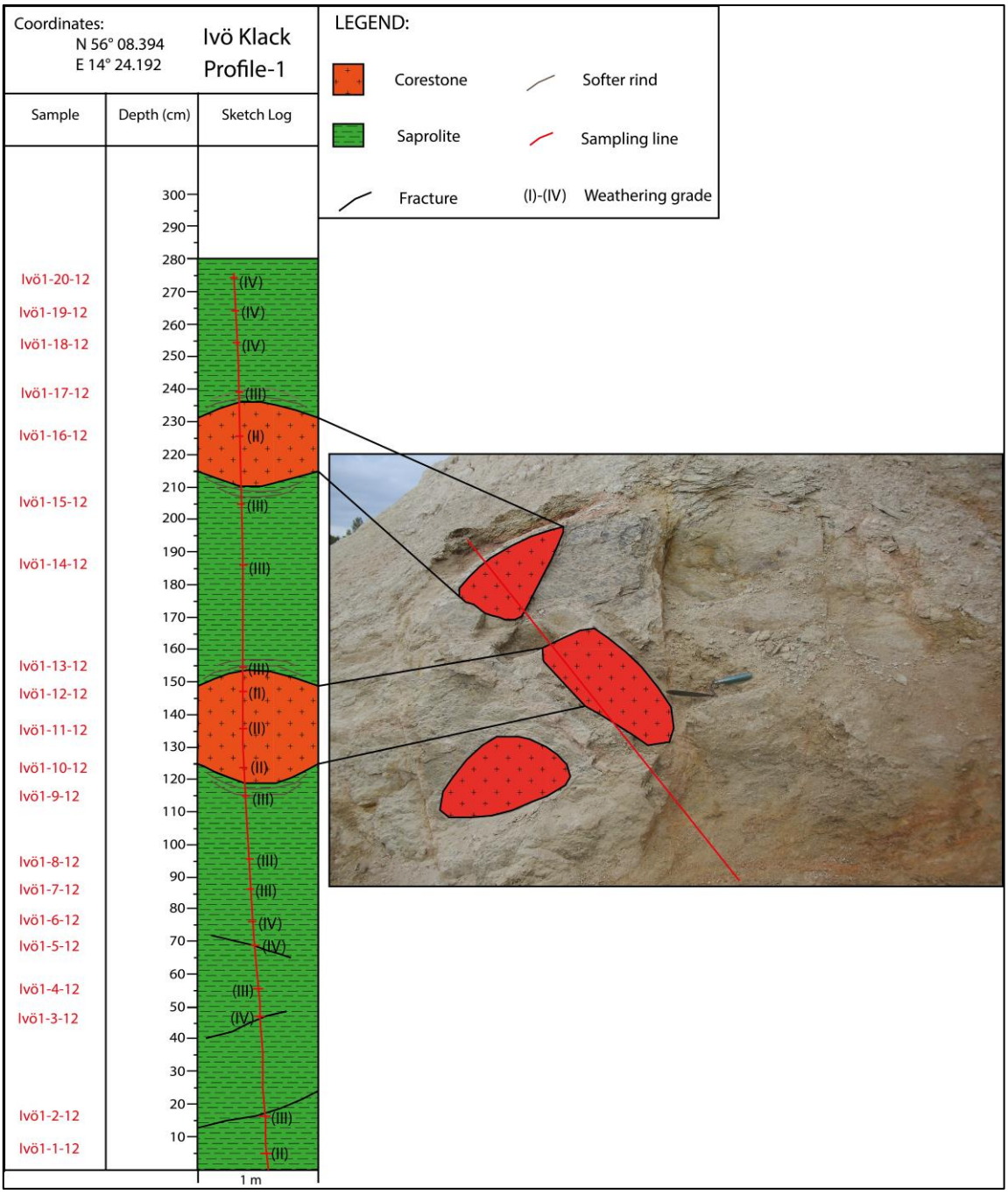

Figure 18: Sketch log along with a photograph from base to top of profile-1. Sample names along with weathering grade and boulders are represented. Red line in both sketch log and photograph show sampling line. Three corestones observed two within the profile-1 and one to the lower left. Weathering grade is shown in roman numbers for each sample of the weathering profile.

This weathering profile was covered with reworked material which was cleared before sampling. The red line in both, sketch log and photograph represent sampling line (along which samples were collected).

Corestones have fresher look then surrounding saprolite. Weathering grade (II-IV) is given to different parts of saprolite along the weathering profile based on intensity of weathering, color, wetness and adhesion of solid rock. Intense weathering of saprolite is observed at the uppermost part. Total length of profile-1 is 2.8 (along x-axis of sketch log) m consisting of fractures of varying orientation. Y-axis of sketch log represent 1 m width of weathering profile-1.Weathering of saprolite is more evident along the fractures, and edges are more weathered than interior of the corestones. The increase in white material (kaolinite) is observed in samples of more weathered saprolite away from corestones in the field.

5.1.1.2. Profile-2:

Figure 19 represents sketch log of profile-2 devoid of any corestone. The sample location along the sampling line (red line) is shown with different weathering grade. Total length of this profile is 50 cm, increase in weathering intensity upwards is observed. Profile-2 is situated 5 m east of profile-1.

5.1.1.3. Profile-3:

Figure 20 depicts the position of four samples collected from weathering profile-3. Three corestones are observed in this profile with various fractures with different orientations.This profile was not logged from bottom to top and Figure 20 represent a sketch. Profile-3 is located approximately 25 m east of profile-1.

5.1.1.4. Profile-4:

Figure 21 shows sketch log and a photograph (taken after sampling) of weathering profile-4 which is intensely weathered. A corestone is observed close to profile-4. The yellow measuring tape in the photograph and red line in sketch log represent the line along which samples were collected. A fracture filled with white mass (kaolinite) is visible in the photograph. Profile-4 is located approximately 170 m to the east of profile-1. The fracture crosses the sampling line (represented with red line) at Ivö-4-5-12. Weathering grade is also represented for each weathered sample in profile with roman numbers.

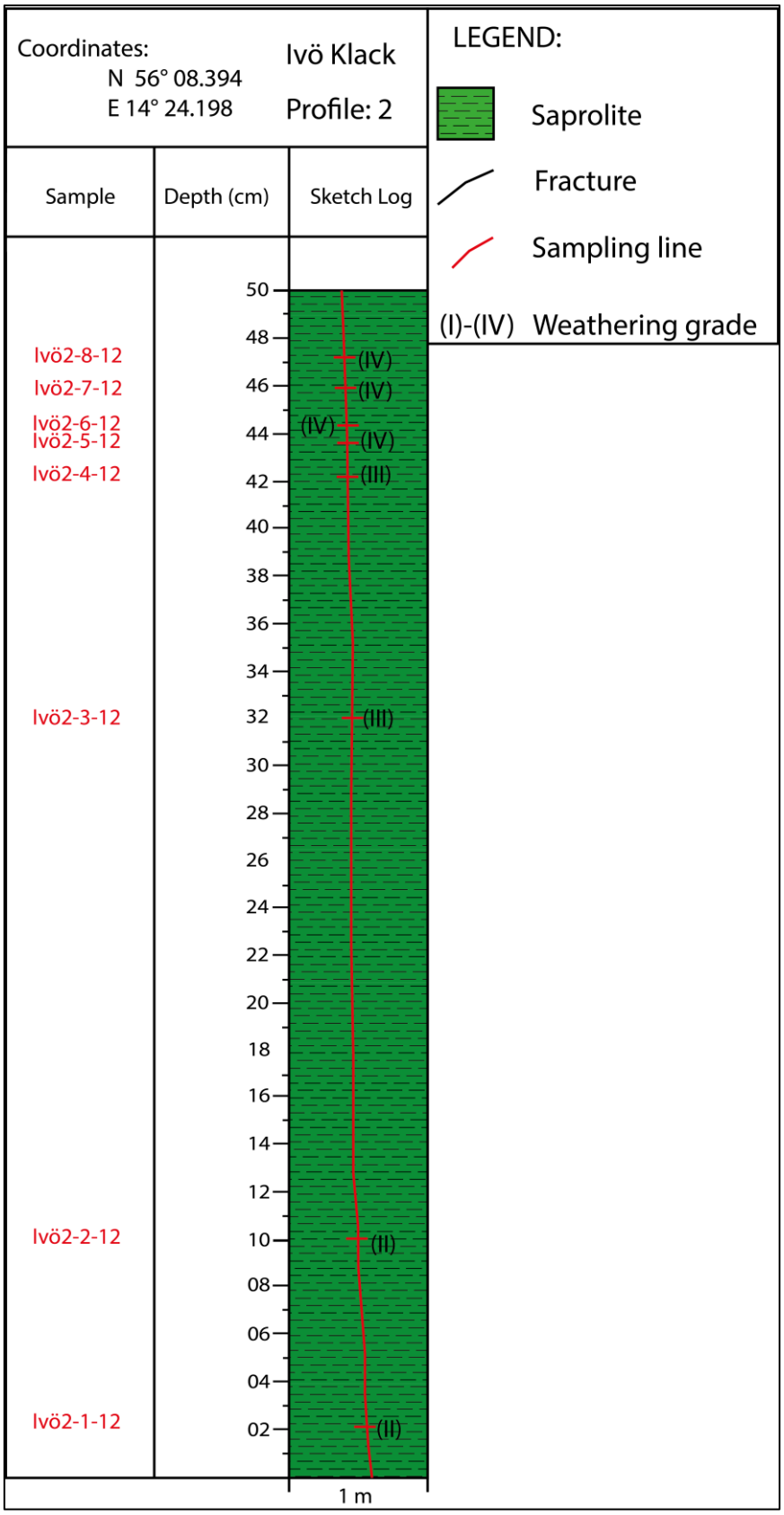

Figure 19: Sketch log of profile-2. Red line represents sampling line along which samples are collected. No corestone was observed in the weathering profile. Weathering grade is represented by roman numbers for every sample in the weathering profile.

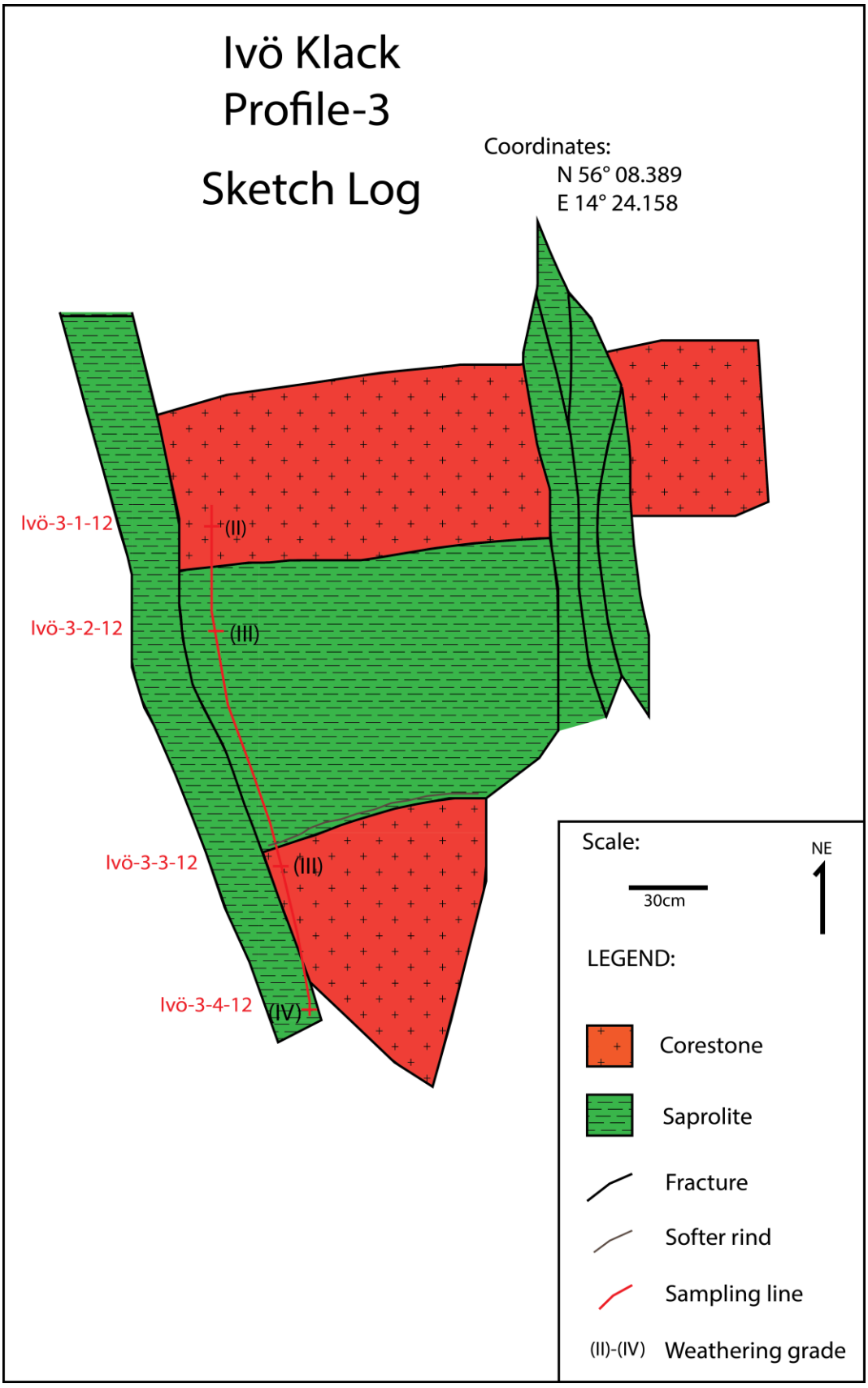

Figure 20: Sketch log of profile-3. Representing sampling line, corestones and fractures. The profile was not logged from bottom to top. Weathering grade for each sample of the weathering profile is shown in roman numbers.

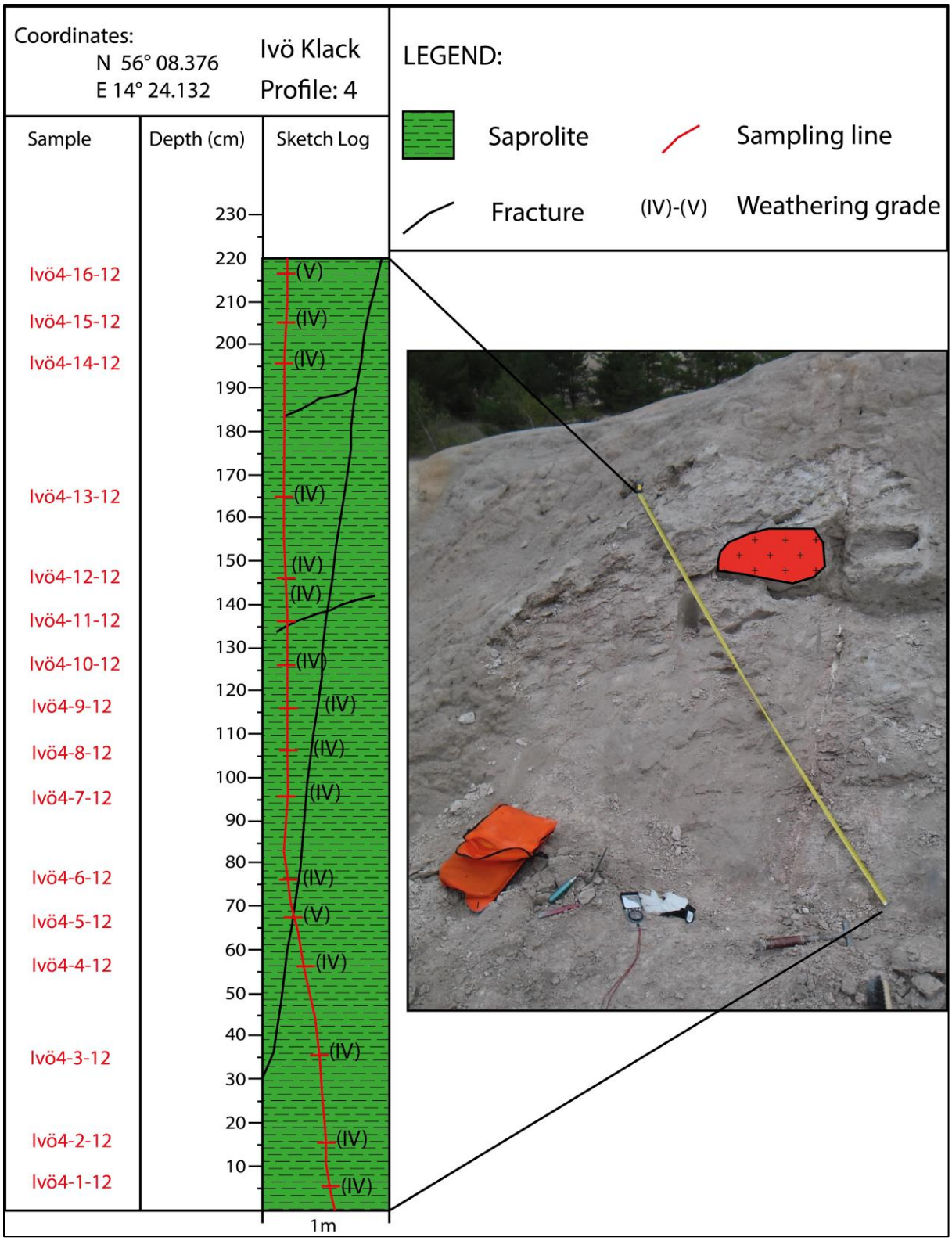

Figure 21: Sketch log of profile-4. Red line represents sampling line, one corestone visible to the right of weathering profile. Fracture filled with kaolinite is visible in the photograph intersecting profile-4 at sample Ivö-4-5-12. Weathering grade for every sample in the weathering profile is written in roman number.

5.1.1.5. Profile-5:

The sketch log of profile-5 which is located 2 m apart from profile-1 is displayed in Figure 22. Unlogged portion of the profile represents reworked material. One corestone is observed in this profile. Weathering intensity increases upwards the profile. The weathering profile is 2.9 m in length along which samples were collected.

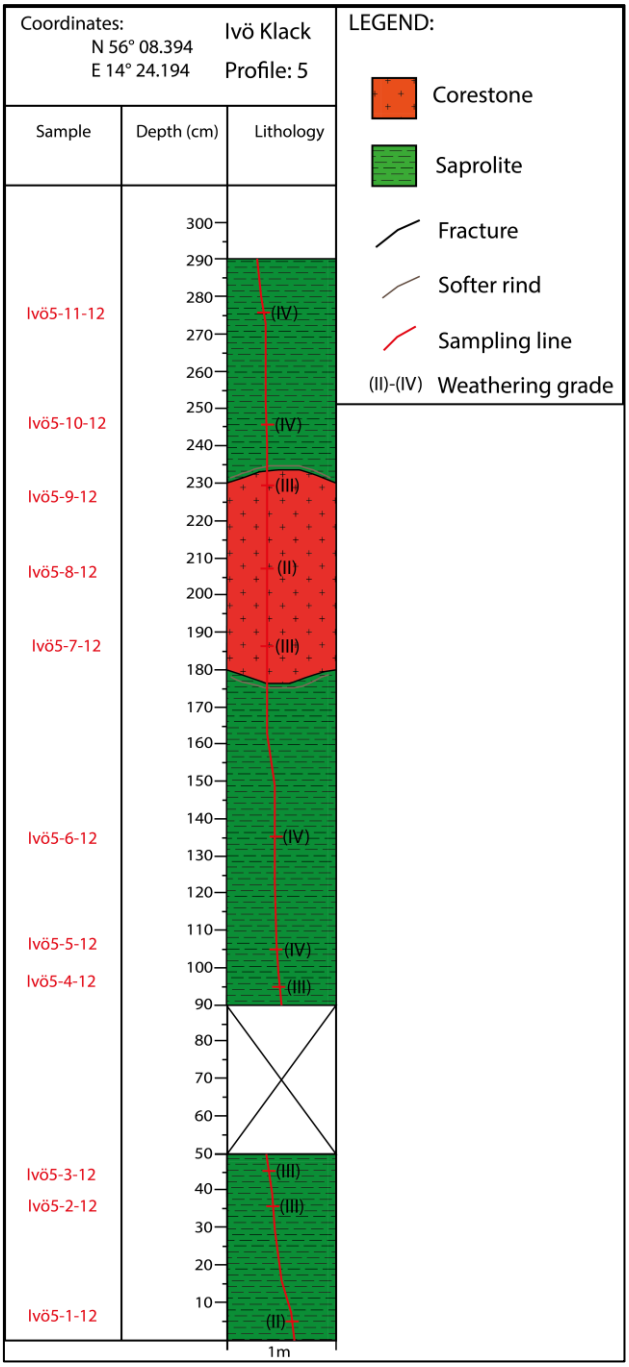

Figure 22: Sketch log of profile-5. Red line represent sampling line, area with a cross in sketch log represents transported material. One corestone is observed in the profile, and weathering grade for every sample is shown in roman numbers.

5.2. Thin Sections:

The detailed results from thin section description of selected samples and mineral point counting are given in Appendix 1 and Appendix 2 respectively.

5.2.1. Fresh granite:

Figure 23 shows a photograph of pink/red colored fresh granite (the Vånga Granite).

Figure 23: Fresh granite with pink/red color (courtesy Lars Riber).

One thin section from fresh granite has been studied. The dominant minerals observed is feldspars, K-feldspar is abundant and has larger crystals than plagioclase. Figure 24 illustrates the fresh granite composition on QAP diagram; at the boundary between monzogranite and syenogranite. Equaling three mineral percentages (from point counting) to 100%, each mineral (quartz, plagioclase, K-feldspar) percentage was calculated and plotted into Streckeisen diagram. Calculated values are: quartz 38%, plagioclase 23% and K-feldspar 39%.

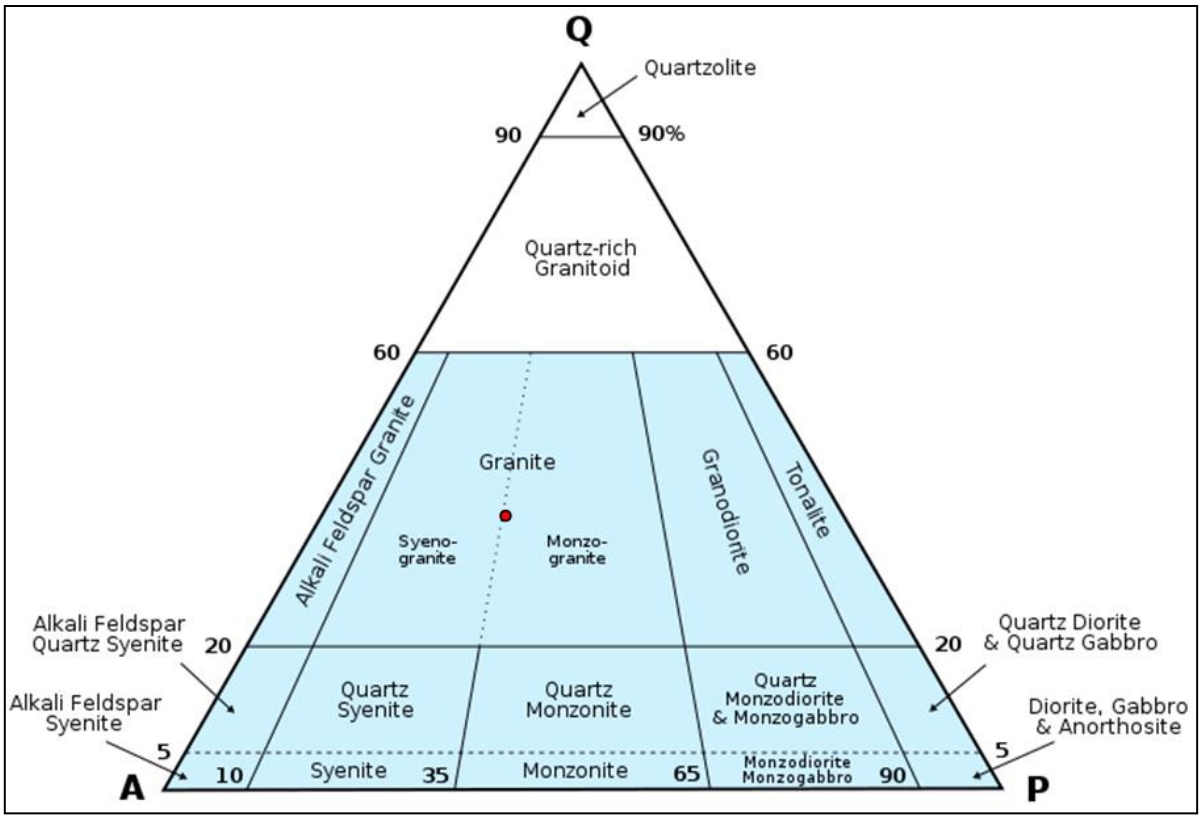

Figure 24: QAP diagram showing granite composition (red dot) based on thin section results (modified from Streckeisen, 1979). Granite composition lies at the boundary between monzogranite and syenogranite.

Most feldspar crystals are visually unaltered but sericite needles can be seen in the plagioclase crystals. These needles have the composition of potassic-muscovite (Figure 25 & 26), and are developed in unevenly manner.

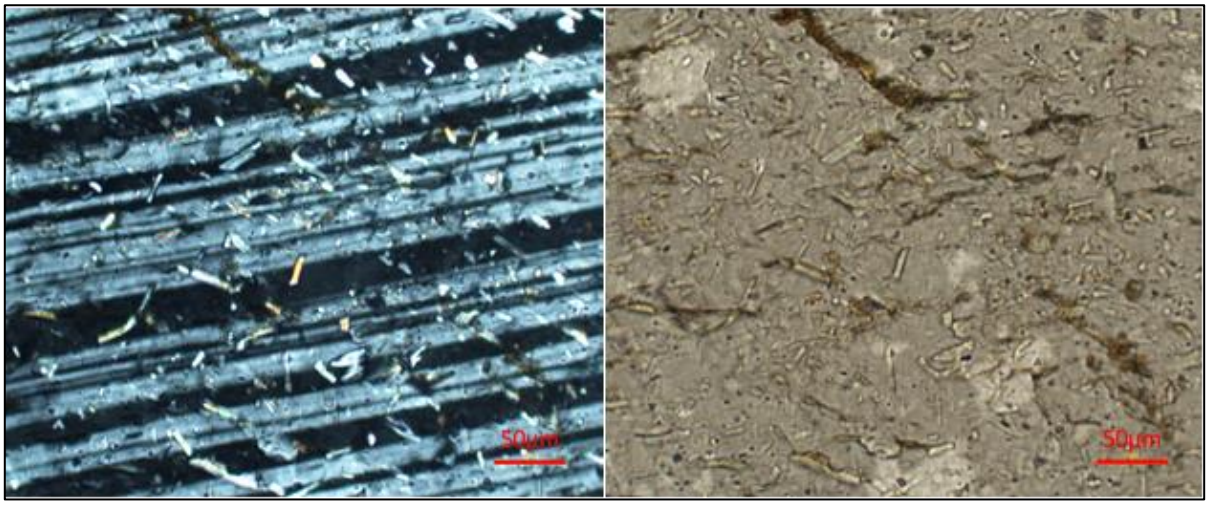

Figure 25: Sericitization (small birefringent needles) of plagioclase visible under microscope. Left image under cross polarized light right image under plane polarized light.

A peculiar feature of these needles is that they are mostly found in center of the plagioclase grain rather than at grain margins. The needles show birefringence when viewed under microscope in cross polarized light.

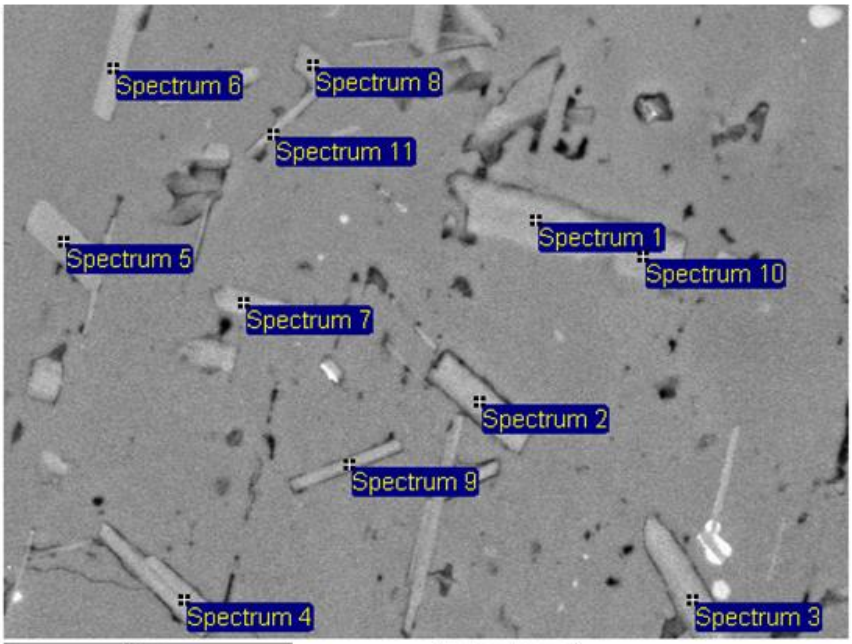

Spectrum No.	In stats.	O	Al	Si	K	Fe	Total
Spectrum 1	Yes	29.69	21.04	31.74	13.27	4.27	100.00
Spectrum 2	Yes	28.22	19.30	33.29	11.75	7.45	100.00
Spectrum 3	Yes	27.45	20.59	32.17	13.74	6.05	100.00
Spectrum 4	Yes	27.41	21.39	32.83	11.97	6.40	100.00
Spectrum 5	Yes	26.39	21.24	33.99	13.07	5.31	100.00
Spectrum 6	Yes	29.59	18.03	32.57	12.70	7.12	100.00
Spectrum 7	Yes	30.52	19.35	37.34	10.53	2.25	100.00
Spectrum 8	Yes	28.59	21.81	32.28	13.35	3.96	100.00
Spectrum 9	Yes	29.83	19.08	39.26	8.78	3.05	100.00
Spectrum 10	Yes	27.99	21.10	30.13	13.22	7.56	100.00
Spectrum 11	Yes	32.62	16.74	45.33	2.79	2.52	100.00
Mean		28.94	19.97	34.63	11.38	5.08	100.00
Max.		32.62	21.81	45.33	13.74	7.56	
Min.		26.39	16.74	30.13	2.79	2.25	

Figure 26: Composition of sericite determined under SEM.

Figure 27 shows the image acquired from back scattered electron analysis under scanning electron microscopy, the lower part of the figure shows the weight percentage of the various elements in sericite. High percentage of potassium by weight makes it potassium-muscovite.

In thin section the K-feldspar (microcline with tartan twinning and perthite) looks relatively fresh, containing very few sericite grains. The albite twining is visible in plagioclase while K-feldspar can be distinguished by its tartan twining. The biggest feldspar crystals, around 3.5mm, have perthitic texture.

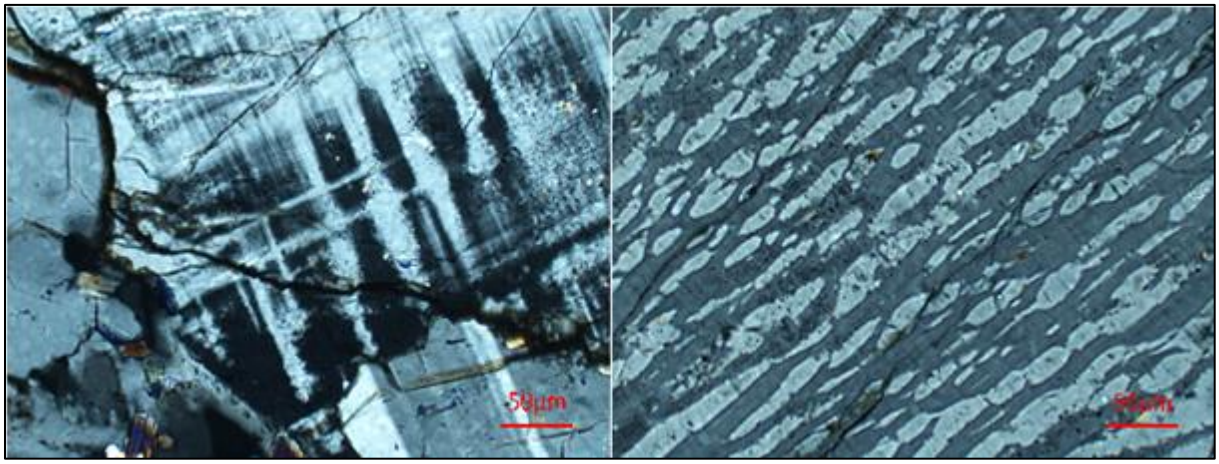

Figure 27: Left) Tartan twinning in microcline, Right) Perthitic texture of feldspar.

Both micas are seen with biotite being the most abundant mica mineral. The quartz grains, which show undulose extinction, are mostly monocrystalline but polycrystalline quartz is also present. Some heavy mineral inclusions can be seen on quartz crystals. All the mineral grains look fresh devoid of any dissolution laminae and porosity.

The plagioclase composition of the fresh granite is determined using Michel-Lévy technique from Nesse (2009) described in chapter-4 (Figure 28). Table-4 shows the extinction angles for six different plagioclase grains with albite twins. By repeating the process for around half dozen plagioclase grains with albite twins the largest average extinction angle measured is 19.5º. When plotted on Figure 29, approximately 35% anorthite is determined by using Michel-Lévy technique.

Table 4: Extinction angle measured on six different plagioclase grains with albite twins.

Grain number	Angle measured during clockwise rotation	Angle measured during counter-clockwise rotation	Mean
01.	13º	13º	13º
02.	12º	13º	12.5º
03.	11º	13º	12º
04.	21º	18º	19.5º
05.	16º	19º	17.5º
06.	16º	20º	18º

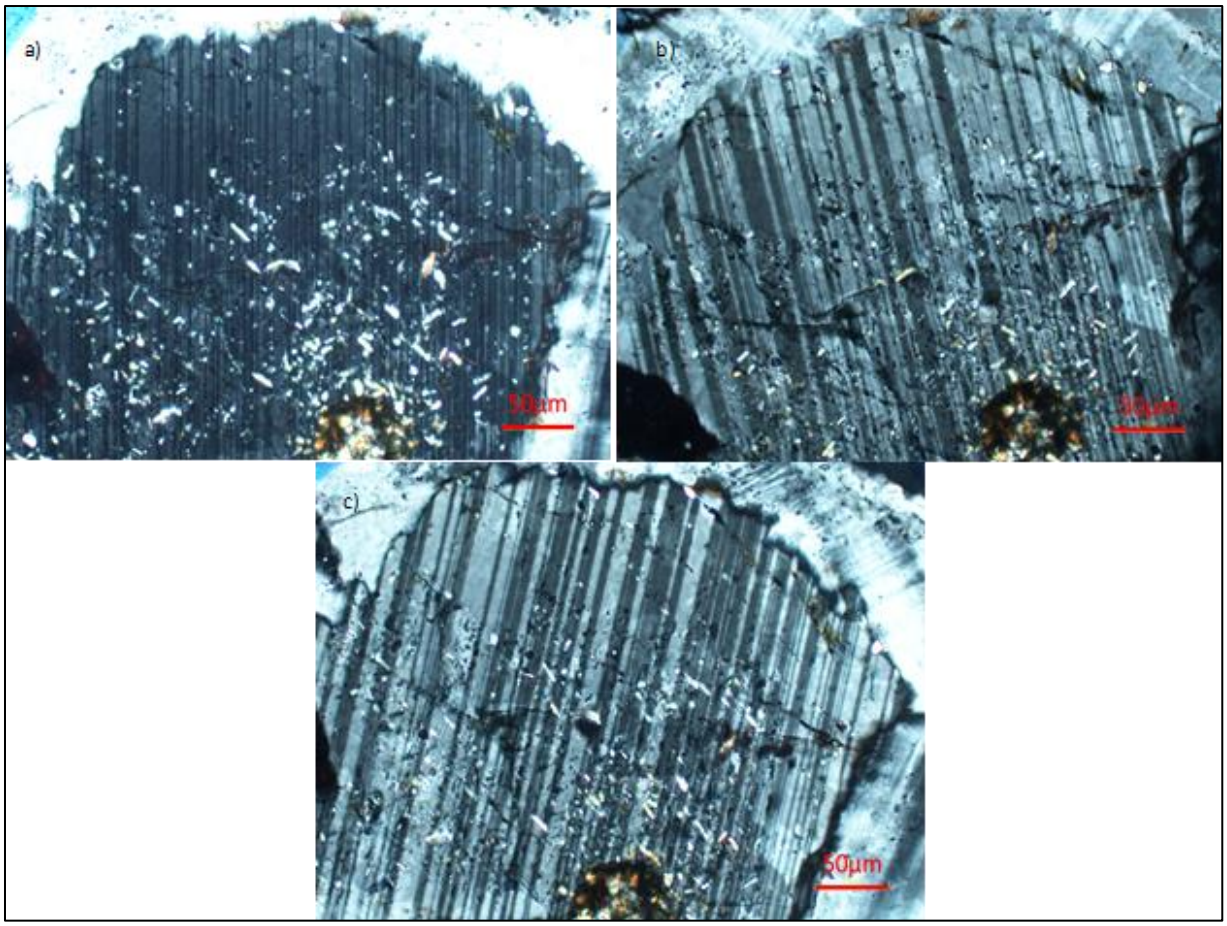

Figure 28: a) (010) composition plane of albite twins, b) counter-clockwise rotation of grain and c) clockwise rotation of grain.

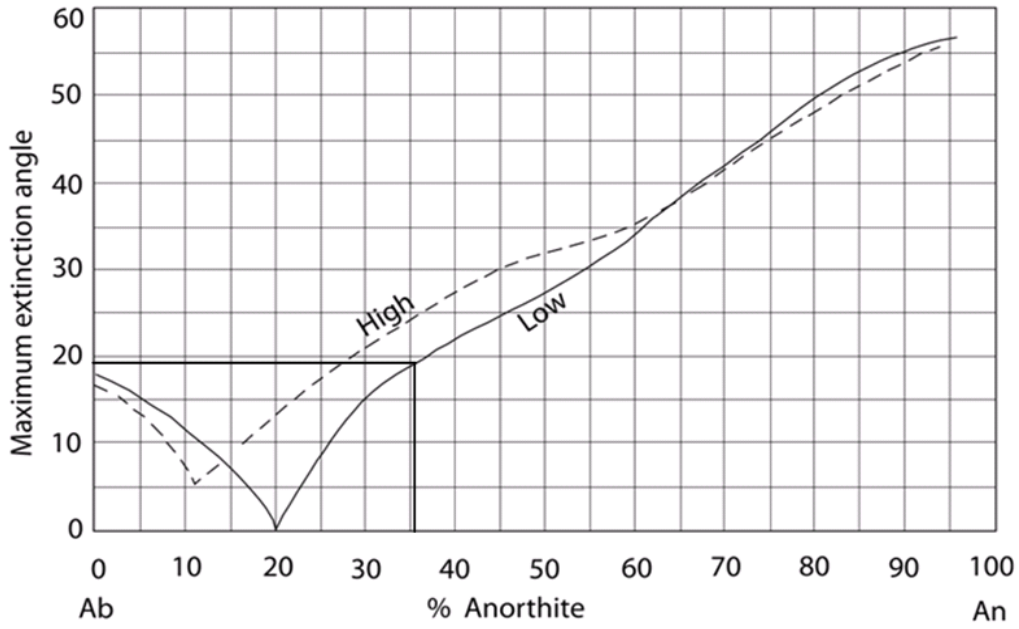

Figure 29: Maximum extinction angle of albite twin for plutonic (low) and volcanic (high) plagioclase (modified from Nesse, 2009).

Two grains of plagioclase with albite twins were studied under electron microscope to determine the anorthite percentage in these grains (Figure 30). Approximately 17% anorthite is calculated from the weight percentage of the elements.

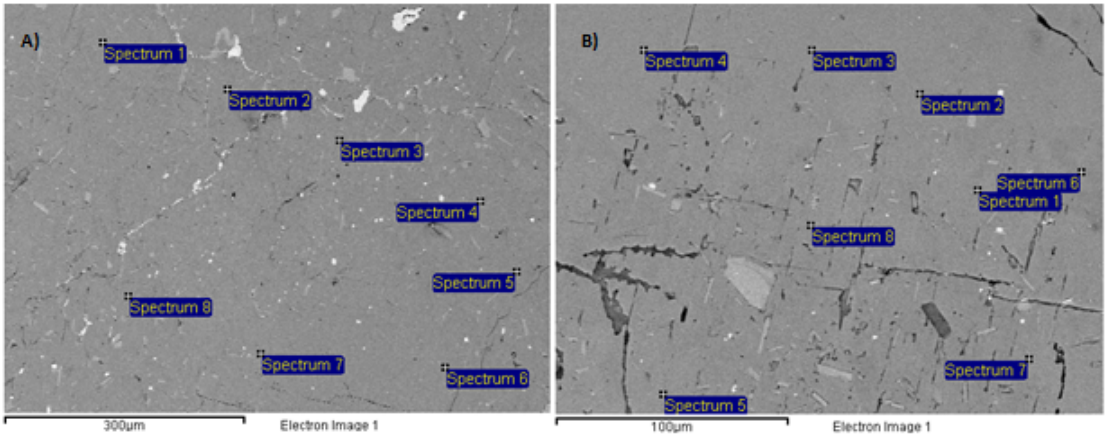

Spectrum **A**	In stats.	O	Na	Al	Si	Ca	Total
Spectrum 1	Yes	30.25	6.42	13.50	48.51	1.33	100.00
Spectrum 2	Yes	28.68	6.36	13.32	49.85	1.78	100.00
Spectrum 3	Yes	30.23	7.31	12.77	48.22	1.47	100.00
Spectrum 4	Yes	31.06	7.00	13.27	46.54	2.13	100.00
Spectrum 5	Yes	31.15	7.31	13.29	47.48	0.76	100.00
Spectrum 6	Yes	31.07	7.23	14.05	46.84	0.80	100.00
Spectrum 7	Yes	31.14	6.98	12.86	47.47	1.56	100.00
Spectrum 8	Yes	29.91	8.05	13.35	47.97	0.73	100.00
Mean		30.44	7.08	13.30	47.86	1.32	100.00
Max.		31.15	8.05	14.05	49.85	2.13	
Min.		28.68	6.36	12.77	46.54	0.73	

Spectrum **B**	In stats.	O	Na	Al	Si	Ca	Total
Spectrum 1	Yes	31.10	6.94	13.95	46.45	1.56	100.00
Spectrum 2	Yes	31.43	6.70	13.03	46.70	2.14	100.00
Spectrum 3	Yes	30.11	7.46	12.70	48.33	1.40	100.00
Spectrum 4	Yes	31.50	6.53	14.17	46.04	1.76	100.00
Spectrum 5	Yes	30.31	7.34	14.23	46.19	1.93	100.00
Spectrum 6	Yes	30.50	6.85	13.75	48.21	0.70	100.00
Spectrum 7	Yes	31.49	7.41	12.65	48.09	0.36	100.00
Spectrum 8	Yes	28.28	7.34	13.73	48.36	2.29	100.00
Mean		30.59	7.07	13.53	47.29	1.52	100.00
Max.		31.50	7.46	14.23	48.36	2.29	
Min.		28.28	6.53	12.65	46.04	0.36	

Figure 30: Anorthite percentage calculated from scanning electron microscope analysis.

5.2.2. Profile-1:

Figure 18 illustrates sample location and location of two corestones in profile-1 (lower and upper corestone). Starting with the thin section made from the sample taken at the base of the

profile-1 (Ivö-1-1-12), effects of alteration of the primary minerals are visible especially in the plagioclase crystals. The clays can be identified, partially replacing plagioclase grains in the sample Ivö-1-1-12. A general trend of increase in the porosity and the quartz mineral is observed from samples Ivö-1-1-12 to Ivö-1-7-12 (Appendix 1). Figure 31 shows five thin section photographs, illustrating different degree of weathering (I-V) based on exsolution of perthite laminae and dissolution of feldspar. All the photographs are taken under microscope in plane polarized light.

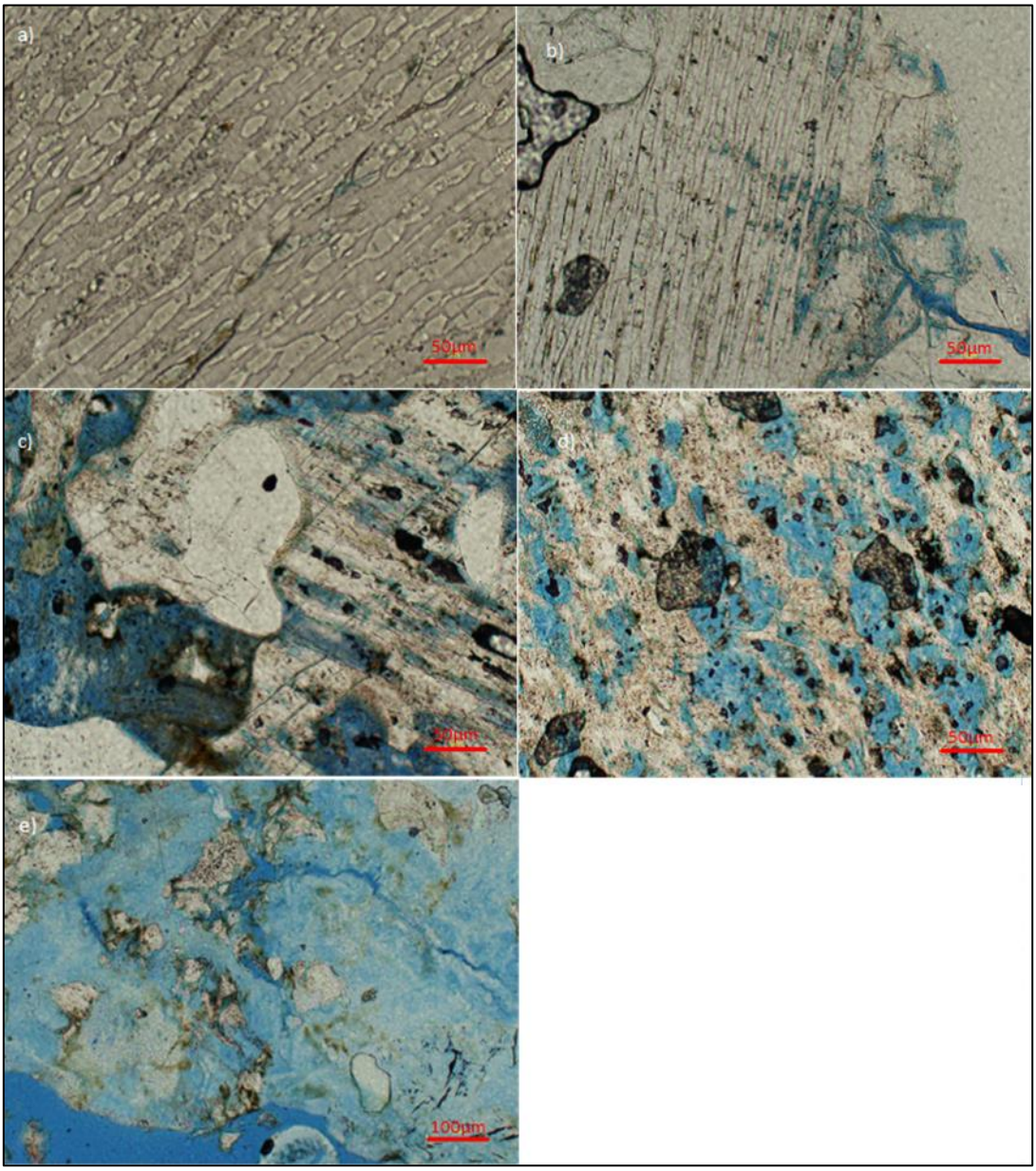

Figure 31: Dissolution laminae seen (a, b, c and d) in plane polarized light under microscope. (a) Ivö-Extra 1-12, all laminae intact (I). (b) Ivö-1-1-12, dissolution is observed along a fracture (II). (c) Ivö-1-2-12, less than half of perthitic texture gone (III). (d) Ivö-1-3-12, more than half of laminae gone due to dissolution (IV) and (e) Ivö-4-5-12, all primary minerals transformed to secondary minerals (V).

Moving from (a) to (e), the increasing trend of weathering is evident. In (a) perthite grain is fresh and devoid of any dissolution, (b) shows a fracture and dissolution of feldspar along it. When viewed in plane polarized light (c) depicts half of the laminae of perthite are gone because of dissolution. In (d), degree of weathering intensifies as more than 50% of perthite laminae are dissolved. Last photograph is taken from a sample in profile-4 along a fracture (to illustrate all weathering grades from I to V), in which only illitic clays are visible and original mineral grain is absent.

From point counting (Appendix 2) biotite content appears to be high than muscovite, and the micas are randomly oriented. The porosity is interconnected due to fracturing. Increased amount of the micas observed in sample-2 and micas are present in varying amount in the thin sections of profile-1. Most of the dissolution is seen in fractures and dissolution laminae are identified especially in feldspars of perthitic texture. The clays are replacing primary minerals. The heavy mineral inclusions are present on the quartz grains.

One of the main features of increasing trend of the dissolution is the scarcity of plagioclase grains. In contrast to the above trend, the porosity and dissolution laminae look to decrease from the sample-8 to sample-12 (from base of lower corestone upwards into its interior as seen in Figure 18). All the mineral grains are less altered in sample-11 and sample-12 with almost zero porosity. Fewer amounts of the visible dissolution lamellae are evident in these two samples. These two thin sections along-with thin sections of sample-15 & sample-16 (upper corestone) resemble the thin section of the fresh granite. In between these, sample-13 and sample-14 show dissolved laminae and porosity.

From the sample-17 to sample-20 there is a marked increase in porosity, decrease in average grain size and grains are suspended in the clay matrix. The grains are largely in-equigranular across the profile and the visible grain size varies between 0.1-4mm. Another main feature in these thin sections is the large size of perthitic feldspar and quartz grains. The quartz grains, mostly monocrystalline, with the undulose extinction are present in all the thin sections. In thin sections containing more illitic clays and dissolved lamellae the average grain size of quartz is small as compared to the thin sections that are less altered.

5.2.3. Profile-2:

Contrary to the mineralogical description obtained in the profile-1, the general trend of increasing porosity and increasing dissolution laminae across the profile-2 is quite smooth

(Appendix 1 and 2). Figure 19 represent sketch log depicting sample location of eight samples acquired in the field along profile-2. Figure 32 & 33 shows two extremes of weathering intensity in relatively fresh sample (left, Ivö-2-1-12) and a more weathered sample (right, Ivö-2-8-12). The process of weathering has just started in fresh sample along the fractures whereas in more weathered sample close to surface almost all the primary minerals have been converted to the respective clays. Increase in porosity is visible from comparison of two samples studied in plane polarized light under microscope. In cross polarized light tartan twinning, a peculiarity of microcline can be observed.

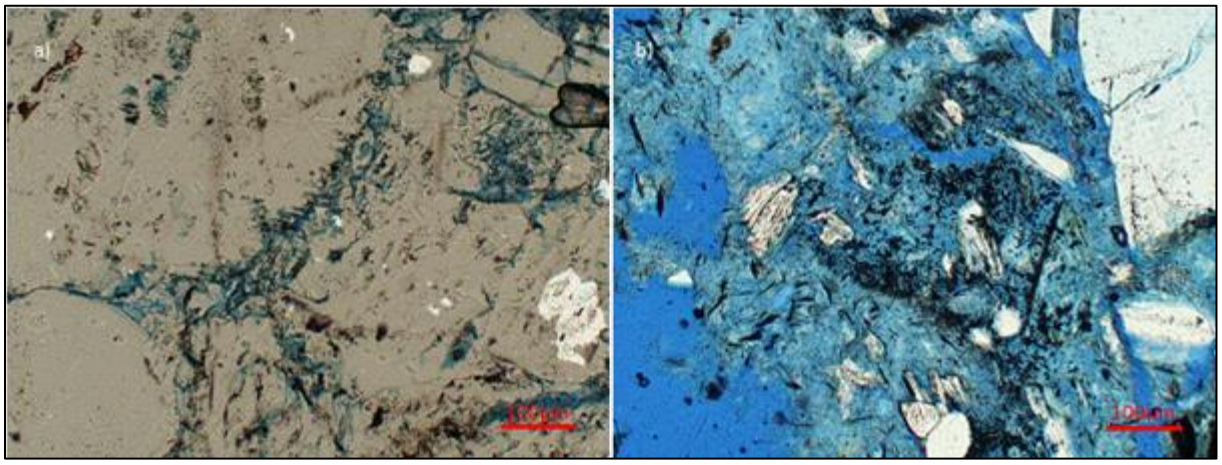

Figure 32: Thin section photographs taken in plane polarized light under microscope. (a) Ivö-2-1-12, dissolution of primary grain along micro-fractures. (b) Ivö-2-8-12, total dissolution of primary minerals and increase in porosity is visible.

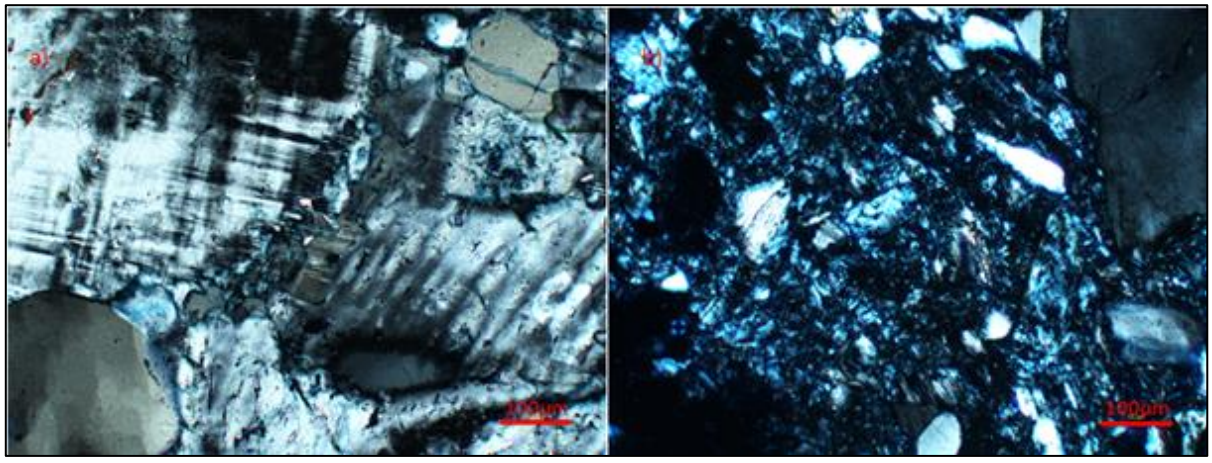

Figure 33: Thin section photographs taken in cross polarized light under microscope. (a) Ivö-2-1-12, tartan twining in microcline. (b) Ivö-2-8-12, increased porosity due to dissolution of primary minerals.

The biotite is dominant of the two micas, and perthite with the exsolved lamellae is the dominant feldspar. Sericitization of the plagioclase is observed in sample-2. Alteration of

perthite grains is intense in sample-3 where half of the laminae are dissolved and illitic clays have replaced them. Dissolution is increased in sample-4 with scattered biotite grains still present. The average grain size is decreasing in thin sections of samples from 4 to 8, and grains are in-equigranular across the whole profile. The quartz is the dominant grain in more altered samples, and clays can be seen where feldspar have been dissolved.

5.2.4. Random samples:

One sample from profile-4 along the fracture filled with kaolinite was also studied (Figure 21). The sample under consideration is taken from the fracture filled with kaolinite. Few highly altered feldspars are distinguished with a good representation of dissolution of the primary mineral is observed (Figure 31e). Some mica (muscovite) grains are identified and the quartz grain is the dominant grain. The primary mineral grains are dissolved with clays replacing it but prints of the primary mineral grains still visible. Similarly feldspars seem to be replaced by illitic clays in the thin section made from the sample taken of kaolinite cover. No feldspar grain is observed and average grain size is smaller than the average grain size observed in the less altered samples. The intense weathering of the bedrock is quite evident in photograph (Figure 21), especially along the fracture in profile-4. Kaolinite that has been formed by the chemical weathering of primary minerals has been concentrated along this fracture. The material, consisting of white soft clay, from the fracture was observed closely at the site.

Two samples from profile-6 (carbonates) have been studied under microscope, abundant fossils are observed (Figure 34).

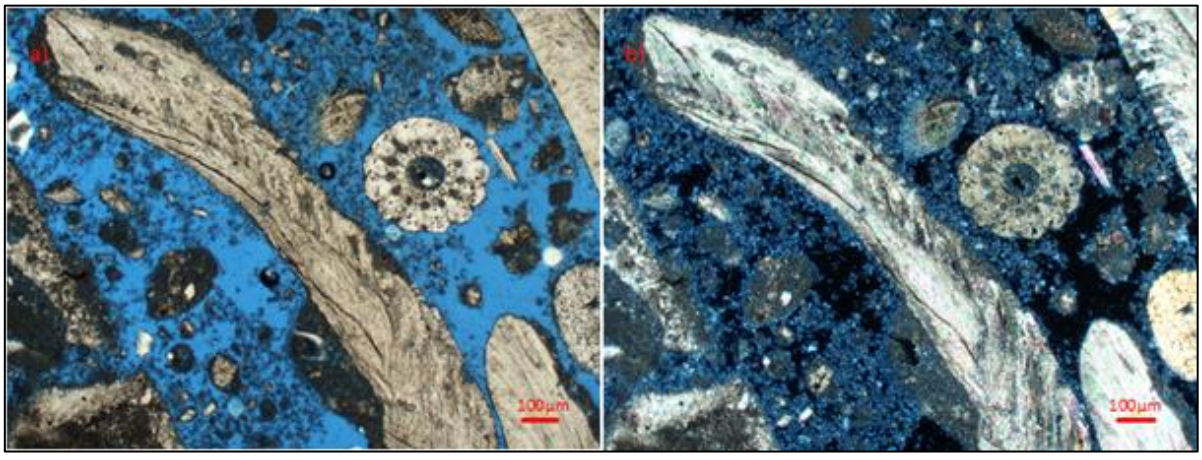

Figure 34: Thin section photo of Ivö-6-2-12. (a) Taken in plane polarized light. (b) Taken in cross polarized light

Calcite grains with cleavage planes and low birefringence are visible. Samples are studied to investigate the effects of carbonate deposition on bedrock weathering.

A sample from the thin veneer (kaolinite) above saprolite has also been studied along-with a sample from transported sand (close to profile-1). Only quartz grains are visible as rest of the mineral grains have been dissolved (Figure 35a). Some mica grains are also visible in Figure 35a, but no feldspar grains are observed. The thin section prepared from the transported sand close to profile-1 contains quartz grains as the dominant mineral, very few intensely altered feldspar are also identified.

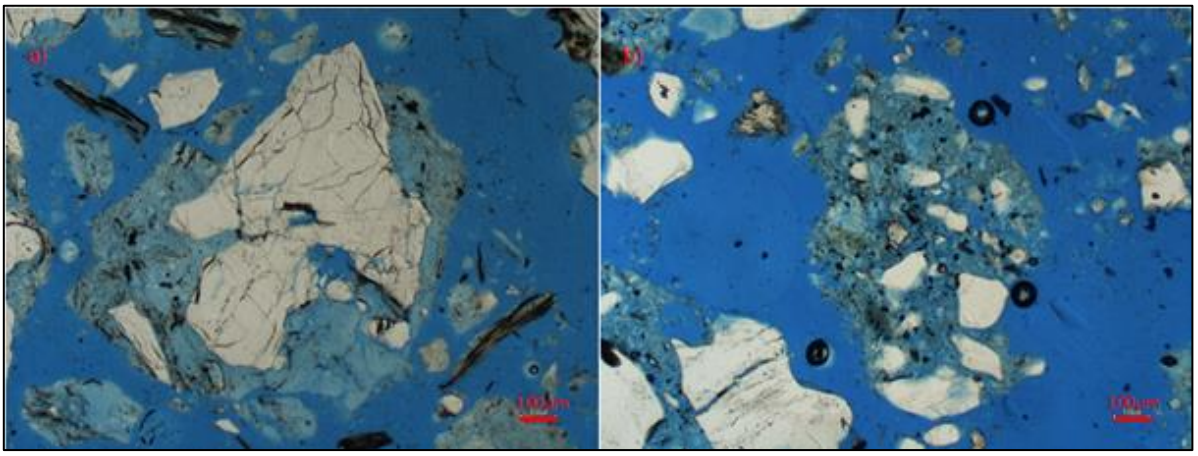

Figure 35: Two photographs in plane polarized light under microscope. (a) Ivö-K-1-12, no feldspar visible with some mica still intact. (b) Ivö-Sand-12, intense dissolution of all primary minerals and only quartz grains are visible.

5.3. X-Ray Diffraction (XRD) analyses:

5.3.1. Bulk Analyses:

Both clay minerals and non-clay minerals are identified and semi-quantified by bulk analyses of the samples (Appendix 3). These results illustrate the mineralogical variations across the two profiles due to weathering and diagenesis.

5.3.1.1. Fresh Granite:

Feldspar is the dominating mineral group with 61 XRD%, where plagioclase (P) is 33 XRD% and K-feldspar (A) is 28 XRD% making plagioclase/total feldspar ratio of 0.55. Quartz (Q) being the second most abundant mineral with 28 XRD% making the quartz/total feldspar ratio of 0.3. The carbonates constitute 7 XRD%, with the calcite (4 XRD%) being the abundant

mineral. The micas make up 6 XRD% of the fresh granite. No clays were identified in this sample.

5.3.1.2. Profile-1:

All the samples from profile-1 were analyzed (Appendix 3); XRD percentages of all the minerals vary according to the location of sample taken along the profile (Figure 36).

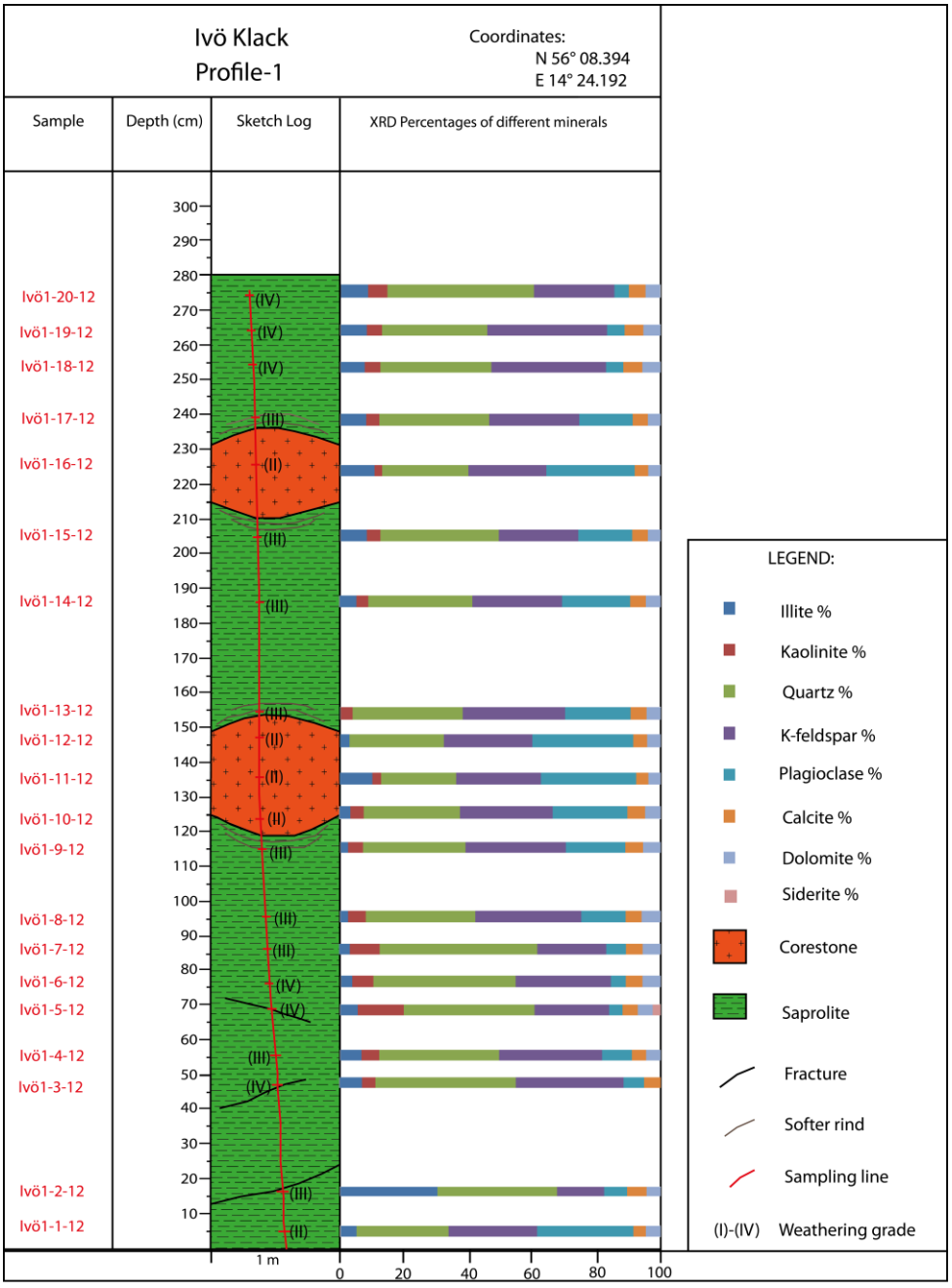

Figure 36: Sketch log of profile-1 with bulk XRD percentages of various minerals. Decreased feldspars and quartz content in samples outside corestone. Quartz and kaolinite content increased away from corestones, while plagioclase content decreases.

The total feldspars range between 22-59 XRD% with the ranges of 5-31 XRD% and 15-37 XRD% of the plagioclase and K-feldspar respectively. Relatively minor variations in K-feldspar XRD% with respect to plagioclase XRD% are observed across this weathering profile. Plagioclase content decreases upwards in profile-1 (up to Ivö-1-7-12), and increase on approaching lower corestone (Ivö-1-8-12 to Ivö-1-12-12). Another decrease in plagioclase content is observed in samples Ivö-1-13-12, Ivö-1-14-12 and Ivö-1-15-12. In Ivö-1-16-12 (sample from corestone) plagioclase content increases again and decreases to 5 XRD% in Ivö-1-20-12.

The quartz varies from 23 to 49 XRD%, and quartz content decreases in two corestones. Carbonates XRD% range is 8-12. The XRD% of 10Å (illite) peak varies from 0-10 with abnormally high 30 XRD% in one of the sample (Ivö-1-2-12). Kaolinite has a range of 0-14 XRD% across the profile. In sample Ivö-1-16-12 kaolinite XRD% reduces to only 2 while an increase in illite XRD% is observed. Only one sample (Ivö-1-5-12) in the whole profile contains siderite with 2 XRD% of the total mineral percentage.

Three ratios have been calculated using bulk XRD analysis viz, plagioclase/total feldspar (Figure 37), kaolinite/kaolinite+total feldspar (Figure 37) and quartz/quartz+total feldspar (Figure 38) which range, 0.13-0.53, 0-0.34 and 0.29-0.64 respectively.

In Figure 37, two ratios (plagioclase/total feldspar and kaolinite/total feldspar) are displayed for a comparison along with sketch log of profile-1. Plagioclase/total feldspar ratio (Figure 37) varies from 0.13 to 0.53 while kaolinite/total feldspar ratio (Figure 37) varies from 0 to 0.34 across profile-1. It is observed that both ratios are inversely proportional to each other. Two colours have been assigned to make distinction between increase (red line) and decrease (black line) in ratios. Decrease in plagioclase/total feldspar ratio is observed in samples Ivö-1-1-12 to Ivö1-6-12 (upwards in profile) followed by increase in samples Ivö-1-7-12 to Ivö-1-12-12 and two decreasing trend (from Ivö-1-13-12 to Ivö-1-15-12 and from Ivö-1-16-12 to Ivö-1-20-12) of ratio in rest of the above samples.

Kaolinite/kaolinite+total feldspar ratio increases from base of profile-1 to Ivö-1-5-12 (Figure 37), and an inverse trend in comparison to plagioclase/total feldspar ratio is observed in rest of the weathering profile. The inverse trend of two bar graphs can be seen across the profile-1 especially from samples Ivö-1-7-12 to Ivö-1-12-12. The variations in these ratios can be attributed to the location of two corestones in the weathering profile

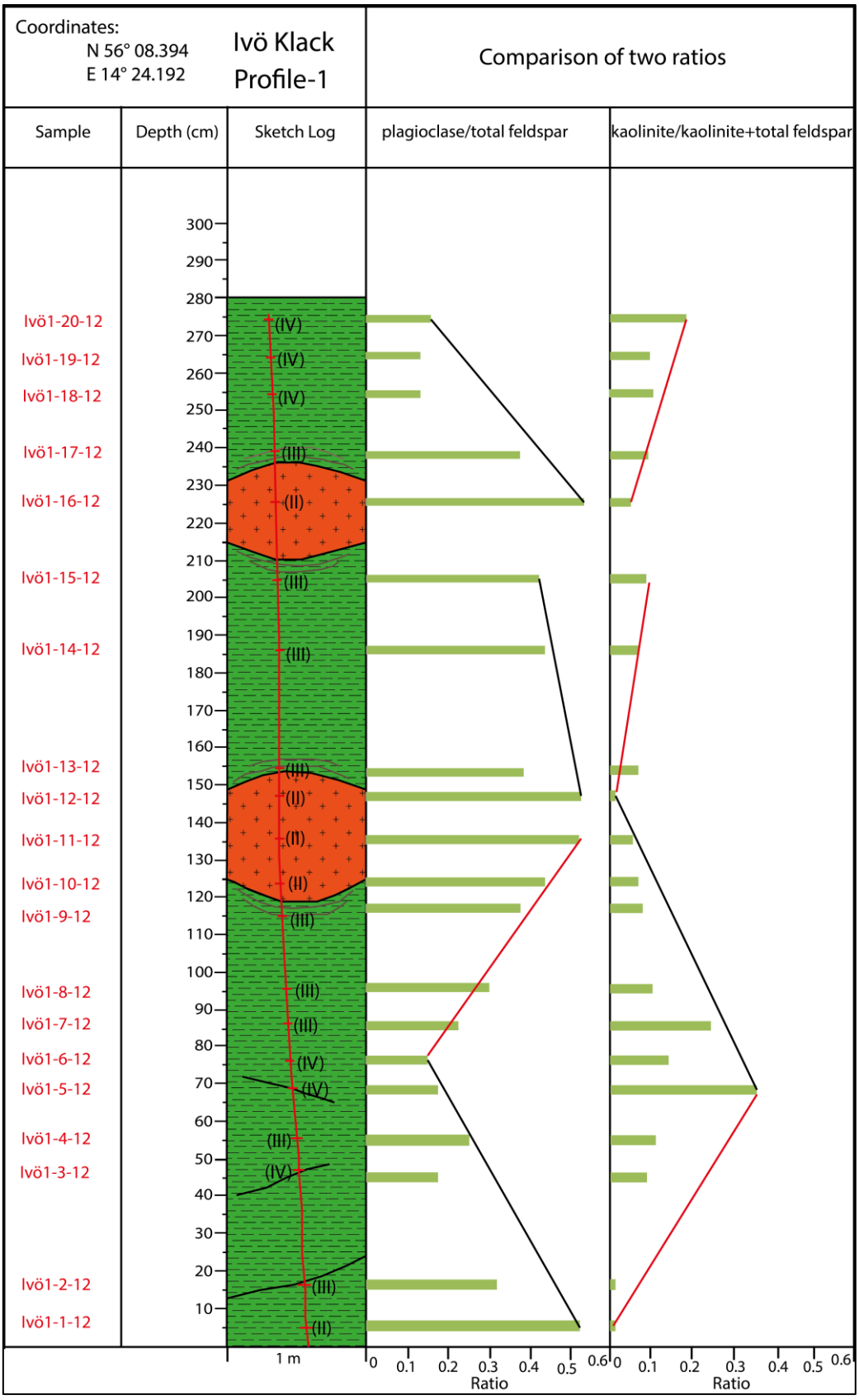

Figure 37: Ratio comparison of plagioclase/total feldspar and kaolinite/kaolinite+total feldspar from bulk XRD analysis along with sketch log of profile-1. Red and black lines represent increase and decrease in ratios respectively. Kaolinite content increases away from corestones while plagioclase content increases.

The percentage change in total feldspar content across profile-1 with respect to total feldspar content of fresh granite compared with the quartz/total feldspar ratio in 20 samples of profile-1 is shown in Figure 38 using two line graphs. X-axis in both line graphs below represents sample number (1-20). While y-axis in upper line graph (Figure 38a) represent percentage change (increase or decrease) in total feldspar concentration along profile-1 with respect to total feldspar concentration of fresh granite and in lower line graph (Figure 38b) represent simple ratio.

The upper line graph (Figure 38a) is made using the concept of mathematical equation from Nesbitt, (1979) elaborated in Materials and method. This graph illustrates changes in mineral (readily altered) concentration along a weathering profile against a more resistant mineral. The eq. 14 uses quartz as an immobile mineral (resistant to weathering) and feldspars being mobile minerals (more easily altered). In three samples (Ivö-1-11-12, Ivö-12-12 and Ivö-1-16-12) from corestones across profile-1, total feldspar concentration is close to total feldspar concentration of fresh granite. The straight red lines in graph (Figure 38a) shows increase in percentage change in feldspars content along weathering profile-1 and black lines shows decreasing trend of percentage change in feldspars content across profile-1 (both changes are considered with respect to feldspars content of fresh granite).

An abrupt increase in quartz/quartz+total feldspar ratio followed by variation across the profile-1 is observed from lower line graph (Figure 38b). Red lines depict increase in ratio while black lines illustrate decrease in this ratio along profile-1.

Following five trends can be marked comparing two line graphs:

1. From Ivö-1-1-12 to Ivö-1-7-12, increase in percentage change of feldspars concentration along profile-1 w.r.t feldspars concentration of fresh granite and increase in quartz/quartz+total feldspar ratio as well.
2. From Ivö-1-7-12 to Ivö-1-11-12, decrease in percentage change of feldspars concentration along profile-1 w.r.t feldspars concentration of fresh granite and decrease in quartz/quartz+total feldspar ratio as well.
3. From Ivö-1-11-12 to Ivö-1-15-12, increase in percentage change of feldspars concentration along profile-1 w.r.t feldspars concentration of fresh granite and increase in quartz/quartz+total feldspar ratio as well.

4. From Ivö-1-15-12 to Ivö-1-16-12, decrease in percentage change of feldspars concentration along profile-1 w.r.t feldspars concentration of fresh granite and decrease in quartz/quartz+total feldspar ratio as well.
5. From Ivö-1-16-12 to Ivö-1-20-12, increase in percentage change of feldspars concentration along profile-1 w.r.t feldspars concentration of fresh granite and increase in quartz/quartz+total feldspar ratio as well.

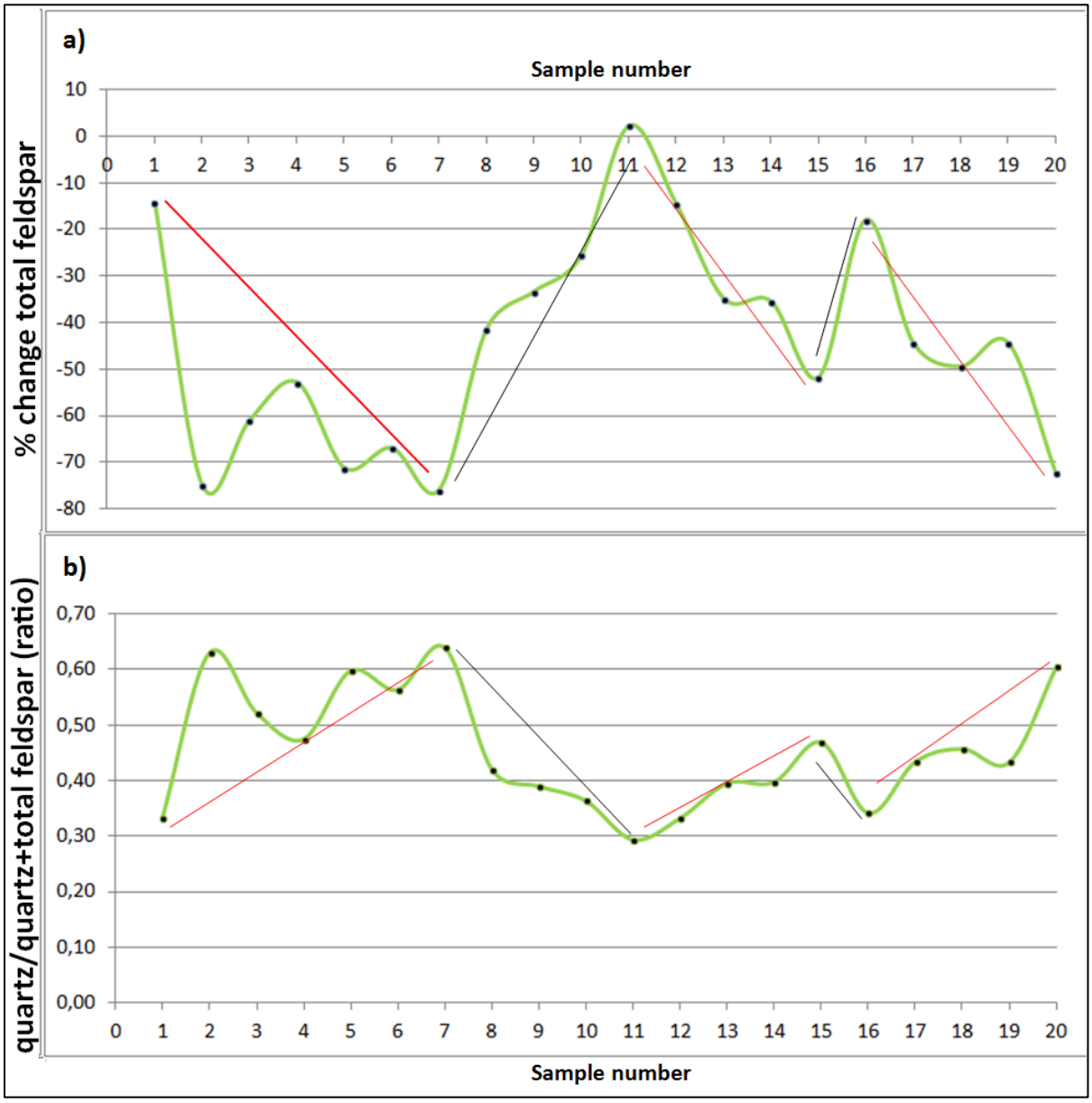

Figure 38: Comparison of two line graphs. (a) Percentage change in total feldspar concentration across profile-1 with respect to total feldspar concentration of fresh granite, (b) Line graph showing quartz/quartz+total feldspar ratio across profile-1. Red lines (increase) and black lines (decrease) depict trends across the profile-1.

5.3.1.3. Profile-2:

All the samples of profile-2 were analyzed (Appendix 3); Figure 39 displays a sketch log and the results.

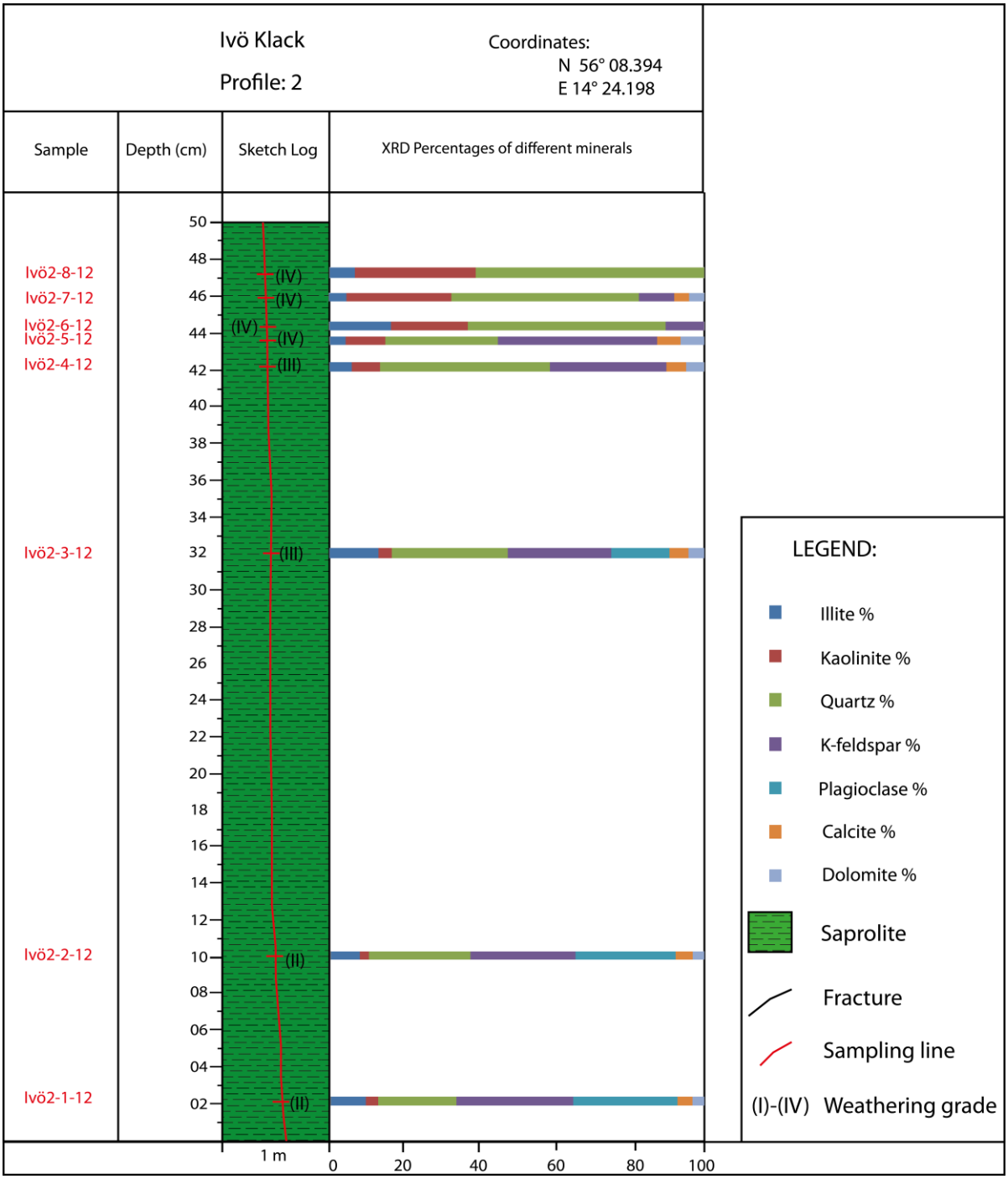

Figure 39: Sketch log of profile-2 with bulk XRD percentages of various minerals. Red line in log represents sampling line and increasing intensity of weathering. Feldpars (plagioclase and K-feldspar) concentration is decreasing upwards in profile-2, while kaolinite content is decreasing. Carbonates are missing in the uppermost sample of the profile-2.

The feldspars vary from 0-59 XRD% while the plagioclase ranges from 0-28 XRD% and the K-feldspar from 0-42 XRD%. Plagioclase XRD% decreases upwards considerably from Ivö-2-1-12 to Ivö-2-3-12 and becomes zero in last five samples of profile-2. While XRD% of K-feldspar remains roughly same (30 XRD%) in first four samples (Ivö-2-1-12 to Ivö-2-4-12) and increases in sample five up to 42XRD%. A decrease in K-feldspar content is observed in Ivö-2-6-12 and Ivö-2-7-12 (10 XRD%) before finally reaching 0 XRD% in Ivö-2-8-12.

The quartz content in this profile varies between 21-61 XRD%. An increasing trend in quartz XRD% can be observed across profile-2. The carbonates range from 0-12 XRD% and a variation of 4-16 XRD% in 10Å (illite) peak. Variation in 10 Å peak can be observed across the weathering profile-2.

A range of 2-32 XRD% belongs to kaolinite. Same as quartz a general increasing trend in kaolinite content is detected across profile-2. Highest kaolinite content (32 XRD%) is observed in Ivö-2-8-12.

Following the same procedure three ratios are calculated for profile-2 viz, plagioclase/total feldspar (Figure 40), kaolinite/kaolinite+total feldspar (figure 40) and quartz/quartz+total feldspar (Figure 41) which range, 0-0.49, 0.05-1.0 and 0.26-1.0 respectively.

Figure 40 displays sketch log of profile-2 along with the comparison of two ratios; plagioclase/total feldspar and kaolinite/kaolinite+total feldspar.

The plagioclase/total feldspar ratio decreases in first three samples (Ivö-2-1-12, Ivö-2-2-12 and Ivö-2-3-12) from a maximum of 0.49 to 0.36, whereas a very slight increase in kaolinite/kaolinite+total feldspar ratio from 0.05 to 0.08 is observed for the same samples. The plagioclase/total feldspar ratio decreases to almost zero in samples Ivö-2-4-12 to Ivö-2-8-12 in contrast to kaolinite/kaolinite+total feldspar ratio which has increased abruptly (from 0.19 to 1.0) in these samples (Figure 40).

An inverse trend between two ratios is evident from two bar graphs. The black line shows decrease in plagioclase/total feldspar ratio, while red line depicts increase in kaolinite/kaolinite+total feldspar. Upwards in the weathering profile, weathering degree of samples is increasing (weathering grade).

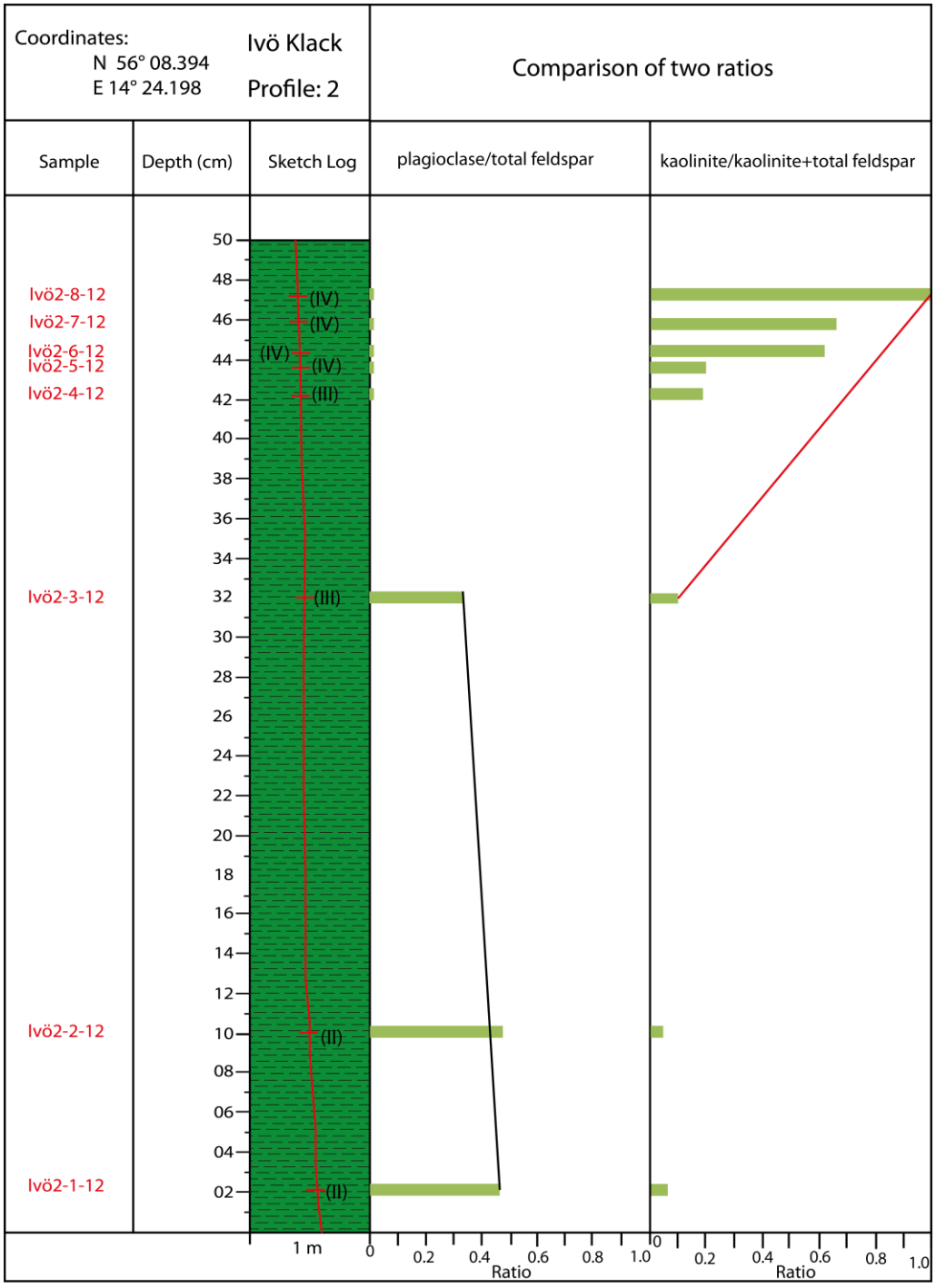

Figure 40: Ratio comparison of plagioclase/total feldspar (reaches zero following a decrease in first three samples indicated by black line), and kaolinite/kaolinite+total feldspar (continuously increasing upwards shown by red line and reaches 1).

Two more line graphs are displayed in Figure 41, one is a line graph (Figure 41a) made using equation 14 while other is a simple ratio (Figure 41b), quartz/quartz+total feldspar ratio increases across the profile from 0.26 to 1.0 and percentage change in total feldspar content also generally increases (apart from a slight deviation due to Ivö-2-5-12) through profile-2.

Both the trends are marked by red lines. The line graphs are made using bulk XRD%. The sample Ivö-2-5-12 shows a slight deviation from the general trend of the graphs, resulting in slight bulge upwards in upper graph and downwards in lower graph. The general trend in both line graphs increase upwards in profile-2 apart from the bulge created due to Ivö-2-5-12.

The x-axis in both line graphs (Figure 41) depicts the sample number, while y-axis in Figure 41a represents the percentage change in total feldspar content with respect to total feldspar content of fresh granite and in Figure 41b y-axis represents quartz/quartz+total feldspar ratio.

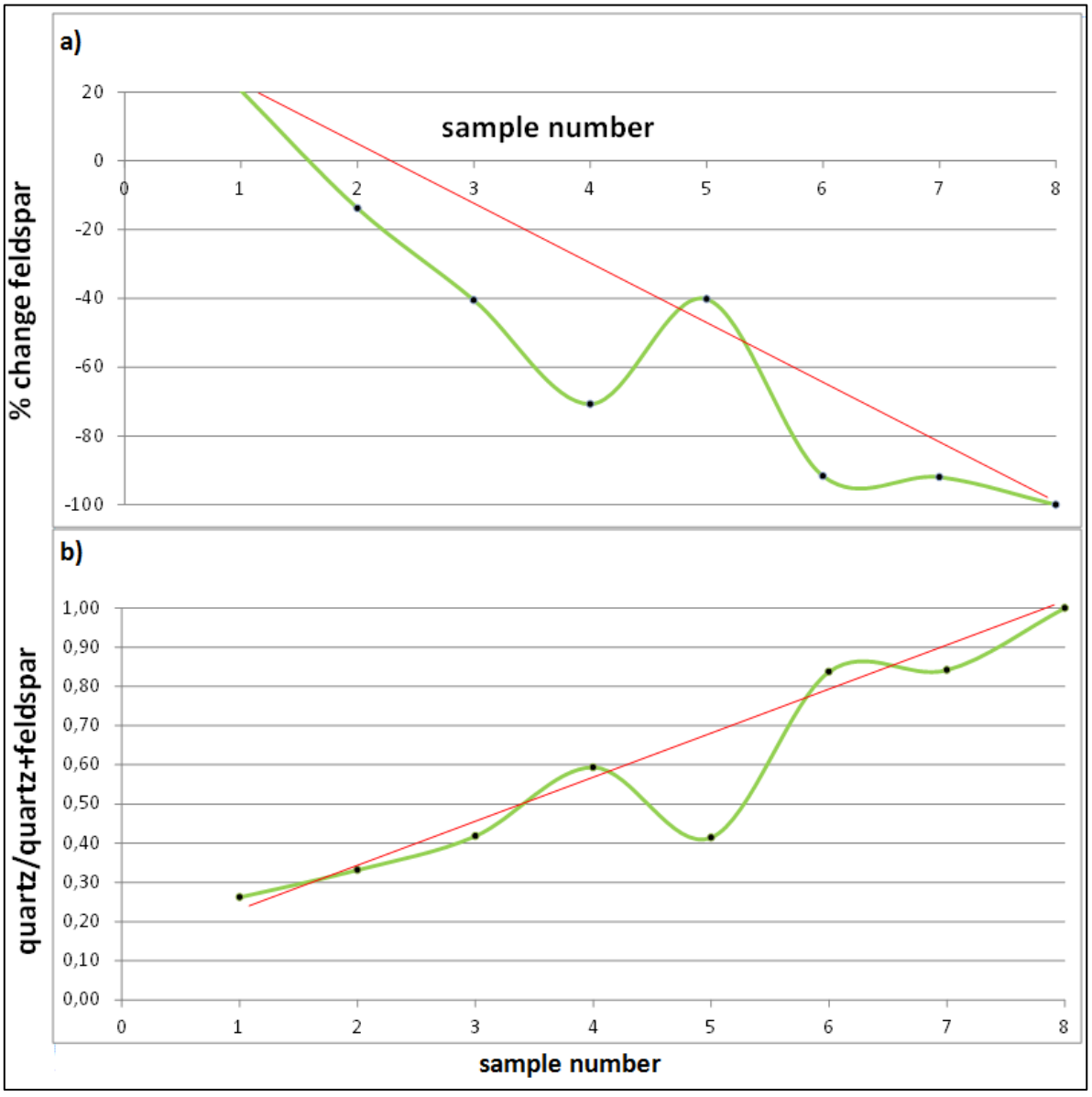

Figure 41: Comparison of two line graphs, (a) percentage change in total feldspar across profile-2, increasing trend is visible apart from sample Ivö-2-5-12 and (b) graph showing quartz/quartz+ total feldspar ratio across profile-2, ratio increases across weathering profile. Red line in both line graphs represent increasing trend.

Figure 42 represents comparison of different weathering stages observed across profile-1 and profile-2 using ternary display based on idea from Nesbitt and Young (1984 and 1989). Axes of ternary display represents three minerals with 100 XRD% namely; A=kaolinite, B=plagioclase and C= K-feldspar. Profile-1 in Figure 42a represents lack of total plagioclase consumption and weathering is limited to initial stage of weathering (ISW). Fresh samples (Ivö-1-1-12 and three samples from corestones) are represented by boxes, plot close to line joining plagioclase and K-feldspar, as weathering intensity increases weathered sample approaches line joining kaolinite and K-feldspar. Absence of advanced stage of weathering

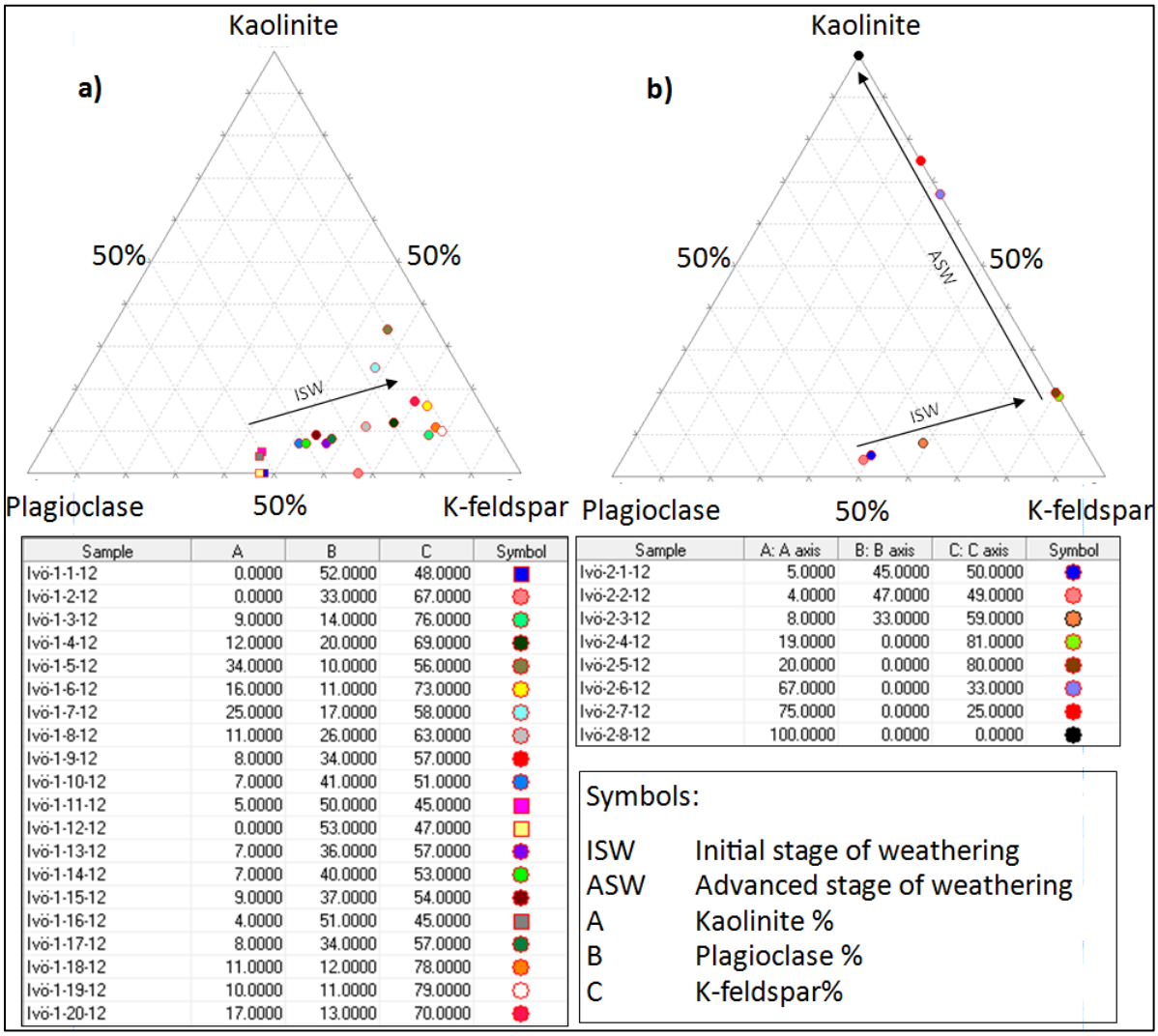

Sample	A	B	C	Symbol
Ivö-1-1-12	0.0000	52.0000	48.0000	
Ivö-1-2-12	0.0000	33.0000	67.0000	
Ivö-1-3-12	9.0000	14.0000	76.0000	
Ivö-1-4-12	12.0000	20.0000	69.0000	
Ivö-1-5-12	34.0000	10.0000	56.0000	
Ivö-1-6-12	16.0000	11.0000	73.0000	
Ivö-1-7-12	25.0000	17.0000	58.0000	
Ivö-1-8-12	11.0000	26.0000	63.0000	
Ivö-1-9-12	8.0000	34.0000	57.0000	
Ivö-1-10-12	7.0000	41.0000	51.0000	
Ivö-1-11-12	5.0000	50.0000	45.0000	
Ivö-1-12-12	0.0000	53.0000	47.0000	
Ivö-1-13-12	7.0000	36.0000	57.0000	
Ivö-1-14-12	7.0000	40.0000	53.0000	
Ivö-1-15-12	9.0000	37.0000	54.0000	
Ivö-1-16-12	4.0000	51.0000	45.0000	
Ivö-1-17-12	8.0000	34.0000	57.0000	
Ivö-1-18-12	11.0000	12.0000	78.0000	
Ivö-1-19-12	10.0000	11.0000	79.0000	
Ivö-1-20-12	17.0000	13.0000	70.0000	

Sample	A: A axis	B: B axis	C: C axis	Symbol
Ivö-2-1-12	5.0000	45.0000	50.0000	
Ivö-2-2-12	4.0000	47.0000	49.0000	
Ivö-2-3-12	8.0000	33.0000	59.0000	
Ivö-2-4-12	19.0000	0.0000	81.0000	
Ivö-2-5-12	20.0000	0.0000	80.0000	
Ivö-2-6-12	67.0000	0.0000	33.0000	
Ivö-2-7-12	75.0000	0.0000	25.0000	
Ivö-2-8-12	100.0000	0.0000	0.0000	

Symbols:

ISW	Initial stage of weathering
ASW	Advanced stage of weathering
A	Kaolinite %
B	Plagioclase %
C	K-feldspar%

Figure 42: Ternary display of kaolinite (A-axis), plagioclase (B-axis) and K-feldspar (C-axis) across two weathering profiles. Symbols for weathered samples and fresh samples from both weathering profile is given by circles and boxes respectively. (a) Arrow indicates initial weathering stage upwards in weathered samples across profile-1; corestones locate on approximately 0 XRD% kaolinite content represented by boxes. (b) Two weathering stages (initial and advanced) marked by arrows across profile-2, advance stage of weathering starts from total consumption of plagioclase and reaches upto 100 XRD% of kaolinite. The initial weathering stage across both weathering profiles is parallel (based on idea from Nesbitt and Young, 1984 and 1989).

can be attributed to presence of plagioclase in every weathered sample of the profile-1.

Two weathering stages (initial and advanced) are detected in profile-2 based on mineral concentration of kaolinite, plagioclase and K-feldspar (Figure 42b). Initial weathering stage has been marked from mineral concentration of first three weathered samples of profile-2 just before total consumption of plagioclase. As soon as all the plagioclase is consumed, the weathering of K-feldspar moves the weathering trend to more aluminous rich (kaolinite) composition. The weathering continues until all the K-feldspar is dissolved and 100 XRD% of kaolinite is achieved in the uppermost sample of profile-2. This stage of weathering is named as advanced stage of weathering (ASW).

5.3.1.4. Random samples:

The sample from the fracture of profile-4 contains 15 XRD% quartz and its main mineral constituent is kaolinite with 74 XRD% (Appendix 3). K-feldspar is 7XRD% and10Å peak contains 4 XRD%. Two samples out of a total 9 nine samples have been picked for the analysis from profile-6. Only two minerals are identified, the calcite (98 XRD%) and the quartz (2 XRD%) in both samples.

One sample collected from the uppermost veneer of the reworked material was also analyzed. The feldspars were absent in the sample whereas the quartz make up the 60 XRD%. The carbonates constitute 8 XRD% with the 4 XRD% each of the calcite and dolomite (Appendix 3). One sand sample has also been analyzed, the quartz being the dominant makes up 68 XRD%. Out of the two feldspars only K-feldspar was present with 7 XRD%. The calcite constitute 4 XRD% (Appendix 3).

5.3.2. Analysis of clay separated samples:

Identification and quantification of clay fraction (2µm) has been acquired using EG-solvated diffractograms in Diffrac-Eva. The qualitative analysis of 2µm-fraction minerals was done by observing a total of four diffractograms (air-dried, treated with ethylene glycol, 350 ºC heated and 550 ºC heated). The EG treated peak changed its position relative to air-dried which indicates presence of swelling component (smectite). Absence of peak between 5.02 and 5.61 denies the possibility of illite content present as interlayered mixed-layered clay mineral (Reynolds and Hower, 1970; Moore and Reynolds, 1997). Appendix 4 gives mineral estimations (XRD%) from clay separated samples.

Three clay minerals have been identified based on the XRD analysis of clay separated samples kaolinite, illite and smectite across profile-1 (Figure 43).

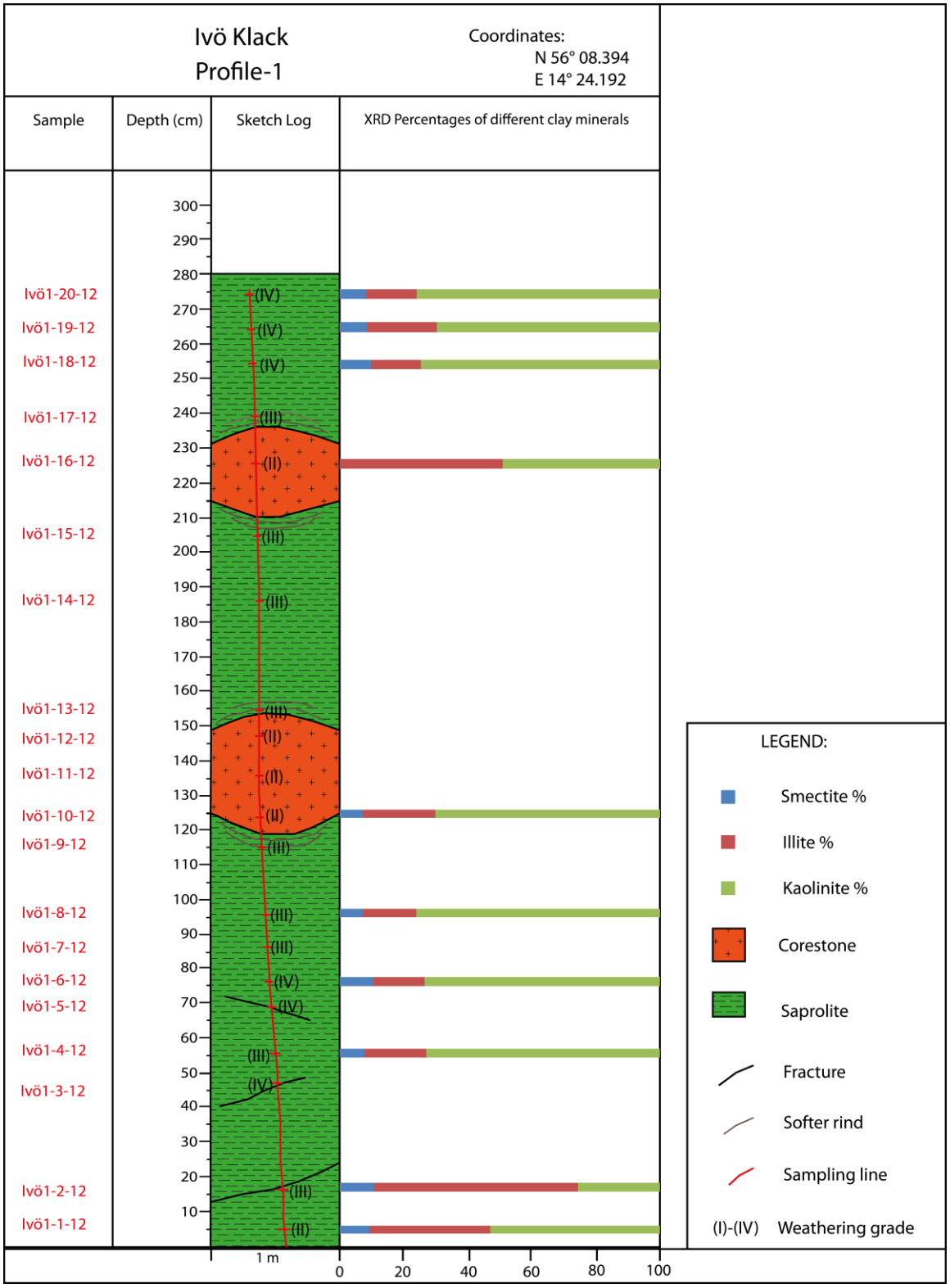

Figure 43: Sketch log of profile-1 with XRD percentages of various minerals (clay separated), kaolinite is the dominant clay mineral across the profile-1 and high illite XRD% in Ivö-1-2-12 and Ivö-1-16-12. Ivö-1-16-12 is collected from corestone.

In most samples kaolinite is the dominant clay with XRD percentages around 50 and more. Smectite (expanding clay mineral) has the lowest 7-11 XRD% and illite varies from 16 to 64 XRD%. In samples Ivö-1-2-12 and Ivö-1-16-12 illite is the dominant clay mineral. Ivö-1-16-12, collected from a corestone, is the only sample in the whole profil-1 which lacks smectite. Illite XRD% decreases from 64 XRD% in Ivö-1-2-12 to 17 XRD% in Ivö-1-7-12 and increases in Ivö-1-10-12 (sample from the bottom of lower corestone). XRD% of illite (around 20 XRD%) and kaolinite (around 70 XRD%) is constant for last three samples of profile-1.

Figure 44 represents the ratio kaolinite/kaolinite+illite of clay separated samples (profile-1) based on XRD analysis.

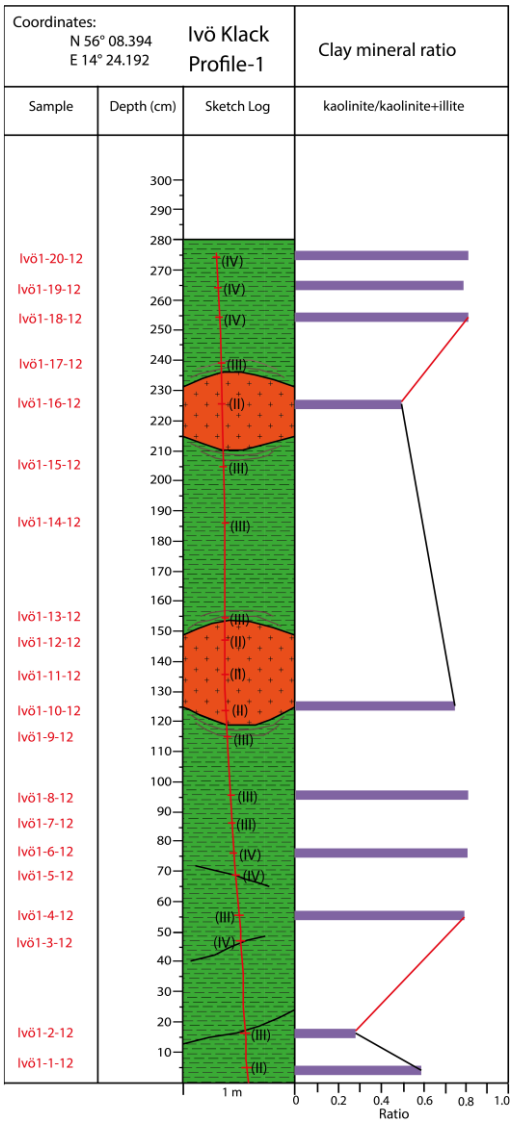

Figure 44: Ratio kaolinite/kaolinite+illite from XRD analysis of clay separated samples of profile-1. Red and black lines represent increase and decrease in ratio respectively.

The ratio varies from 0.29 to 0.83, a decrease of ratio in samples Ivö-1-2-12 and Ivö-1-16-12 is evident from the bar graph. The red lines represent increase while black lines depict decrease in kaolinite/kaolinite+illite. High kaolinite content in most of the samples in profile-1 is evident from bar graph in Figure 43. The ratio decreases to 0.29 in Ivö-1-2-12 and 0.49 in Ivö-1-16-12 which is sample collected from a corestone.

The same three clay minerals were identified in clay separated samples of profile-2 (Figure 45).

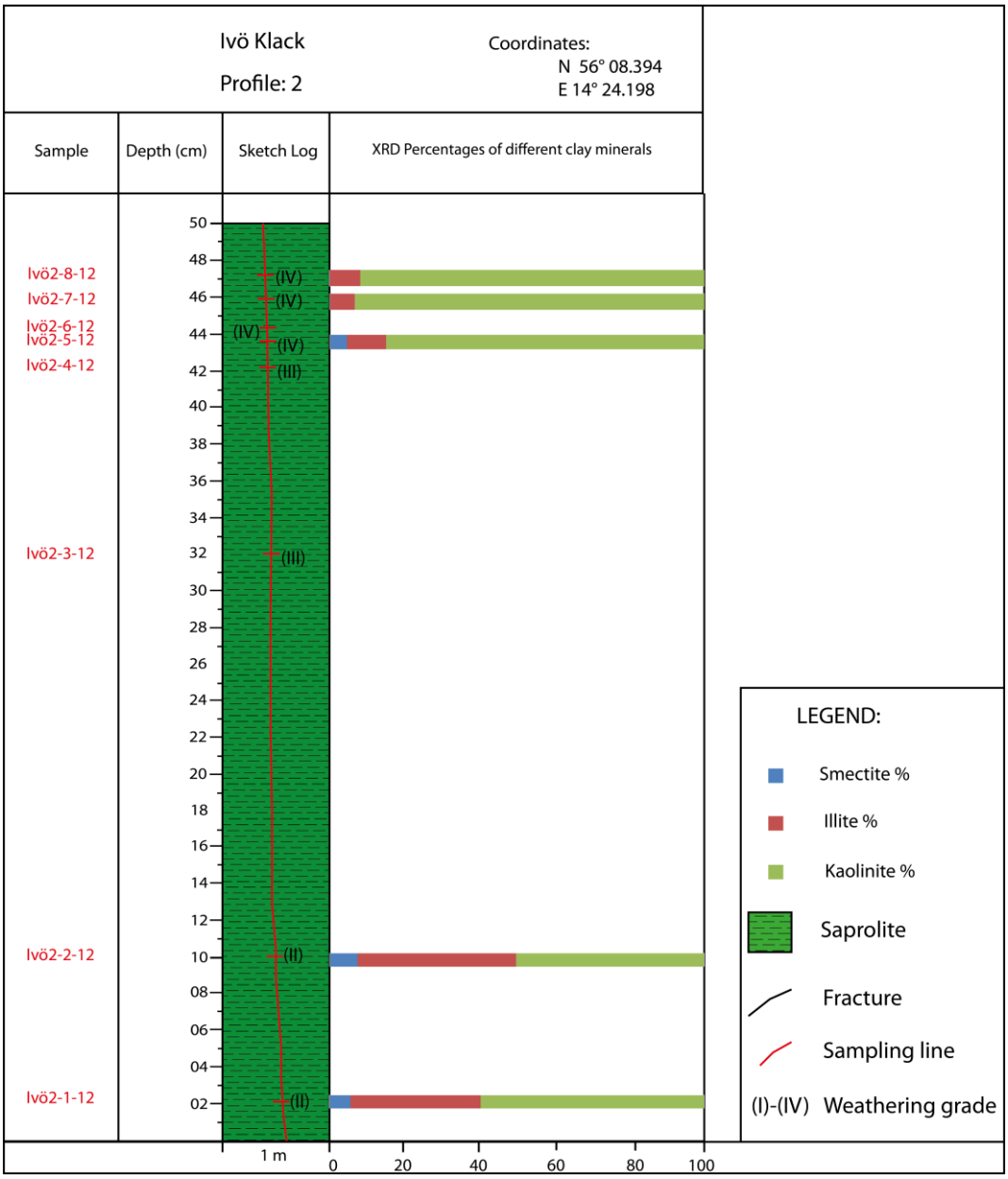

Figure 45: Sketch log of profile-2 with XRD percentages of various minerals (clay separated). Kaolinite seems dominant clay mineral across profile-2, illite and smectite content decreasing upwards in the weathering profile. Smectite is absent in last two samples of profile-2.

Kaolinite is the dominant clay with 61-94 XRD%, while smectite is absent in the uppermost two samples in this profile. Illite being the second most dominant clay varying 7-42 XRD% across the profile-2. Large illite content is observed in the two lowermost samples (Ivö-2-1-12 with 35 XRD% and Ivö-2-2-12 with 42 XRD%). Kaolinite content is increasing from base to top along profile-2, while illite and smectite contents are decreasing. Smectite is absent in the uppermost two samples (Ivö-2-7-12 and Ivö-2-8-12) of profile-2.

In Figure 46 ratio kaolinite/kaolinite+illite of clay separated samples (profile-2) based on XRD analysis is displayed.

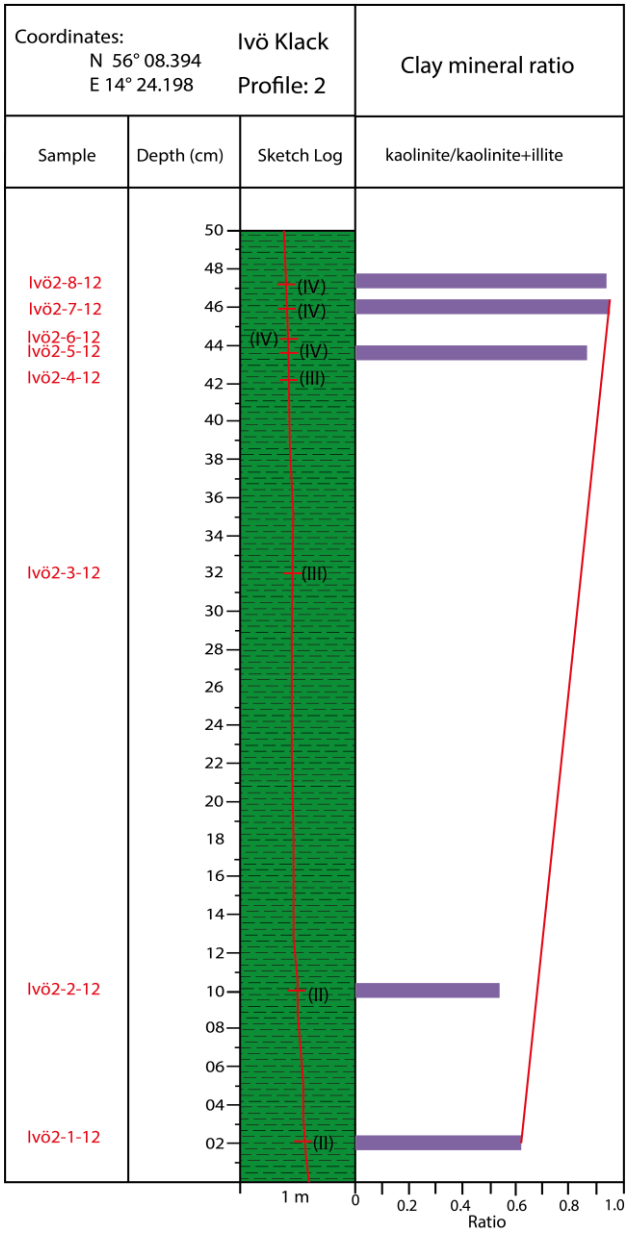

Figure 46: Ratio kaolinite/kaolinite+illite from XRD analysis of clay separated samples of profile-2. Increase in kaolinite content across weathering profile is marked with red line.

Increase in kaolinite content across the profile is observed, and represented by a red line. The first two samples (Ivö-2-1-12 and Ivö-2-2-12) have a ratio of 0.63 and 0.54 respectively, and increased to around 90 XRD% in the last three samples (Ivö-2-6-12, Ivö-2-7-12 and Ivö-2-8-12) of profile-2.

Figure 47 illustrates the ternary display of clay minerals (smectite, illite and kaolinite) of profile-1 and profile-2. Aggregate clay mineral content of all the samples from two profiles is represented in different colors. Three axes of triangles A, B and C shown in Figure 47 represents smectite, illite and kaolinite respectively. Increase in kaolinite content (apart from minor variations along profile-1 due to occurrence of corestone) upwards in both profiles show increased weathering of primary minerals. Smectite content is clearly very less in both weathering profiles. In profile-1 (Figure 47a), three samples (Ivö-1-1-12, Ivö-1-2-12, and Ivö-1-16-12) and in profile-2 (Figure 47b) two samples (Ivö-2-1-12 and Ivö-2-2-12) have appreciable amounts of illite. The arrows in Figure 47 depict the direction of increased weathering across both weathering profiles.

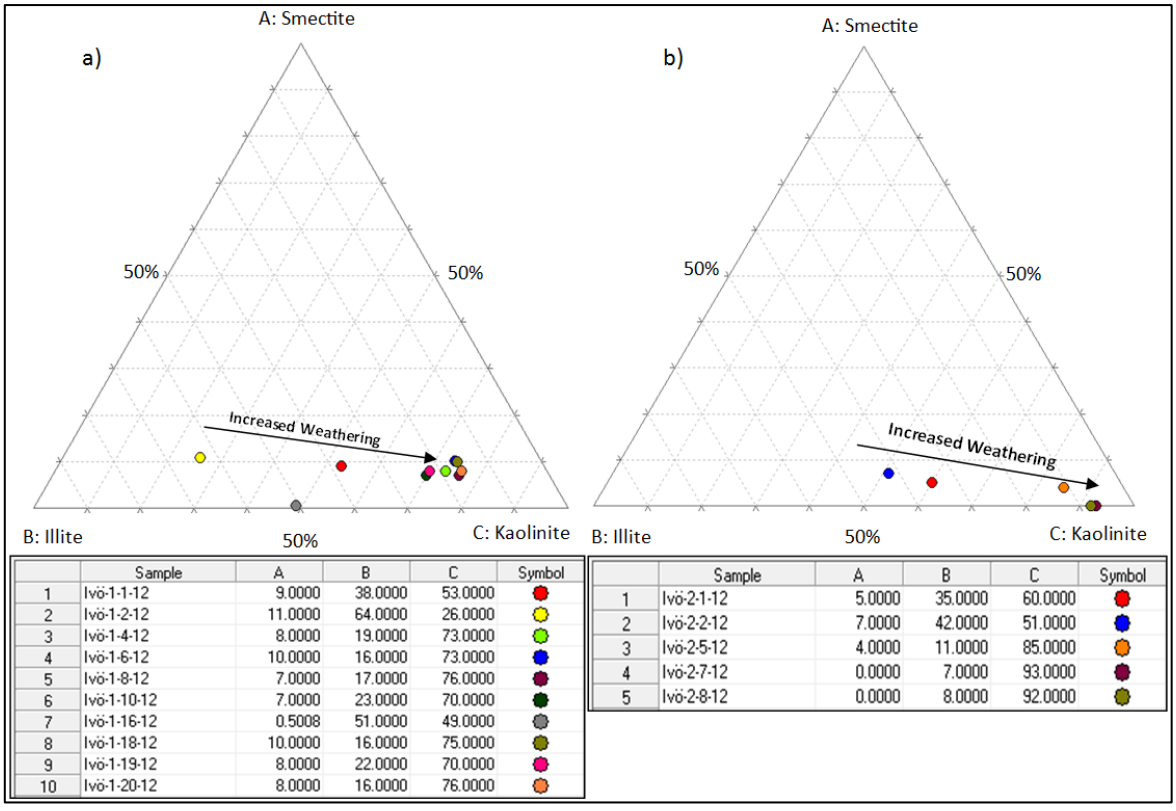

	Sample	A	B	C	Symbol
1	Ivö-1-1-12	9.0000	38.0000	53.0000	
2	Ivö-1-2-12	11.0000	64.0000	26.0000	
3	Ivö-1-4-12	8.0000	19.0000	73.0000	
4	Ivö-1-6-12	10.0000	16.0000	73.0000	
5	Ivö-1-8-12	7.0000	17.0000	76.0000	
6	Ivö-1-10-12	7.0000	23.0000	70.0000	
7	Ivö-1-16-12	0.5008	51.0000	49.0000	
8	Ivö-1-18-12	10.0000	16.0000	75.0000	
9	Ivö-1-19-12	8.0000	22.0000	70.0000	
10	Ivö-1-20-12	8.0000	16.0000	76.0000	

	Sample	A	B	C	Symbol
1	Ivö-2-1-12	5.0000	35.0000	60.0000	
2	Ivö-2-2-12	7.0000	42.0000	51.0000	
3	Ivö-2-5-12	4.0000	11.0000	85.0000	
4	Ivö-2-7-12	0.0000	7.0000	93.0000	
5	Ivö-2-8-12	0.0000	8.0000	92.0000	

Figure 47: Ternary display of clay minerals from profile-1 (a) and profile-2 (b). Samples from both profiles represented with different colors (shown in legend), and 'A' represents 100 % smectite, 'B' represents 100 % illite and 'C' represents 100% kaolinite. Arrows represent increase of weathering intensity across two profiles (based on idea from Riber, 2009).

5.4. SEM (scanning electron microscopy):

Analysis under scanning electron microscope has been carried out on various samples. Figure 48 displays backscattered electron image of two extreme samples (Ivö-1-1-12 and Ivö-1-20-12) from profile-1. These images display activity of dissolution on perthitic feldspar, in Figure 48a, kaolinite has replaced half of the plagioclase lamina and K-feldspar is intact. Whereas in Figure 48b no plagioclase if observed, only kaolinite and K-feldspar are present. Another observation from back scattered electron images below is absence and presence of porosity in Ivö-1-1-12 and Ivö-1-20-12 respectively.

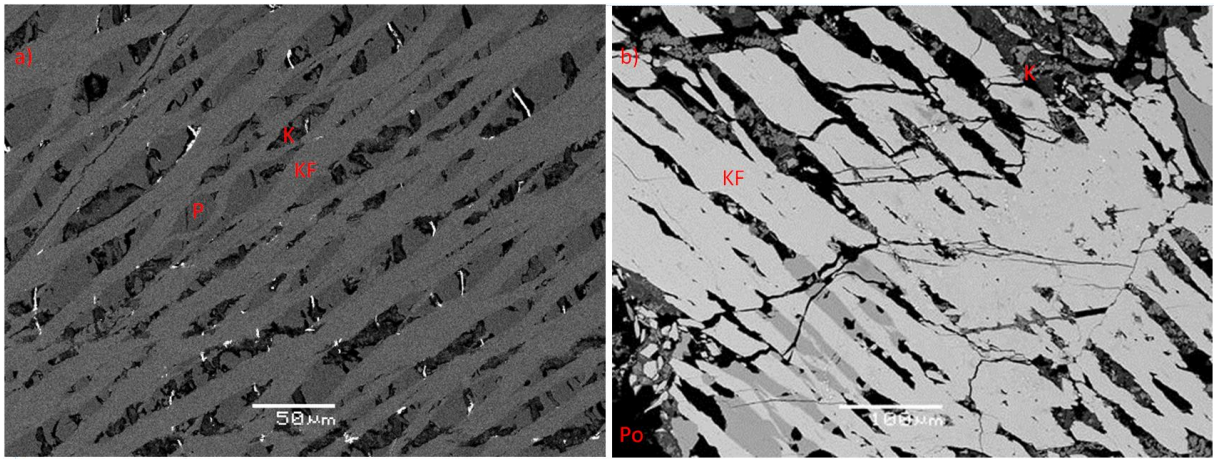

Figure 48: Dissolution pattern in feldspar (backscaterred electron images). (a) Ivö-1-1-12, K-feldspar, plagioclase and kaolinite can be seen. (b) Ivö-1-20-12, only kaolinite and K-feldspar are visible along with some porosity. Symbols: KF= K-feldspar, P= plagioclase, K=kaolinite and Po=porosity.

Figure 49 displays transition from fresh granite to the weathered samples and shows increasing degree of feldspar dissolution and formation of clay minerals, especially kaolinite. The dissolution pits and formation of secondary minerals are clearly visible, except in Ivö-Extra1-12 sample of fresh granite (Figure 49a) where only fresh feldspar (K-feldspar and plagioclase) grains are observed. Formation of both, the secondary mineral (kaolinite) and dissolution pit can be seen in Ivö-1-1-12 (Figure 49b). Kaolinite seems to be transformed material after part of feldspar is dissolved.

In Ivö-1-5-12 (Figure 49c) needle like mineral is observed (halloysite or illite). These needles look more like illite, and also characteristic 8.1 Å peak for halloysite in XRD analysis is absent. Complete dissolution of primary minerals and formation of secondary minerals (mainly kaolinite) is observed in sample Ivö-4-5-12 (Figure 49d). In addition different

structures of kaolinite minerals are observed (Figure 49d and 50). This describes the possibility of transformation of primary minerals into various forms of secondary minerals.

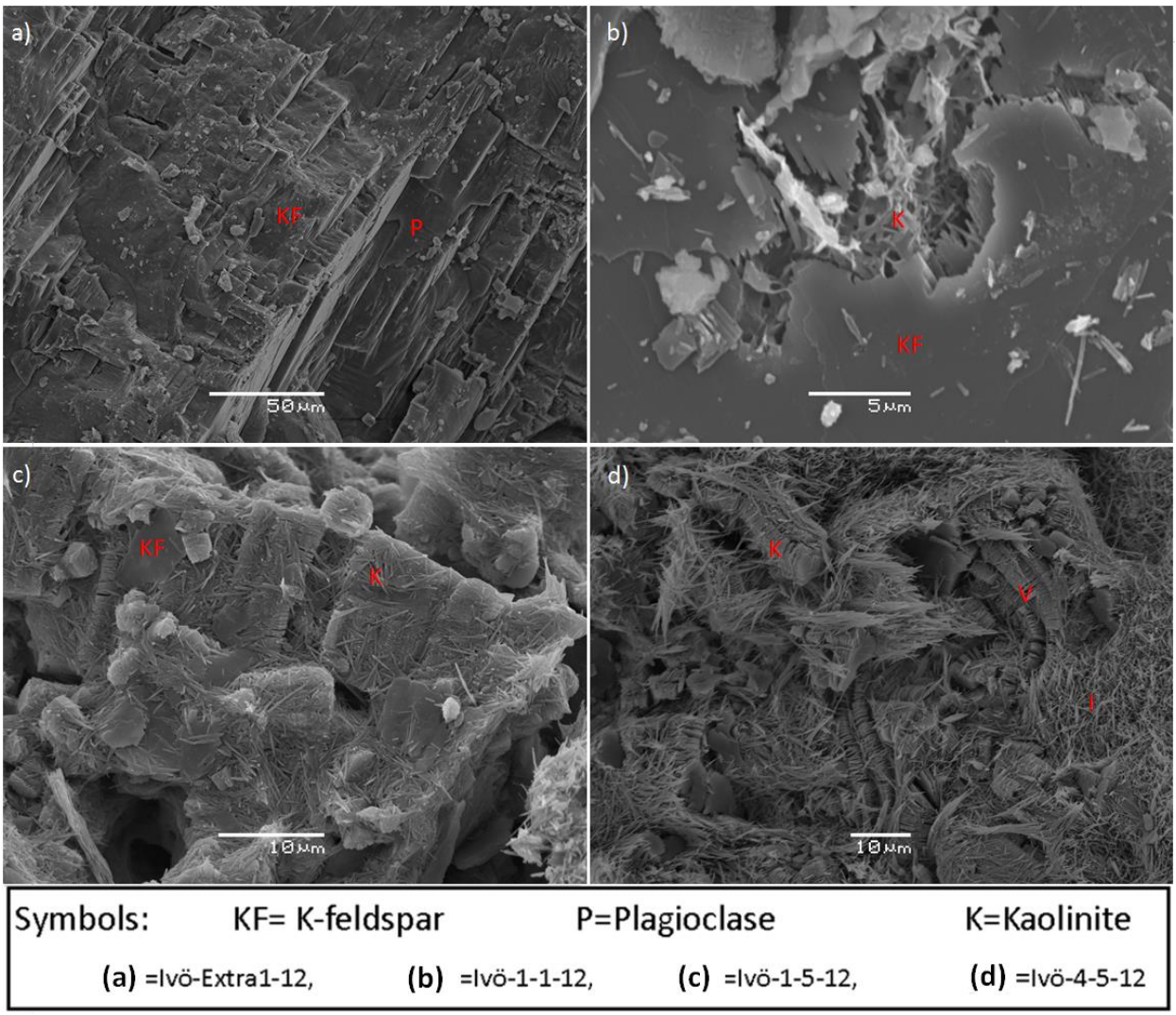

Figure 49: Different samples showing transformation of feldspars to secondary minerals. (a) Ivö-Extra1-12, fresh K-feldspar and plagioclase crystals visible (I). (b) Ivö-1-1-12, a dissolution pit in which kaolinite is precipitated due to feldspars dissolution (II). (c) Ivö-1-5-12, secondary minerals precipitated from dissolution of feldspars (IV). (d) Ivö-4-5-12, no primary mineral observed and various forms of kaolinite present.

Various structural forms of kaolinite are visible in Figure 50. Right image is enlarged to view booklets of kaolinite in Figure 50. Vermiculite and illite are the other clay mineral component seen in this sample. Booklets of kaolinite confirm their diagenetic origin (precipitated as a result of primary mineral dissolution).

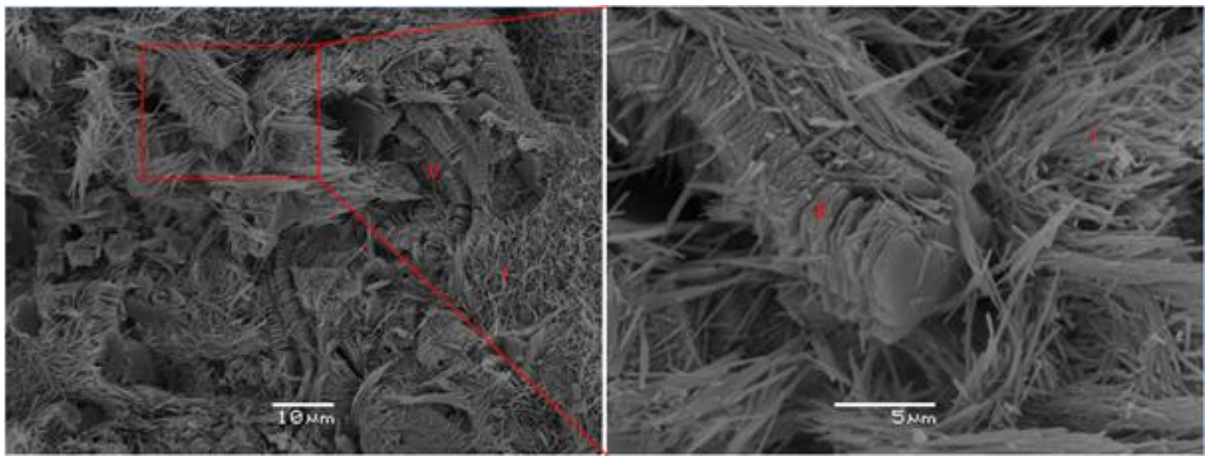

Figure 50: Various structures of kaolinite in Ivö-4-5-12(V). Symbols: V= vermiculite, K= kaolinite (booklet) and I= illite.

The two images displayed in Figure 51 shows formation of recrystallized plagioclase distinguished by the help of BEC (back scattered electron image) and cathodoluminescence images. Cathodoluminescence analysis is done to look for any authigenic mineral present in the sample from fresh granite. Recrystallized plagioclase mineral is observed.

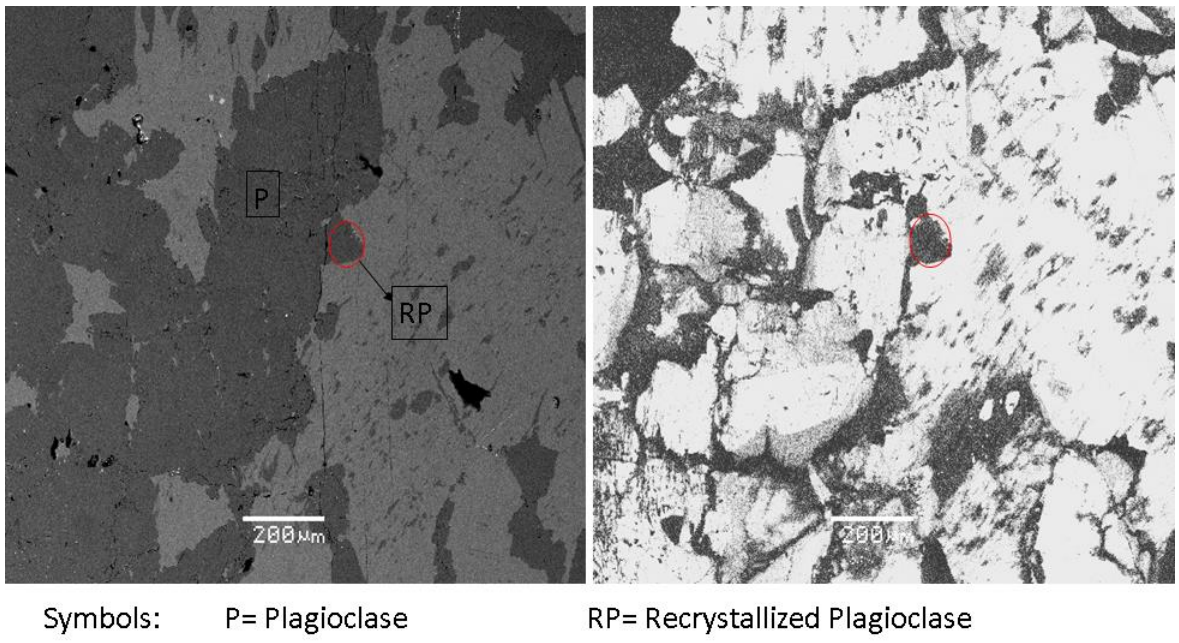

Figure 51: Left) Back scattered electron image, right) Cathodoluminescence image. (Ivö-Extra1-12)

6. Discussion:

Firstly, elaboration of the results acquired from different analyses of fresh granite and weathering profiles will be presented, focusing on secondary minerals formation associated with the composition of primary minerals and climatic conditions. This then followed by the discussion on kaolinite weathering and preservation in the study area along with some theoretical considerations. In the end, comparison of weathering profiles developed at Ivö Klack with the weathering profiles formed in different parts of the world and some benefits of this study to Utsira Project will be discussed briefly.

6.1. Fresh granite:

The fresh granite sample (Ivö-Extra1-12) of Vånga granite falls at the boundary of monzogranite and syenogranite inside Streckeisen diagram (QAP diagram) on the basis of its mineral composition determined from mineral point counting. Mineral XRD% gives semi-quantification which is not usable for such classification. Mostly, the granite consists of medium to coarse grained crystals which approves its plutonic origin (Åberg, 1985). Mineral XRD percentages vary from mineral percentages calculated from mineral point counting, the reason could be the complex procedure followed for the XRD mineral identification and semi-quantification using Diffac.Eva (software).

Sericitization of plagioclase is well-developed in all the plagioclase grains observed under microscope. The replacement of the core of plagioclase with sericite is associated with transformation of biotite to chlorite. The occurrence of sericite needles on plagioclase could be due to both, the post-magmatic alteration of the fresh granite (Que and Allen 1996) or due to the slight weathering of fresh granite (Kato, 1964). The presence of sericite depicts that even fresh granite has suffered alteration. Sericitization is mostly confined to the more porous, calcic core of the plagioclase grain and generation of pores in plagioclase crystal could be of various origins (Que and Allen 1996). However, pores in the plagioclase were not observable even under high-magnification (400= 40×10) of microscope. The composition of sericite resembles muscovite which explains the phenomenon for it being birefringent. Anorthite percentage of the plagioclase is also affected by its sericitization, margins are found to be more anorthite rich than the cores, which could be a possible reason for difference in anorthite percentage measured from the Michel-Lévy technique and XRD analysis (Que and Allen 1996). Another reason attributed to this difference in anorthite composition is XRD analysis

specifications. Although micro-fracturing is visible on plagioclase grains but sericitization is not developed along these fracture. This approves that sericitization occur earlier than fracturing of grains as a result of retrograde metamorphism. Fracturing of the mineral grains in the fresh granite can be associated to exfoliation.

Only one grain of chlorite is observed in the fresh granite sample under scanning electron microscope. This chlorite grain can be attributed to the post-magmatic alteration of biotite (Que and Allen 1996; Murphy et al., 1998). No chlorite is observed in weathered samples from thin section analysis and XRD analysis (clay separated) which approves chlorite is readily altered in the weathering profile (Fordham, 1990; Que and Allen 1996; Murphy et al., 1998).

Basu et al. (1975) devised a scheme based on undulosity and polycrystallinity of detrital quartz crystal to decipher the original rock type of sand samples collected from a stream (plutonic, low-grade metamorphic or high grade metamorphic). Table 5 represents undulosity of 12 quartz grains measured under microscope and number of crystal units per grain of 12 different polycrystalline quartz grains in Ivö-Extra1-12. Based on scheme developed by Basu et al. (1975), Ivö-Extra1-12 falls under the category of plutonic rocks.

Assuming quartz a resistant mineral against processes of weathering, erosion, transportation and sedimentation, here we can use a comparable technique to describe nature of 'fresh granite'. Four parameters can be useful in determining the parent rock of quartz viz, (a) amount of quartz with undulose extinction, (b) amount of quartz with non-undulose extinction, (c) amount of polycrystalline quartz and (d) number of crystals per polycrystalline quartz grain, Figure 6 of Basu et al. (1975).

Monocrystalline quartz based on its undulosity can be categorized into (i) undulolatory (>5º undulosity), (ii) non-undulolatory (≤5º undulosity). Quartz grain of plutonic origin is non-undulose with mean true undulosity of 3.6º whereas metamorphic quartz grains have a mean undulosity of 7.9 º. Low-grade metamorphic monocrystalline quartz grain contains both undulose and non-undulose extinction. Polycrystalline plutonic quartz is coarsely crystalline while polycrystalline metamorphic quartz is more finely crystalline. Plutonic quartz contains less amount of polycrystalline quartz with 2-3 crystal units per grain whereas low-grade metamorphic quartz contains larger amounts of polycrystalline quartz with greater than 3 crystals per grain (Basu et al., 1975).

Table 5: Undulosity of 12 quartz grains and number of crystal units per grain of 12 different polycrystalline quartz grains.

Quartz grain	Undulosity	Polycrystalline quartz	Crystal units per grain
Grain-1	5º	**Polycrystalline-1**	3
Grain-2	4º	**Polycrystalline-2**	2
Grain-3	5º	**Polycrystalline-3**	3
Grain-4	3º	**Polycrystalline-4**	5
Grain-5	5º	**Polycrystalline-5**	3
Grain-6	5º	**Polycrystalline-6**	3
Grain-7	4º	**Polycrystalline-7**	4
Grain-8	3º	**Polycrystalline-8**	5
Grain-9	5º	**Polycrystalline-9**	2
Grain-10	5º	**Polycrystalline-10**	3
Grain-11	5º	**Polycrystalline-11**	3
Grain-12	4º	**Polycrystalline-12**	2

6.2. Weathering Profiles:

Based on the sketch logs, the results from thin section analysis and XRD analysis we can observe a systematic alternating trend of primary and secondary mineral presence throughout the profile-1.Whereas there is a progressive trend of transformation from primary minerals to secondary minerals across profile-2. Variations across the profile-1 indicates that saprolite does not have a smooth, regular surface but in contrast consist of corestones that have been formed by weathering along fractures. Two corestones are identified in the field from profile-1, display a composition close to fresh granite as indicated by petrographic and XRD analyses and have low porosities where they occur. The variations in primary and secondary minerals found in both profiles will be discussed first, then followed by possible reasons of formation of secondary minerals in different environments.

6.2.1. Profile-1:

Smooth changes in mineral types due to weathering depict uniform composition of bedrock all through the weathering profile (Kato, 1964) and somewhat same climatic conditions prevailed during formation of saprolites (Tardy et al., 1973). Apart from one drastic change in mineral type of sample (Ivö-1-2-12) in profile-1where illite reaches up to 30 XRD% in bulk sample and 64 XRD% in clay separated sample. Three causes can be credited to this change, 1) firstly; this could be attributed to the increased amount of sericite seen on plagioclase grains in the sample plus beginning of mica weathering. 2) Another reason for this deviation

can be attributed to unfortunate poor collection of this sample in the field. Increased amount of illite found in the Scandinavian clays is not in accordance with the amount of mica occurring in the basement rock. Rosenqvist (1961) concluded that Scandinavian clays were derived from the soils containing illite which covered the area before Ice Age and illite is eroded and transported by ice and water (Gjems, 1967). 3) A strong mineral XRD% correlation can be observed comparing this sample (Ivö-1-2-12) with Ivö-1-12-12 and Ivö-1-16-12 (both collected from corestones). Consequently, Ivö-1-2-12 could be a sample from a corestone that is no more visible in weathering profile-1 due to intense weathering around corestone.

By examining feldspars with perthitic texture under microscope one can represent different stages of weathering by amounts of mineral laminae removed. As proved by SEM analysis the first mineral to weather between feldspars is plagioclase, in addition it also clarifies that anorthite content of the feldspar is the most weatherable. Blum (1994) generally stated that plagioclase weathers much more easily than K-feldspar in natural environments, which has also been confirmed in this study from results of different analyses (thin section, XRD and SEM). The conversion of primary minerals present in the granite to intermediate and end products under different climates will be discussed later in this chapter. Examination of feldspar grain morphology of different samples in a weathering profile through scanning electron microscope reveals increased size of dissolution pits with increased weathering (Berner and Holden, 1979). Precipitation of kaolinite is observed in pits fromed due to feldspar dissolution.

Increase in quartz percentage with parallel decrease of feldspars confirms more resistant nature of quartz grains against weathering agents. From comparison of two line graphs in Figure 38, it is evident that two corestones have the quartz/quartz+total feldspar ratio and feldspar composition very close to the fresh granite. These two corestones form the least weathered part of saprolite, weathering away from corestones is evident in field and from results (thin section analysis, XRD analysis and SEM). Chemical weathering is most effective in the parts of saprolite with good permeability and porosity, generally along fractures, where water can flow easily (Grant, 1964; Nesbitt, 1979). Change in total feldspar XRD% of the weathered samples compared with the total feldspar XRD% of parent rock illustrates the degree of weathering across profile-1, and change in XRD% is directly proportional to degree of weathering (Nesbitt, 1979).

The amount of K-feldspar across profile-1 decreases in the parts of intense weathering, as represented by the results. In contrast plagioclase percentages fall abruptly everywhere in the weathering sequence. The minerals with intermediate stability (K-feldspar) reduce (to a certain amount) in advanced stages of weathering (Nesbitt and Young, 1984). Consequently, the concentration of these minerals in the weathering product depends on their resistance to chemical weathering (Kato, 1964). In general, porosities are high in near surface saprolite and/or more weathered part of saprolite and decreases with when approaching unweathered bedrock. According to Thomas (1994), dissolution of plagioclase in granitoid rocks generates volume loss which results in the physical degradation of bedrock and formation of a porous, friable saprolite. Figure 37 divides the profile-1 into three distinct portions based on weathering degree of the primary mineral (plagioclase) in the saprolite. There is a clear difference in ratio plagioclase/total feldspar from weathered sample below and above of more fresh corestone. Besides, on approaching the corestone from both directions (above and below) plagioclase content increases. This approves weathering degree of the softer rinds is lesser than more weathered below and above portions of corestone but greater than more fresh corestones. Another important observation is the inverse relationship of two ratios viz, (i) plagioclase/total feldspar and (ii) kaolinite/kaolinite+total feldspar. An inference can be made here that primary mineral (plagioclase) is converting into secondary mineral (kaolinite). Grant (1964) mentioned that under good drainage condition and warm climate, the first unstable weathering products of plagioclase are gibbsite and allophane which converts to stable secondary mineral kaolinite. In addition Nesbitt and Young (1984) stated that kaolinite group minerals are formed at the expense of plagioclase. Intermediate minerals (gibbsite and allophane) formed from plagioclase are missing in the weathering profiles found at the locality.

Biotite is the principle type of mica abundant in the weathering profile, whereas only muscovite grains are seen in thin sections of the most weathered samples. According to Leonard and Weed (1970) biotite weathers more rapidly than muscovite under same conditions of weathering. An intermediate mineral vermiculite, product of biotite weathering is observed under scanning electron microscope, confirms biotite alteration in the weathering profile (Gjems, 1967; Tardy et al., 1973). Two main types of carbonates (calcite and dolomite) identified in XRD analysis can be attributed to the calcite veins in the granite or leaching of limestones from sub-Cretaceous cover above saprolite. The latter is more probable phenomenon as saprolite is more porous near the base of Cretaceous limestone (evident from

mineral point counting results), in addition with the far and few occurrence of the calcite veins in the outcrop.

After discussing the general trends of primary minerals present in the profile-1, we will now discuss trends of secondary minerals found across the profile. This discussion will be based on the results acquired from both bulk and clay separated XRD analyses. The three secondary mineral detected from these analyses have their own significances. General weathering trend from both the profiles shows kaolinite>> illite> smectite. By looking into ratio kaolinite/illite+kaolinite made from XRD results of clay separated samples in Figure 44, the sample from corestone Ivö-1-16-12 shows an erratic decrease which is understandable due to the fact corestone is less weathered than surrounding saprolite. Increase in illite content in sample Ivö-1-2-12 is already discussed. Kaolinite seems to be the principal secondary mineral in the weathering profile defining the weathering intensity in the saprolite. An interesting fact is observed that samples from more weathered parts of profile have greatest kaolinite content in them. Nearly all the aluminium produced upon weathering of plagioclase and biotite seems to have incorporated in forming kaolinite. Samples from the profile-1 having the greater amount of kaolinite have experienced greater intensity of weathering (Grant, 1964; Steinmann et al., 1994). Vermiculite which is an intermediate mineral during the weathering of biotite mineral is observed in scanning electron microscope (Murphy et al., 1998). Absence of chlorite in the samples from weathering profile can be credited to the fact that all the chlorite is converted to the kaolinite (Murphy et al., 1998).

6.2.2. Profile-2:

In comparison with weathering profile-1, this section shows a gradual increase in degree of weathering towards the top which was also seen in the field. It can be divided in two parts namely, (i) lower part (consisting of first three samples) and (ii) upper part (consisting of last five samples). The reason of this division is increased weathering intensity (absence of plagioclase and increment in kaolinite content from Ivö-2-4-12 to Ivö-2-8-12) across the profile. This profile lack presence of any corestone which is the main reason of a gradual change from dominance of primary minerals in lower part to the dominance of secondary minerals in the upper part of the profile. An abrupt change in mineralogy is observed both in thin sections and XRD percentages from sample Ivö-2-3-12 to sample Ivö-2-4-12. Another difference that can be attributed to this profile from profile-1 is the utter absence of feldspar in the uppermost sample.

The first primary mineral to be affected from the weathering process is plagioclase which decreases in amounts considerably in first three samples before vanishing almost completely in samples above it. From the Figure 40 it can be inferred that its dissolution is contrasted by the formation of kaolinite (Nesbitt and Young, 1989). This result supported by Blum's (1994) general interpretation of weathering of plagioclase before K-feldspar.

K-feldspar is more resistant to weathering than plagioclase (Kato, 1964; Nesbitt and Young, 1989; Blum, 1994), shows an increase in XRD% in sample Ivö-2-5-12 than its original value in less weathered samples. Upwards, in next three samples its K-feldspar XRD% starts decreasing until it reaches to zero XRD% in the last sample (near surface). This validates the total consumption of feldspars resulting in the formation of kaolinite as evident from increased kaolinite XRD% in both bulk and clay separated samples.

The accessory minerals of biotite, muscovite, calcite and dolomite display the same trend as observed in profile-1. The absence of chlorite in weathered samples proves the instability of this post-magmatic alteration product (Murphy et al., 1998). The Only difference observed between the two profiles is the absence of carbonates from two samples of profile-2 which can be attributed to the dissolution of carbonates due to near surface location of samples.

Figure 41 illustrates comparison of two line graphs, the upper line graph (Figure 41a) shows a general increase in the total feldspar XRD% change across the profile with respect to total feldspar XRD% of fresh granite. Whereas the upper line graph shows increase in quartz/quartz+ total feldspar ratio resulting from increased weathering upwards in the profile. Both graphs depict the increased weathering degree upwards in the profile-2. Both line graphs, at one point (sample Ivö-2-5-12) shows a slight discrepancy from the general trend. These line graphs are made from the XRD% values of quartz and feldspar. The reason for deviation of both graphs from general trend is due to increased value of K-feldspar XRD% (resulted from intermediate stability of K-feldspar towards weathering) in Ivö-2-5-12 (Kato, 1964).

Figure 42 gives a comparison of weathering stages (initial and advanced) between profile-1 and profile-2, advanced stage of weathering starts in profile-2 after total consumption of plagioclase. In advanced stage of weathering aluminous phase (kaolinite) precipitate at the expense of potassic phases (K-feldspar and illite) (Nesbitt and Young, 1989).

As in profile-1, profile-2 also contains same three secondary precipitates. For the lower part kaolinite> illite >smectite, but for the upper part kaolinite >> illite >smectite (Figure 45). In the last two samples of upper part of the profile-2 smectite is completely missing, which indicates its conversion to kaolinite (Singer, 1984). The effect of weathering on the lower part of the profile is less intense in comparison to the upper part of the profile, where the most dominant secondary mineral is kaolinite with XRD% of around 90. The kaolinite/illite +kaolinite ratio displayed in Figure 46 shows kaolinite increase upwards in the profile. Presence of kaolinite is itself explain the intensity of weathering as it is a secondary mineral formed in the later stages of weathering (Gjems, 1967; Tardy et al., 1973).

6.2.3. Random samples:

Sample Ivö-4-5-12 collected from a fracture along profile-4 displays kaolinite with 96 XRD% (clay separated), depicting kaolinite is the most stable mineral in this environment. It can be deduced this because aqueous solution movement is intense along fractures. Thin section of the particular sample shows imprints of primary minerals, which have been replaced by more stable secondary minerals. The presence of vermiculite in Ivö-4-5-12 represents the ongoing process of biotite weathering (Figure 49 and 50). Transported sand sample as expected shows high sand (quartz) content along-with kaolinite being second dominant mineral and minute amount of K-feldspar. This confirms intermediate stability of K-feldspar in comparison with plagioclase which is readily weathered.

6.3. Formation of secondary minerals:

According to Tardy et al. (1973), the interpretation of any weathering profile can be achieved from three interpretive viewpoints, 1) presence of secondary minerals in the weathering profile, 2) weathering of primary minerals and 3) geo-chemical association on ions in solution. Here the discussion will be limited to the first two viewpoints. There are three main agents of weathering viz, chemical, mechanical and biological. Weathering illustrates the alteration of primary minerals found in the rocks to more stable secondary minerals. The suitable conditions for the formation of a particular secondary mineral resulted from the weathering of primary minerals involves, i) relative accumulation of secondary mineral under certain climatic conditions and ii) composition of primary mineral, as seen in Figure 53 (Tardy et al., 1973). As less stable minerals reduces more rapidly as weathering proceeds, the

stable minerals during chemical weathering accumulate in the weathered product (Kato, 1964).

The origin of montmorillonite as secondary mineral in granites can be associated with two processes, (i) by transformation of biotite or (ii) authigenesis in feldspars. First process is limited to semi-arid climates where montmorillonite formed is ferriferous. Montmorillonite formed due to second process contains more aluminium than its precursor (plagioclase) and found in humid tropical climate (Tardy et al., 1973). Vermiculite is also an intermediate mineral formed during weathering of both plagioclase and biotite. Its transformation from the biotite has a certain relationship with the climate, in humid tropical areas it is only confined to bottom of the saprolites and is a common weathering product of biotite in temperate areas (Tardy et al., 1973). In humid tropical regions, kaolinite is the common alteration product of K-feldspar, plagioclase and biotite while in temperate areas it only appears as secondary mineral of feldspars (Tardy et al., 1973). Illite which is intermediate weathering mineral can be formed from K-feldspar and muscovite (Nesbitt and Young, 1984 and 1989). Trioctahedral illite is unstable in acidic soil horizons whereas amount of dioctahedral illite increases upward in a soil horizon (Gjems, 1967).

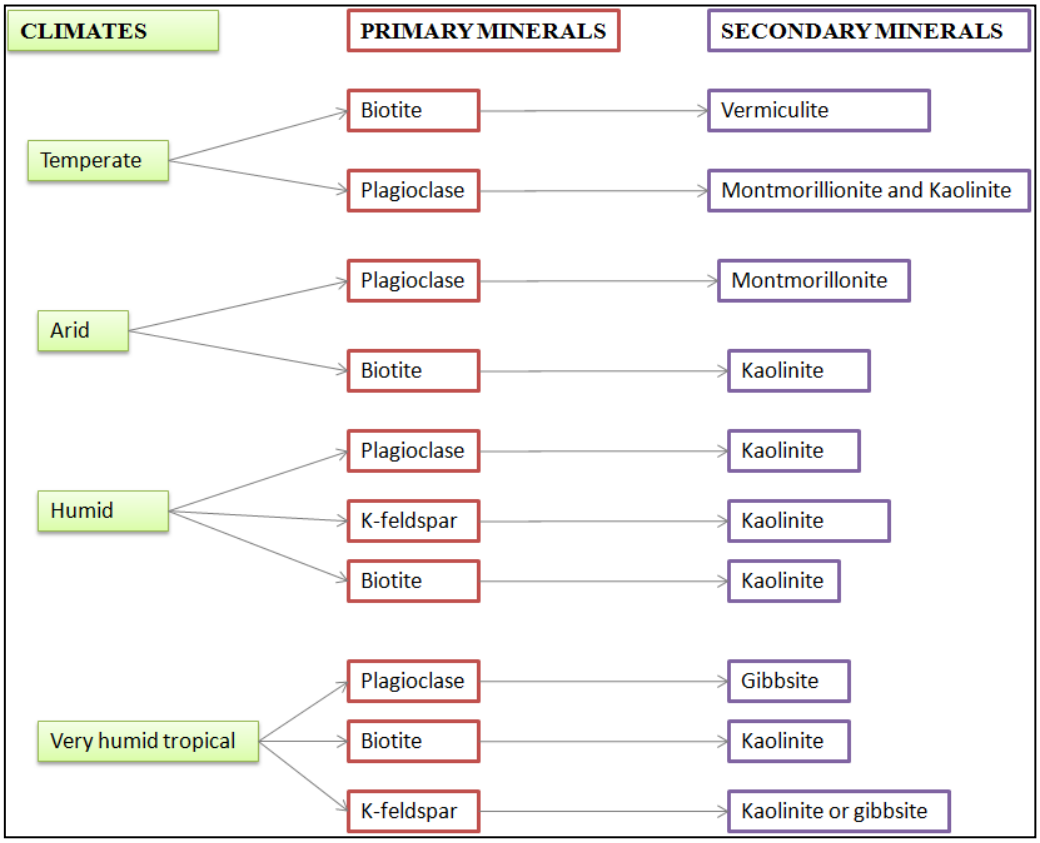

Figure 52: Transformation of primary minerals to secondary minerals in different climates.

Mineral associations formed by dissolution of microcline were briefly discussed in chapter 2. Most of the secondary minerals formed by the alteration of primary minerals come under the definition of phyllosilicates (vermiculite, montmorillonite, kaolinite, chlorite, illite and various mixed-layered clay minerals) (Bregaya, 2006). Gibbsite is considered by many scientists to be the end member (in extreme weathering conditions) of the weathering sequence for aluminosilicate minerals' (Sequeira et al., 2002).

Smectite, kaolinite and gibbsite may represent advanced stage of chemical weathering, while illite and vermiculite are considered unstable intermediate minerals. In addition, kaolinite which is indicator of humid climate has a higher preservation potential during subsequent aridity after its formation. Whereas, smectite which is arid climate indicator, suffers transformation during subsequent humid climate (Singer, 1984; Ahlberg et al., 2003a). Out of above mentioned weathering products, illite and kaolinite can be found in fresh granites (Gjems, 1967). Illite can be presented as sericite (Gjems, 1967), and is also a common weathering product of K-feldspar (Nesbitt and Young, 1984).

6.4. Kaolinite weathering and preservation:

Apart from Cambrian and Silurian period, Precambrian bedrock in Sweden was exposed to weathering processes throughout Paleozoic. The formation of kaolinite in southern Sweden can be attributed to the possible tropical to sub-tropical climates through Devonian to Late Tertiary period (Lidmar-Bergström, 1981; 1982). The kaolinitic weathering initiated in the Late Triassic and continued throughout Mesozoic (Lidmar-Bergström, 1995). Formation of deep kaolinized saprolites of the area are attributed to i) long-term mid-latitude hot and humid climate, ii) low pH, iii) fractured bedrock, iv) vegetation and v) carbondioxide rich Mesozoic atmosphere and hydrosphere (Ahlberg et al., 2002; Ahlberg et al., 2003a; Lidmar-Bergström et al., 1997). Intense Mesozoic weathering can be attributed to increased amounts of the carbonic acid in soils which in turn is linked to the Mesozoic greenhouse atmosphere (Ahlberg et al., 2003a). The effect of the Mesozoic deep weathering can be obsereved in saprolites below cover rocks and the sediment record in the adjacent sedimentary basins (Lidmar-Bergström et al., 1997).

The long lasting humid, warm conditions from the Rhaetian and onwards provided conditions for the development of vegetation cover. This cover helped in binding sediments, accumulating organic matter and peat, increasing acidity of soils, flourishing fauna and

increased flushing of meteoric water (Ahlberg et al., 2003a). The Late Cretaceous transgression and deposition of carbonates on weathered Precambrian basement in Ivö Klack is responsible for the good preservation of the kaolinized saprolites (Lidmar-Bergström, 1982).

The shift of smectite rich beds to kaolinite rich beds from Norian-Rhaetian (Late Triassic) is characterized by three observations described by Ahlberg (1994).

1. From sediments devoid of fossils to rich in flora and fauna.
2. From underdeveloped, organic matter free red-beds to chemically mature, organic rich siliciclastics.
3. From diagenetic calcrete and ferric oxide to transformation of feldspars to kaolinite and dissolution of carbonates due to meteoric water flushing.

From the results of Lidmar-Bergström et al., (1997) it is evident in Scania, kaolinite dominates the uppermost parts of soil profiles and smectite concentration increases downwards. At a locality (Odersberga) north of Kristianstad town, kaolinite is dominant clay mineral near surface while at 30 m depth kaolinite content decreases and smectite appears (Lidmar-Bergström, 1982). This observation helps us in concluding the area had tropical climate with seasonal contrast (Tardy et al., 1973). Ahlberg et al., (2003a) discussed clay mineralogy of sedimentary basins in of south Sweden and concluded that smectite content is much higher in beds near the base of the Rhaetian (Late Triassic) succession while kaolinite and illite are the dominant clay minerals in beds deposited after Late Triassic. This conclusion is in accordance with the results of this study as kaolinite and illite are the dominant clay minerals found in both weathering profiles.

Kaolinite content increases upwards in a weathering profile in well drained areas compared to poorly drained profiles (Gjems, 1967). Decreased amounts of smectite in Late Triassic-Jurassic beds depict that aridity never came back to Scania during Mesozoic period except in Late Jurassic (Ahlberg et al., 2003a). Increased smectite content and evaporite minerals in Late Jurassic depicts that Scania was located at northern boundary of Laurasia in northwards growing aridity belt (Ahlberg et al., 2003a).

The ice movement during Pleistocene glaciation resulted in the removal of kaolinite cover, at some places in Sweden, and formation of new relief, but relief of basement rock surface is

pre-glacial. A boring at Råbelöv reached fresh basement rocks only after penetrating 40 m of weathered Precambrian rocks (Lidmar-Bergström, 1982).

6.5. Theoretical considerations:

Out of all the minerals exposed to weathering on earth's surface, 75% of them are readily prone to chemical weathering (Nesbitt and Young, 1984 and 1989). Feldspars are stable in waters with high cation/H^+ values or high silica content. The water (rain water) infiltrating weathering profiles is mainly rain water which is (frequently) acidic in nature due to dissolution of atmospheric carbon dioxide or carbon dioxide derived from organic matter oxidation (Nesbitt and Young, 1984 and 1989). Waters that plot outside stability field of a particular mineral (Figure 54) has the potential to react with that mineral (Nesbitt and Young, 1984 and 1989). Clay mineral study of the samples from both weathering profiles at Ivö Klack represents three clay mineral phases (kaolinite, illite and smectite) which are in (partial) equilibrium with water solution. These three clay minerals and gibbsite according to Nesbitt and Young (1984) are the products resulting from the dissolution of feldspars, and water composition must travel through the stability field of these clay minerals to achieve stability field of feldspars (Figure 5, 6 and 54).

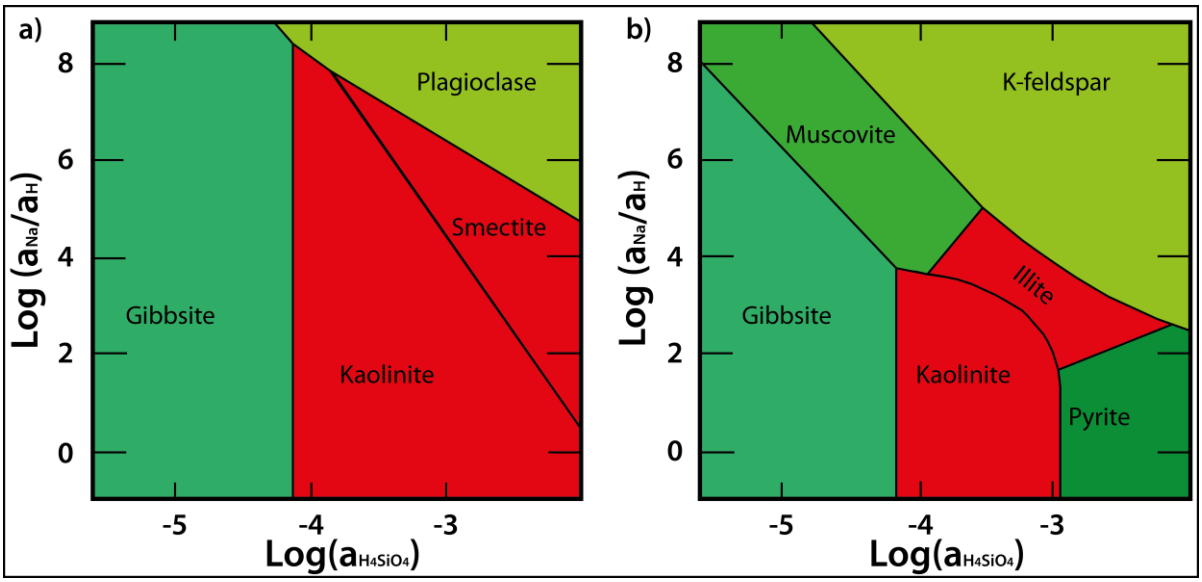

Figure 53: Stability diagram between some common minerals and weathering solutions. Red portion (kaolinite, illite and smectite) in both 'a' and 'b' represent mineral assemblage found at the locality (Ivö Klack). Pore waters of both the weathering profiles are in partial equilibrium with these three mineral phases (modified from Nesbitt and Young, 1989).

The red portions in the stability diagram (Figure 54a and b) represent clay minerals found in study area. Kaolinite can be formed by dissolution of feldspars (plagioclase and K-feldspar) (Nesbitt and Young, 1984 and 1989; Blum, 1994), formation of illite occurs at the expense of K-feldspar (Nesbitt and Young, 1984 and 1989) and smectite can be produced at the expense of biotite and chlorite (Nesbitt and Young, 1984 and 1989) or plagioclase (Tardy et al., 1973). Dominance of kaolinite as clay mineral in study area can be attributed to its formation from feldspars which constitutes around 60% of fresh granite (Appendix 2 and 3). In addition, biotite weathered at very early stage of weathering (Appendix 2), also contributes to the formation of kaolinite (Tardy et al., 1973; Nesbitt and Young, 1989).

Figure 55 illustrates nomenclature of weathering solutions and zones associated with acidity and different minerals found in different parts of a weathering profile (Nesbitt and Young, 1984, Murphy et al., 1998). Primitive weathering solutions display low cation/H^+ and are generally associated with gibbsite, kaolinite and quartz. These minerals are stable in acidic solutions, and are found in residual weathering zone which forms uppermost part of a weathering profile (Nesbitt and Young, 1984). Similarly two other weathering zones (intermediate weathering zone and incipient weathering zone) associated with weathering solutions (evolved weathering solutions and mature weathering solutions) are named in a weathering profile by Nesbitt and Young (1984 and 1989). Intermediate weathering zone with evolved weathering solutions of moderate acidity consist of the mineral groups of illites, smectites or vermiculites. Mature weathering solutions achieve equilibrium with respect to feldspars and muscovite and are commonly associated with incipient weathering zone.

<table>
<tr><th>Weathering profile</th><th>Weathering solution</th><th>Weathering zone</th><th>Acidity</th><th>Minerals</th></tr>
<tr><td>Soil</td><td rowspan="2">Primitive weathering solutions.</td><td rowspan="2">Residual weathering zone.</td><td rowspan="2">High</td><td rowspan="2">Gibbsite, kaolinite and quartz.</td></tr>
<tr><td rowspan="3">Saprolite</td></tr>
<tr><td rowspan="2">Evolved weathering solutions.</td><td rowspan="2">Intermediate weathering zone.</td><td rowspan="2">Moderate</td><td rowspan="2">Illite, smectite.</td></tr>
<tr><td>Saprock</td></tr>
<tr><td>Bedrock</td><td>Mature weathering solutions.</td><td>Incipient weathering zone</td><td>Low</td><td>Feldspars and muscovite.</td></tr>
</table>

Figure 54: Weathering solutions and zones in a weathering profile. Solutions with different pH represent equilibrium with different mineral phases across a weathering profile. Time and space affects progressive deepening of each weathering zone (made using idea from Nesbitt and Young, 1989 and Murphy et al., 1998).

According to Nesbitt and Young, 1984, there is a close connection between weathering zones and weathering solutions in space and time. As weathering continues residual weathering zone gradually advances over intermediate weathering zone, and similarly intermediate weathering zone encroaches beyond incipient weathering zone (Nesbitt and Young, 1984 and 1989; Steinmann et al., 1994). With time and progressive weathering, each of the weathering zone advances to greater depths (Nesbitt and Young, 1984; Steinmann et al., 1994). Occurrence of thick kaolinite cover (40 m) above bedrock (before quarrying) in Scania (Lidmar-Bergström, 1983; Lidmar-Bergström et al., 1997) can be attributed to prolonged weathering of bedrock in acidic waters through Late Triassic to Late Cretaceous (Lidmar-Bergström, 1983). As shown in Figure 6, intermediate weathering zone consisting of illite and smectite is quantitatively unimportant (Steinmann et al., 1994).

As evident from Figures 5 and 54 formation of gibbsite is credited to extreme weathering conditions (Nesbitt and Young, 1984 and 1989; Steinmann et al., 1994). The stability diagrams illustrates gibbsite is only stable in waters with low cation/H^+ and low silica content. Any changes in water composition (pH or silica content) make gibbsite unstable and it transforms into kaolinite (Steinmann et al., 1994). Absence of gibbsite in weathering profiles at Ivö Klack approves metastable nature of mineral and acidic pore water composition with intermediate silica content.

6.6. Comparison with other localities:

In the Early Quaternary humid temperate climate existed in Portugal which resulted in arenization (sand formation) and transformation of primary minerals in granites to kaolin minerals and gibbsite (Braga et al., 2002). In contrast at Ivö Klack, absence of gibbsite in both weathering profiles as secondary mineral is observed. The probable reason for this difference has already been discussed earlier in this chapter. Braga et al. (2002) identifies a climatic zonation of clay minerals found in granitic saprolites from Scandinavia to Portugal. The degree of weathering, as evident from secondary minerals present, increases southwards with the gibbsite dominance in the southernmost weathered granites. The process of arenization is active in temperate regions and is a form of skeleton weathering resulting in separation of mineral grains with minimal clay formation. On the other hand argillization (clay formation), as seen at Ivö Klack, is a process more active in humid tropical regions resulted by deep weathering of bedrock (Braga et al., 2002). The immature saprolites within southern Sweden

can be distinguished from more mature ones on the basis of grain size, finer the grain size more mature is the saprolite (Lidmar-Bergström et al., 1997).

The moderate intense weathering in the Luquillo Mountains, Puerto Rico, is confirmed by the presence of biotite in the saprolite and contrasts with the tropical environment where weathering is intense (White et al., 1998). Intensity of chemical weathering is low in temperate climates where less weathered primary minerals are found in saprolites. In contrast to moderate weathering intensity in the saprolites found in this locality, the weathering rate is extremely rapid and is the fastest as documented of the granites on the Earth's surface (White et al., 1998). In the saprolites of Luquillo Mountains, the inverse relationship between biotite and kaolinite concentration upwards in a saprolite confirms the transformation of biotite to kaolinite directly. But the presence of 14 Å peak in some samples validate the existence of expandable vermiculite, an intermediate mineral phase in the weathering of biotite to kaolinite (Murphy et al., 1998). Biotite has surface area higher and density (2.5 g/cc) lower than kaolinite (2.6-2.8 g/cc). Biotite weathers and re-precipitates as kaolinite on biotite crystal, minimizing contact of solution with biotite that ultimately results in decreased rate of biotite weathering (Murphy et al., 1998).

Nesbitt and young (1984 and 1989) studied chemical weathering trends in granites and granodiorites occurring in different parts of world. They considered four granites and granodiorite from different areas viz, the Toorongo Granodiorite (South Australia), the Mazaruni Granite (British Guiana), the Ricany Granite (Bohemian Massif) and the Stone Mountain Granite (Georgia, USA). Following is a small descriptive note on chemical weathering trends in these four localities based on results of Nesbitt and Young (1984 and 1989).

1. The Toorongo Granite is located in hilly cool temperate climate with annual rainfall of 800 mm approximately. Weathering profile has a rate of biotite weathering comparable to rate of plagioclase weathering (Nesbitt and Young, 1984 and 1989). Plagioclase alters rapidly to precipitate kaolinite and is consumed completely as weathering continues. The residue which is left contains aluminous phases (kaolinite) and potassic phases (illite or K-feldspar). Potassium ion rather than aluminium ion is released upon further dissolution of potassic phases. In advanced stages of weathering only kaolinite precipitates as a weathering product (Nesbitt and Young, 1984 and 1989).

2. The Mazaruni Granite is situated in tropics of British Guiana with a very high annual rainfall of 2418 mm approximately. Plagioclase is first to alter in comparison with K-feldspar during initial stages of weathering. As weathering progressed plagioclase is destroyed completely leaving behind potassic and aluminous phases in the residues. During later stages of weathering, release of potassium ion to solutions is preferred than aluminium ion release (Nesbitt and Young, 1984 and 1989). Although above discussed two bedrocks are compositionally different but their chemical weathering trends are qualitatively alike (Nesbitt and Young, 1984 and 1989). In addition, chemical weathering in both the weathering profiles at Ivö Klack represent the same chemical trends as followed by the Toorongo Granite and the Mazaruni Granite.
3. The Ricany Granite is located in a temperate climate and is compositionally similar to the Mazaruni Granite. The weathering at the Ricany Granite also resembles the chemical weathering trend followed by the Mazaruni Granite, although the climatic conditions are different (Nesbitt and Young, 1984 and 1989).
4. The Stone Mountain Granite is situated in a warm temperate climate and weathering profile here also follows the above discussed weathering trends (Nesbitt and Young, 1984 and 1989).

The calculated weathering trends of weathering profiles observed at Ivö Klack mimic weathering trends detected from four different localities of Nesbitt and Young (1984 and 1989).

6.7. Utsira project:

Parallel study on two weathering profiles at Nygård kaolin pit which is situated northwest of the town Rønne on Bornholm (Danish island shown in Figure 1) has being conducted by Nikolas Oberhardt. The fresh granite (Rønne Granite) sample falls near the boundary of monzogranite and quartz monzonite when plotted in Streckeisen diagram (through personal communication with Oberhardt in May, 2013). Sericite and chlorite are present in fresh granite describing the possibility post magmatic alterations (Que and Allen, 1996). In contrast to the Vånga Granite (red colored), the Rønne Granite (dark gray colored) has a total 18% (approximately) of mafic minerals (hornblende, ilmenite and biotite). Studies from the two weathering profiles (profile-B and profile-D) at Nygård kaolin pit confirmed the presence of four main clay minerals namely; smectite, chlorite, illite and kaolinite (Oberhardt, 2013). Illite and smectite contents of both profiles are low as compared with chlorite and kaolinite when

semi-quantified from clay separated samples. In profile-B, kaolinite consist of 50-70 XRD% and chlorite is 20-30 XRD% whereas in profile-D kaolinite constitutes 60-90 XRD% and chlorite make up 10-30 XRD% (Øberhardt, 2013).

The increased amount of chlorite can be attributed to neoformation (personal communication with Oberhardt) or to late diagenetic reactions of trapped sea waters with minerals in the weathering profile (Nesbitt and Young, 1989). According to Nesbitt and Young (1989), during and after burial of a weathering profile illite, smectite and chlorite can be produced at the expense of kaolinite due to metasomatism. This conversion is dependent on two factors, 1) temperature and 2) magnesium ion concentration (Nesbitt and Young, 1989). Considering aluminium as immobile phase the reaction can be given as:

$$Mg_5Al_2Si_3O_{10}(OH)_8 + 10H^+ = Al_2Si_2O_5(OH)_4 + SiO_2 + 5Mg^{2+} + 7H_2O$$

(Chlorite) (Kaolinite) (Silica)……. eq. 15

The reaction moves to left as temperature increases even if magnesium is present in small amounts (Nesbitt and Young, 1989). The presence of abundant chlorite mineral in weathering profiles from Nygård kaolin pit itself explains the weathering environment was different from Ivö Klack, studies of weathering profiles of Nesbitt and Young (1984 and 1989), results of Braga et al. (2002) and observations of White et al. (1998). According to Lidmar-Bergström (1983), the kaolin minerals of Scania are sub-aerial in origin whereas kaolin in Bornholm is of different origin. Detailed studies on two weathering profiles of Nygård kaolin pit will be presented by Nikolas Obehardt in June, 2013.

Present study provides us with a model against which paleo-chemical weathering of ancient weathering profiles (e.g. Utsira High) can be compared. The weathering profiles on Utsira High are under investigation (based on cores) by Lars Riber. Present research gives lateral as well as vertical details about weathering processes active at the locality, whereas data from cores of a weathering profile lacks lateral extent of information. In addition, argillization (clay formation) is a process active during the development of saprolites, and clays (fine grained material) addition to coarser lithology reduces the porosity and permeability (Marion et al., 1992). These two reservoir parameters define the quality of the reservoir (Bjørlykke and Jahren, 2010).

7. Conclusion:

Based on results and discussions present in this research following conclusions can be inferred:

- The Vånga Granite of intrusive origin has composition between monzogranite and syenogranite when plotted on Streckeisen diagram.
- Sericitization of fresh granite is mainly attributed to post-magmatic alterations.
- Sharp mineral transitions in weathering degree can be observed around corestones in a saprolite.
- Primary minerals, plagioclase along with biotite are first to alter. And anorthite content of plagioclase mineral weathers earlier than albite content. Whereas K-feldspar is intermediately weatherable.
- Increment in size of dissolution pits (due to dissolution of feldspars) is directly related to weathering degree.
- Percentage change in total feldspar content with respect to total feldspar percentage of fresh granite is proportional to degree of weathering.
- In acidic environments plagioclase is readily consumed leaving behind equilibrium between kaolinite, K-feldspar and illite phases. Upon further dissolution of potassic phase (K-feldspar and illite), potassium ion is liberated instead of aluminium ion to precipitate more kaolinite.
- Waters with a composition that plot outside stability diagram of a mineral have the tendency to react with that mineral to achieve equilibrium.
- Quartz is a more resistant mineral against weathering agents.
- Chemical weathering is most effective in parts of saprolite with good porosity and permeability, and is high in near surface saprolite.
- In areas of intense weathering biotite can be transformed directly to kaolinite with no intermediary minerals, e.g. vermiculite.
- Muscovite grains visible even in intensely weathered samples when viewed under microscope approve its stability against chemical weathering.
- Calcite and dolomite occurring in the weathering profiles are products of early diagenesis.

- Kaolinite is the dominant clay mineral which is precipitated as a result of feldspars dissolution that is understandable due to 60% feldspars content of fresh granite. Besides, kaolinite is end product of biotite weathering.
- Even though only one grain of chlorite has been detected in fresh granite, absence of chlorite in weathering profiles depicts its less resistant nature and denies the possibility of any late diagenetic reaction occurring at the locality.
- Main contributor of smectite mineral in weathering profiles is plagioclase.
- Humid tropical to sub-tropical climatic conditions can be attributed to the formation of weathering profiles at Ivö Klack.
- Two weathering stages (initial and advanced) can be differentiated with respect to consumption of plagioclase in weathering profile. Advance stage of weathering starts on total consumption of plagioclase where potassic phases (K-feldspar and illite) are transformed to aluminous phase (kaolinite).
- Absence of gibbsite mineral in the saprolite illustrates absence of extreme weathering conditions.
- Kaolinite weathering in the study area started in the Late Triassic (Rhaetian) times.
- A number of factors can be attributed to the formation of deep kaolinized saprolites at the locality:
    i. Long lasted humid tropical to sub-tropical climates.
    ii. Vegetation.
    iii. Acidity of soil waters.
    iv. Carbondioxide rich environment of the Mesozoic period.
    v. Fracturing in the bedrock.
- Deep kaolinitization can also be credited to progressive weathering of each weathering zone of a weathering profile in relation with time and space.
- Argillization (clay formation), active in humid tropical regions, is a process also operating in the study area.
- From studies of Nesbitt and Young (1984 and 1989), White et al., (1998), Braga et al., (2002) and this master thesis secondary mineral formation mainly depends on primary mineral composition and its distribution in parent rock.

References:

AHLBERG, A. 1994. *Deposition and diagenesis of the Rhaetian Hettangian succession (Triassic-Jurassic) in southern Sweden*, Lund University Press.

AHLBERG, A., ARNDORFF, L. & GUY-OHLSON, D. 2002. Onshore climate change during the Late Triassic marine inundation of the Central European Basin. *Terra Nova,* 14**,** 241-248.

AHLBERG, A., OLSSON, I. & ŠIMKEVIČIUS, P. 2003a. Triassic–Jurassic weathering and clay mineral dispersal in basement areas and sedimentary basins of southern Sweden. *Sedimentary Geology,* 161**,** 15-29.

AHLBERG, A., SIVHED, U. & ERLSTRÖM, M. 2003b. The Jurassic of Skåne, southern Sweden. *Geological Survey of Denmark and Greenland Bulletin,* 1**,** 527-541.

AMOURIC, M. & OLIVES, J. 1998. Transformation mechanisms and interstratification in conversion of smectite to kaolinite: an HRTEM study. *Clays and clay minerals,* 46**,** 521-527.

BAARTMAN, J. & CHRISTENSEN, O. B. 1975. *Contributions to the interpretation of the Fennoscandian Border Zone,* Reitzel.

BAHAT, D., GROSSENBACHER, K. & KARASAKI, K. 1999. Mechanism of exfoliation joint formation in granitic rocks, Yosemite National Park. *Journal of Structural Geology,* 21**,** 85-96.

BASU, A., YOUNG, S. W., SUTTNER, L. J., JAMES, W. C. & MACK, G. H. 1975. Re-evaluation of the use of undulatory extinction and polycrystallinity in detrital quartz for provenance interpretation. *Journal of Sedimentary Research,* 45.

BEGONHA, A. & BRAGA, S. 2002. Weathering of the Oporto granite: geotechnical and physical properties. *Catena,* 49**,** 57-76.

BERGSTRÖM, J., CHRISTENSEN, W. K., JOHANSSON, C. & NORLING, E. 1973. An extension of Upper Cretaceous rocks to the Swedish west coast at Särdal. *Bulletin of the Geological Society of Denmark,* 22**,** 83.

BERGSTRÖM, J. & SHAIKH, N. A. 1980. *Malmer, industriella mineral och bergarter i Kristianstads län,* Sveriges geologiska undersökning.

BERNER, R. A. & HOLDREN JR, G. R. 1979. Mechanism of feldspar weathering—II. Observations of feldspars from soils. *Geochimica et Cosmochimica Acta,* 43**,** 1173-1186.

BJØRLYKKE, K. & JAHREN, J. 2010. Sandstones and sandstone reservoirs. Petroleum Geoscience. Springer.

BLUM, A. E. 1994. Feldspars in weathering. *Feldspars and their reactions.* Springer, 595-630.

BRAGA, S., PAQUET, H. & BEGONHA, A. 2002. Weathering of granites in a temperate climate (NW Portugal): granitic saprolites and arenization. *Catena,* 49**,** 41-56.

DEARMAN, W. 1975. Weathering classification in the characterisation of rock: a revision. *Bulletin of Engineering Geology and the Environment,* 14**,** 123-127.

ERLSTRÖM, M., THOMAS, S., DEEKS, N. & SIVHED, U. 1997. Structure and tectonic evolution of the Tornquist Zone and adjacent sedimentary basins in Scania and the southern Baltic Sea area. *Tectonophysics,* 271**,** 191-215.

FAIRBRIDGE, W. R. 1968. The Encyclopedia of Geomorphology Reinhold Book Corporation. *New York***,** 302.

FORDHAM, A. 1990. Formation of trioctahedral illite from biotite in a soil profile over granite gneiss. Clays and Clay Minerals, 38, 187-195.

GAÁL, G. & GORBATSCHEV, R. 1987. An Outline of the precambrian evolution of the baltic shield. *Precambrian Research,* 35**,** 15-52.

GJEMS, O. 1967. Studies on clay minerals and clay-mineral formation in soil profiles in Scandinavia. *Norwegian Forest Research Institute, Vollebekk, Norway*, 310-321 & 402-406.

GORBATSCHEV, R. 1980. The Precambrian development of southern Sweden. *Geologiska Föreningen i Stockholm Förhandlingar,* 102**,** 129-136.

GORBATSCHEV, R. 1985. Precambrian basement of the Scandinavian Caledonides. *The Caledonide orogen-scandinavia and related areas,* 197**,** 212.

GORBATSCHEV, R. & BOGDANOVA, S. 1993. Frontiers in the Baltic Shield. *Precambrian Research,* 64**,** 3-21.

GRANT, W. H. 1964. Chemical weathering of biotite-plagioclase gneiss. *Clays Clay Miner,* 12**,** 455-463.

GROUP, E.-S. W. 1988. Crustal structure and tectonic evolution of the transition between the Baltic Shield and the North German Caledonides (the EUGENO-S Project). *Tectonophysics,* 150**,** 253-348.

HALSEY, D., MITCHELL, D. & DEWS, S. 1998. Influence of climatically induced cycles in physical weathering. *Quarterly Journal of Engineering Geology and Hydrogeology,* 31**,** 359-367.

ISRM. 1978. International society for rock mechanics commission on standardization of laboratory and field tests: Suggested methods for the quantitative description of discontinuities in rock masses. *International Journal of Rock Mechanics and Mining Sciences & Geomechanics Abstracts,* 15**,** 319-368.

JOHANNES, W. 1979. Ternary feldspars: Kinetics and possible equilibria at 800 C. *Contributions to Mineralogy and Petrology,* 68**,** 221-230.

KATO, Y. 1964. Mineralogical study of weathering products of granodiorite at Shinshiro City (II) Weathering of primary minerals-Stability of primary minerals. *Soil Science and Plant Nutrition,* 10**,** 34-39.

KUMP, L. R., BRANTLEY, S. L. & ARTHUR, M. A. 2000. Chemical weathering, atmospheric CO_2, and climate. *Annual Review of Earth and Planetary Sciences,* 28**,** 611-667.

LASAGA, A. C., SOLER, J. M., GANOR, J., BURCH, T. E. & NAGY, K. L. 1994. Chemical weathering rate laws and global geochemical cycles. *Geochimica et Cosmochimica Acta,* 58**,** 2361-2386.

LEONARD, R. & WEED, S. 1970. Mica weathering rates as related to mica type and composition. *Clays Clay Miner,* 18**,** 187-195.

LIBORIUSSEN, J., ASHTON, P. & TYGESEN, T. 1987. The tectonic evolution of the Fennoscandian Border Zone in Denmark. *Tectonophysics,* 137**,** 21-29.

LIDMAR BERGSTRÖM, K. 1981. Kaolin och landformer I Sydsverige. *Skånes Natur.* 68, 17-22.

LIDMAR BERGSTRÖM, K. 1983. Pre-Quaternary geomorphological evolution in southern Fennoscandia. *Dissertation abstracts international. C. European abstracts,* 44.

LIDMAR-BERGSTRÖM, K. 1995. Relief and saprolites through time on the Baltic Shield. *Geomorphology,* 12**,** 45-61.

LIDMAR-BERGSTRÖM, K., OLSSON, S. & OLVMO, M. 1997. Palaeosurfaces and associated saprolites in southern Sweden. *Geological Society, London, Special Publications,* 120**,** 95-124.

LUNDEGARDH, H. 1978. The Vanga granite in southernmost Sweden: Sweden, *Geologiska Undersoekning. Serie C. Avhandlingar och Uppsatser. Stockholm,* 72, 11-23.

MARION, D., NUR, A., YIN, H. & HAN, D.-H. 1992. Compressional velocity and porosity in sand-clay mixtures. Geophysics, 57, 554-563.

MATSUOKA, N. 1990. Mechanisms of rock breakdown by frost action: an experimental approach. *Cold Regions Science and Technology,* 17**,** 253-270.

LINNEAMANN, U., ROMER, R, L., PIN, C., ALEKSANDROWSKI, P., BULA, Z., GEISLER, T., KACHLIK, V., KRZEMINSKA, E., MAZUR, S., MOTUZA, G., MURPHY, J. B., NANCE, R. D., PISAREVSKY, S.A., SCHULZ, B., ULRICH, J., WISZNIEWSKA, J., ZABA, J., & ZEH, A. 2008. Precambrian. MCCANN, T. 2008, The Geology of Central Europe: Precambrian and Paleozoic, Geological Society Publishing House, 1-43.

MOORE, D. & REYNOLDS, R. JR., 1997. X-ray diffraction and the identification and analysis of clay minerals. Oxford University.

MURPHY, S. F., BRANTLEY, S. L., BLUM, A. E., WHITE, A. F. & DONG, H. 1998. Chemical weathering in a tropical watershed, Luquillo Mountains, Puerto Rico: II. Rate and mechanism of biotite weathering. *Geochimica et Cosmochimica Acta,* 62**,** 227-243.

NESBITT, H. W. 1979. Mobility and fractionation of rare earth elements during weathering of a granodiorite.

NESBITT, H. & YOUNG, G. 1984. Prediction of some weathering trends of plutonic and volcanic rocks based on thermodynamic and kinetic considerations. *Geochimica et Cosmochimica Acta,* 48**,** 1523-1534.

NESBITT, H. & YOUNG, G. M. 1989. Formation and diagenesis of weathering profiles. The Journal of Geology, 129-147.

NESSE, W. D. 2009. Introduction to optical mineralogy. Oxford University Press New York, 134-141.

NOCKOLDS, S. & KNOX, R. O'B., and Chinner, GA (1978) Petrology for Students. Cambridge University Press, England, 1-20.

NORLING, E. & BERGSTRÖM, J. 1987. Mesozoic and Cenozoic tectonic evolution of Scania, southern Sweden. *Tectonophysics,* 137**,** 7-19.

Oberhardt, N. 2013. Granite weathering, saprolitization and the formation of clay particles, with special emphasis on the mineralogy, Bornholm. Master thesis, UiO. In press.

OLLIER, C. & PAIN, C. 1996. *Regolith, soils and landforms,* John Wiley & Sons.

QUE, M. & ALLEN, A. R. 1996. Sericitization of plagioclase in the Rosses granite complex, Co. Donegal, Ireland. *Mineralogical Magazine,* 60**,** 927-936.

REYNOLDS, R. C. & HOWER, J. 1970. The nature of interlayering in mixed-layer illite-mont-morillonites. *Clays Clay Miner.,* 18**,** 25-36.

RIBER, L. 2009. Paleogene depositional conditions and climatic changes of the Frysjaodden Formation in central Spitsbergen. Master thesis, UiO.

ROSENQVIST, I. 1961. What is the origin of the hydrous micas of Fennoscandia. *Bull. Geol. Univ. Uppsala,* 40, 265-268.

STEINMANN, P., LICHTNER, P. C. & SHOTYK, W. 1994. Reaction path approach to mineral weathering reactions. *Clays and clay minerals,* 42**,** 197-206.

STRECKEISEN, A. 1979. Classification and nomenclature of volcanic rocks, lamprophyres, carbonatites, and melilitic rocks: recommendations and suggestions of the IUGS subcommission on the systematics of igneous rocks. Geology, 7, 331-335.

SURLYK, F. & SØRENSEN, A. M. 2010. An early Campanian rocky shore at Ivö Klack, southern Sweden. *Cretaceous Research,* 31**,** 567-576.

SØRENSEN, A. M. & SURLYK, F. 2010. Palaeoecology of tube-dwelling polychaetes on a Late Cretaceous rocky shore, Ivö Klack (Skåne, southern Sweden). *Cretaceous Research,* 31**,** 553-566.

TARDY, Y., BOCQUIER, G., PAQUET, H. & MILLOT, G. 1973. Formation of clay from granite and its distribution in relation to climate and topography. *Geoderma,* 10**,** 271-284.

TAYLOR, L., LEAKE, J., QUIRK, J., HARDY, K., BANWART, S. & BEERLING, D. 2009. Biological weathering and the long-term carbon cycle: integrating mycorrhizal evolution and function into the current paradigm. *Geobiology,* 7**,** 171-191.

THOMAS, M. F. 1994. *Geomorphology in the tropics: a study of weathering and denudation in low latitudes,* John Wiley & Sons, 83-99.

THOREZ, J. & THOREZ, J. 1976. *Practical identification of clay minerals: a handbook for teachers and students in clay mineralogy*, Lelotte, 1-19.

THYBO, H. 1997. Geophysical characteristics of the Tornquist Fan area, northwest Trans-European Suture Zone: indication of late Carboniferous to early Permian dextral transtension. *Geological Magazine,* 134**,** 597-606.

TOBI, A. C. & KROLL, H. 1975. Optical determination of the An-content of plagioclases twinned by Carlsbad-law; a revised chart. *American Journal of Science,* 275**,** 731-736.

WARR, L. N. 2012. The Variscan Orogeny: the Welding of Pangaea. *Geological History of Britain and Ireland.* John Wiley & Sons, Ltd.

WHITE, A. F., BLUM, A. E., SCHULZ, M. S., VIVIT, D. V., STONESTROM, D. A., LARSEN, M., MURPHY, S. F. & EBERL, D. 1998. Chemical weathering in a tropical watershed, Luquillo Mountains, Puerto Rico: I. Long-term versus short-term weathering fluxes. *Geochimica et Cosmochimica Acta,* 62**,** 209-226.

WWW.YR.NO 2013. Weather statistics for Ivö, Scania (Sweden) access date 22.04.2013. *http://www.yr.no/place/Sweden/Scania/Iv%C3%B6/statistics.html*.

ZIEGLER, P. 1978. North-western Europe: tectonics and basin development. *Geologie en Mijnbouw,* 57**,** 589-626.

ZIEGLER, P. & KENT, P. 1982. Faulting and Graben Formation in Western and Central Europe [and Discussion]. *Philosophical Transactions of the Royal Society of London. Series A, Mathematical and Physical Sciences***,** 113-143.

ÅBERG, G., KORNFÄLT, K.-A. & NORD, A. G. 1985. The Vånga granite, south Sweden-a complex granitic intrusion. *GFF,* 107**,** 153-159.

ŚRODOŃ, J. 2006. Identification and quantitative analysis of clay minerals. BERGAYA, F., THENG, B. & LAGALY, G. 2006, Handbook of clay science. Amsterdam. Elsevier, 765-787.

Appendix 1: Thin section description.

Sample Name	Crystallinity	Crystal Size	Crystal Development	Crystal Orientation	Twining	Heavy minerals Inclusions	Dissolution laminae	Quartz (Mono/polycrystalline)	Weathering Grade	Remarks
Ivö-Extra1-12	Holocrystalline Inequigranular	Fine-medium crystalline (0.25-4mm)	Subhedral-anhedral	Random	Albite, perthite and tartan	Yes, few	No	Both, mostly monocrystalline	I	No porosity, undulose extinction of quartz. Sericite needles on plagioclase.
Ivö-1-1-12	Holocrystalline Inequigranular	Fine-medium crystalline (0.25-4mm)	Subhedral-anhedral	Random	Albite, perthite and tartan	Yes, few to some	Yes, seen close to fractures	Both, mostly monocrystalline	II	Fracturing in some crystals, quartz is undulose, porosity appears.
Ivö-1-2-12	Holocrystalline Inequigranular	Fine-medium crystalline (0.25-4mm)	Subhedral-anhedral	Random	Albite, perthite and tartan	Yes, v.few	Present, increased	Both present	III	Porosity increased. Polycrystalline quartz increased.
Ivö-1-5-12	Holocrystalline Inequigranular	Fine-medium crystalline (0.25-4mm)	Subhedral-anhedral	Random	Tartan and perthite	V.few	Seen prominently	Both present	IV	No plagioclase crystal is seen.
Ivö-1-7-12	Holocrystalline Inequigranular	Fine-medium crystalline (0.25-4mm)	Subhedral-anhedral	Random	Albite, tartan and perthite	Not seen	Yes present in abundance	Both present	III	Increased alteration and fracturing of grains. Feldspars look dominant.
Ivö-1-12-12	Holocrystalline Inequigranular	Fine-medium crystalline (0.25-4mm)	Subhedral-anhedral	Random	Albite, tartan and perthite	V.few	Present	Both present, mostly monocrystalline	II	Porosity decreased considerably, fresh look crystals.
Ivö-1-16-12	Holocrystalline Inequigranular	Fine-medium crystalline (0.25-4mm)	Subhedral-anhedral	Random	Albite, tartan and perthite	V.few	Seen	Both present, mostly monocrystalline	II	Low porosity, plagioclase altered.
Ivö-1-19-12	Holocrystalline Inequigranular	Fine-medium crystalline (0.25-3mm)	Subhedral-anhedral	Random	Tartan and perthite	Few	Presence increased	Monocrystalline	IV	K-feldspar intensely weathered, micas look less altered.

Sample Name	Crystallinity & granularity	Crystal Size	Crystal Development	Crystal Orientation	Twining	Heavy minerals Inclusions	Dissolution laminae	Quartz (Mono/polycrystalline)	Weathering Grade	Remarks
Ivö-1-20-12	Holocrystalline Inequigranular	Fine-medium crystalline (0.2-3mm)	Subhedral-anhedral	Random	Tartan and perthite	None	Present, intense	Monocrystalline	IV	Clays dominating, muscovite seen.
Ivö-2-1-12	Holocrystalline Inequigranular	Fine-medium crystalline (0.25-3.5mm)	Subhedral-anhedral	Random	Perthite and tartan	None	Present	Both, mostly monocrystalline	II	Less porosity, undulose extinction of quartz. Plagioclase not seen. Alteration seen.
Ivö-2-3-12	Holocrystalline Inequigranular	Fine-medium crystalline (0.25-3mm)	Subhedral-anhedral	Random	Perthite and tartan	None	Present, increased	Both, mostly monocrystalline	III	Increased porosity, scattered biotite crystals.
Ivö-2-6-12	Holocrystalline Inequigranular	Fine-medium crystalline (0.1-1.5mm)	Anhedral	Random	None	None	Completely weathered	Both, mostly monocrystalline	IV	Intensely altered. Clays replaced feldspars.
Ivö-2-8-12	Holocrystalline Inequigranular	Fine-medium crystalline (0.1-2mm)	Anhedral	Random	None	None	Completely weathered	Only monocrystalline	IV	Small grains suspended in clays.
Ivö-4-5-12	Holocrystalline Inequigranular	Fine-medium crystalline (0.1-2mm)	Anhedral (only quartz)	Random	None	None	Completely weathered	Only monocrystalline	V	Some mica grains detectable. Imprints of dissolved primary grains can be seen
Ivö-K1-12	Holocrystalline Inequigranular	Fine-medium crystalline (0.1-2mm)	Anhedral (only quartz)	Random	None	None	Completely weathered	Only monocrystalline	V	Some mica grains detectable.
Ivö-Sand-12	Holocrystalline Inequigranular	Fine-medium crystalline (0.1-2mm)	Anhedral (only quartz)	Random	None	None	Completely weathered	Both, mostly monocrystalline	NA	Some mica grains detectable.

Appendix 2: Mineral point counting in thin sections.

Sample Name	Mono-quartz	Poly-quartz	K-feldspar	Plagioclase	Biotite	Muscovite	Porosity	Illitic clays
Ivö-Extra1-12	30.6	3.5	35.3	20.1	6.9	2.4	0	1.2
Ivö-1-1-12	35.5	2.7	46.7	5.2	2.9	5.3	1.4	0
Ivö-1-2-12	40	2.7	28.7	1.7	5.5	1.2	9.5	10.5
Ivö-1-5-12	34.5	4.0	30.5	1.3	4.0	0.6	10.8	13.5
Ivö-1-7-12	26.7	3.2	39	3.7	0	0	7.7	19.5
Ivö-1-11-12	33	2	36.7	5	1.7	0.2	7.7	12.7
Ivö-1-16-12	38	4.8	32.4	13.7	5.1	3.0	0.8	2.2
Ivö-1-20-12	50.9	0.7	16.7	0	1.1	3.1	10.3	15.9
Ivö-2-1-12	35.7	4.7	35.3	8.7	5.6	3.6	2.8	3.6
Ivö-2-8-12	55.5	3.8	2.2	0.8	0	3.0	12.2	22.5
Ivö-K1-12	46.2	1.8	----	----	----	1.8	31.7	18.5
Ivö-Sand-12	59.7	2.1	----	----	----	1.6	26.4	10.2

Appendix 3: Mineral estimation (XRD%) from XRD analysis.

Sample name	Illite %	Kaolinite %	Quartz %	K-feldspar %	Plagioclase %	Calcite %	Dolomite %	Siderite %
Ivö-Extra 1-12	6	0	26	28	33	4	5	0
Ivö-1-1-12	5	0	29	28	30	4	4	0
Ivö-1-2-12	30	0	37	15	7	6	0	0
Ivö-1-3-12	7	4	44	34	6	5	5	0
Ivö-1-4-12	7	5	37	32	9	4	5	0
Ivö-1-5-12	6	14	41	23	4	5	6	2
Ivö-1-6-12	4	7	44	30	5	5	6	0
Ivö-1-7-12	3	9	49	21	6	5	6	0
Ivö-1-8-12	3	6	34	33	14	5	5	0
Ivö-1-9-12	2	5	32	31	19	5	5	0
Ivö-1-10-12	4	4	30	29	23	5	4	0
Ivö-1-11-12	10	3	23	26	30	4	4	0
Ivö-1-12-12	3	0	29	27	31	4	4	0
Ivö-1-13-12	0	4	34	32	20	5	5	0
Ivö-1-14-12	5	4	32	28	21	5	4	0
Ivö-1-15-12	8	4	37	25	17	5	4	0
Ivö-1-16-12	11	2	27	24	28	4	4	0
Ivö-1-17-12	8	4	34	28	17	5	6	0
Ivö-1-18-12	8	5	35	36	5	6	5	0
Ivö-1-19-12	8	5	33	37	5	6	5	0
Ivö-1-20-12	9	6	46	25	5	5	3	0

Sample name	Illite %	Kaolinite %	Quartz %	K-feldspar %	Plagioclase %	Calcite %	Dolomite %	Siderite %
Ivö-2-1-12	9	3	21	31	28	4	3	0
Ivö-2-2-12	8	2	27	28	27	5	3	0
Ivö-2-3-12	13	4	31	28	15	5	4	0
Ivö-2-4-12	6	7	45	31	0	5	5	0
Ivö-2-5-12	4	11	30	42	0	6	6	0
Ivö-2-6-12	16	21	53	10	0	0	0	0
Ivö-2-7-12	5	28	50	9	0	4	4	0
Ivö-2-8-12	7	32	61	0	0	0	0	0
Ivö-4-5-12	4	74	15	7	0	0	0	0
Ivö-6-2-12	0	0	2	0	0	98	0	0
Ivö-6-9-12	0	0	2	0	0	98	0	0
Ivö-K1-12	6	26	60	0	0	4	4	0
Ivö-Sand-12	5	16	68	7	0	4	0	0

Appendix 4: Mineral estimation (XRD%) from XRD analysis of clay separated samples.

Sample name	Smectite %	Illite %	Kaolinite %
Ivö-1-1-12	9	38	53
Ivö-1-2-12	11	64	26
Ivö-1-4-12	8	19	73
Ivö-1-6-12	10	16	73
Ivö-1-8-12	7	17	73
Ivö-1-10-12	7	23	70
Ivö-1-16-12	0	51	49
Ivö-1-18-12	10	16	75
Ivö-1-19-12	8	22	70
Ivö-1-20-12	8	16	76
Ivö-2-1-12	6	35	60
Ivö-2-2-12	7	42	50
Ivö-2-5-12	4	11	85
Ivö-2-7-12	0	7	93
Ivö-2-8-12	0	8	92
Ivö-4-5-12	0	4	96
Ivö-A-6-12	0	48	52
Ivö-B-6-12	0	49	51
Ivö-K1-12	4	10	86
Ivö-Sand-12	0	10	90

Appendix 5: Samples description from logs.

Sample name	Location	Coordinates	Depth above base (cm)	Colour	Weathering grade	Gamma Ray value
Ivö-Extra 1-12	Random	----------	Base	Red, Green.	I	
Ivö-1-1-12	Profile-1	N 56 08.394 E 14 24.192	5	Brown, Red, Grey.	II	115
Ivö-1-2-12	Profile-1	N 56 08.394 E 14 24.192	15	Green, White, Grey.	III	120
Ivö-1-3-12	Profile-1	N 56 08.394 E 14 24.192	45	Red, Brown, Grey.	IV	125
Ivö-1-4-12	Profile-1	N 56 08.394 E 14 24.192	55	Brown, Grey.	III	120
Ivö-1-5-12	Profile-1	N 56 08.394 E 14 24.192	70	Brown, Grey.	IV	112
Ivö-1-6-12	Profile-1	N 56 08.394 E 14 24.192	75	Dark green, Grey.	IV	121
Ivö-1-7-12	Profile-1	N 56 08.394 E 14 24.192	85	Brown, Red.	III	123
Ivö-1-8-12	Profile-1	N 56 08.394 E 14 24.192	95	Grey, Green.	III	116
Ivö-1-9-12	Profile-1	N 56 08.394 E 14 24.192	115	Dark grey, Green.	III	105
Ivö-1-10-12	Profile-1	N 56 08.394 E 14 24.192	125	Green, Red, Grey.	II	114
Ivö-1-11-12	Profile-1	N 56 08.394 E 14 24.192	135	Dark brown, green.	II	103
Ivö-1-12-12	Profile-1	N 56 08.394 E 14 24.192	145	Green, Grey, Brown.	II	104
Ivö-1-13-12	Profile-1	N 56 08.394 E 14 24.192	155	Brown, Dark grey.	III	116
Ivö-1-14-12	Profile-1	N 56 08.394 E 14 24.192	185	Dark grey.	III	128
Ivö-1-15-12	Profile-1	N 56 08.394 E 14 24.192	205	Brown, Dark Grey.	III	135
Ivö-1-16-12	Profile-1	N 56 08.394 E 14 24.192	225	Dark Grey. White	II	135
Ivö-1-17-12	Profile-1	N 56 08.394 E 14 24.192	235	White, Dark Grey.	III	110
Ivö-1-18-12	Profile-1	N 56 08.394 E 14 24.192	255	Red, White, Grey.	IV	110
Ivö-1-19-12	Profile-1	N 56 08.394 E 14 24.192	265	Red, Grey.	IV	101
Ivö-1-20-12	Profile-1	N 56 08.394 E 14 24.192	275	Brown, Red.	IV	101

Sample name	Location	Coordinates	Depth above base (cm)	Colour	Weathering grade	Gamma Ray value
Ivö-2-1-12	Profile-2	N 56 08.394 E	02	Red, Black.	II	105
Ivö-2-2-12	Profile-2	N 56 08.394 E	11	Red, Black, White.	II	118
Ivö-2-3-12	Profile-2	N 56 08.394 E	32	Grey, Red, White.	III	115
Ivö-2-4-12	Profile-2	N 56 08.394 E	42	Grey, White.	III	110
Ivö-2-5-12	Profile-2	N 56 08.394 E	43	Grey, White.	IV	115
Ivö-2-6-12	Profile-2	N 56 08.394 E	44	Grey, White.	IV	99
Ivö-2-7-12	Profile-2	N 56 08.394 E	46	Grey, White.	IV	100
Ivö-2-8-12	Profile-2	N 56 08.394 E	47	Grey, White.	IV	104
Ivö-3-1-12	Profile-3	N 56 08.389 E 14 24.158	NA	Grey, Purple.	II	105
Ivö-3-2-12	Profile-3	N 56 08.389 E 14 24.158	NA	Red, Grey.	III	94
Ivö-3-3-12	Profile-3	N 56 08.389 E 14 24.158	NA	Grey White.	III	91
Ivö-3-4-12	Profile-3	N 56 08.389 E 14 24.158	NA	Dark grey, green.	IV	100

Sample name	Location	Coordinates	Depth above base (cm)	Colour	Weathering grade	Gamma Ray value
Ivö-4-1-12	Profile-4	N 56 08.376 E 14 24.132	05	Red, Brown, Grey, White.	IV	110
Ivö-4-2-12	Profile-4	N 56 08.376 E 14 24.132	15	Red, White, Grey.	IV	110
Ivö-4-3-12	Profile-4	N 56 08.376 E 14 24.132	35	Red, Grey.	IV	106
Ivö-4-4-12	Profile-4	N 56 08.376 E 14 24.132	55	White, Red.	IV	95
Ivö-4-5-12	Profile-4	N 56 08.376 E 14 24.132	65	White, Red.	V	90
Ivö-4-6-12	Profile-4	N 56 08.376 E 14 24.132	75	White, Grey, Red.	IV	95
Ivö-4-7-12	Profile-4	N 56 08.376 E 14 24.132	95	White, Grey.	IV	90
Ivö-4-8-12	Profile-4	N 56 08.376 E 14 24.132	105	Grey, White.	IV	93
Ivö-4-9-12	Profile-4	N 56 08.376 E 14 24.132	115	White, Red, Grey.	IV	100
Ivö-4-10-12	Profile-4	N 56 08.376 E 14 24.132	125	Red, Grey, White.	IV	100
Ivö-4-11-12	Profile-4	N 56 08.376 E 14 24.132	135	White, Grey.	IV	107
Ivö-4-12-12	Profile-4	N 56 08.376 E 14 24.132	145	White, Grey.	IV	101
Ivö-4-13-12	Profile-4	N 56 08.376 E 14 24.132	165	Grey, Red, White.	IV	86
Ivö-4-14-12	Profile-4	N 56 08.376 E 14 24.132	195	Grey, Red, White.	IV	85
Ivö-4-15-12	Profile-4	N 56 08.376 E 14 24.132	205	Grey, White.	IV	85
Ivö-4-16-12	Profile-4	N 56 08.376 E 14 24.132	215	Grey, White.	V	90

Sample name	Location	Coordinates	Depth above base (cm)	Colour	Weathering grade	Gamma Ray value
Ivö-5-1-12	Profile-5	N 56 08.394 E 14 24.194	05	Red, Grey Brown.	II	126
Ivö-5-2-12	Profile-5	N 56 08.394 E 14 24.194	35	Whit, Grey.	III	120
Ivö-5-3-12	Profile-5	N 56 08.394 E 14 24.194	45	White, Red, Grey.	III	115
Ivö-5-4-12	Profile-5	N 56 08.394 E 14 24.194	95	Brown, Red, Grey.	III	121
Ivö-5-5-12	Profile-5	N 56 08.394 E 14 24.194	105	Dark grey, Brown.	IV	130
Ivö-5-6-12	Profile-5	N 56 08.394 E 14 24.194	135	Dark brown, Grey.	IV	115
Ivö-5-7-12	Profile-5	N 56 08.394 E 14 24.194	185	Dark grey, Green.	III	130
Ivö-5-8-12	Profile-5	N 56 08.394 E 14 24.194	205	Dark grey.	II	126
Ivö-5-9-12	Profile-5	N 56 08.394 E 14 24.194	225	Dark grey.	III	120
Ivö-5-10-12	Profile-5	N 56 08.394 E 14 24.194	245	Light brown, grey.	IV	110
Ivö-5-11-12	Profile-5	N 56 08.394 E 14 24.194	275	Grey, White.	IV	140

Sample name	Location	Coordinates	Depth above base (cm) approximate	Colour	Weathering grade	Gamma Ray value
Ivö-6-1-12	Profile-6	N 56 08.348 E 14 24.100	15	White, Yellow.	NA	28
Ivö-6-2-12	Profile-6	N 56 08.348 E 14 24.100	35	White, Yellow.	NA	----
Ivö-6-3-12	Profile-6	N 56 08.348 E 14 24.100	65	White, Yellow, Grey.	NA	29
Ivö-6-4-12	Profile-6	N 56 08.348 E 14 24.100	85	White, Yellow, Grey.	NA	----
Ivö-6-5-12	Profile-6	N 56 08.348 E 14 24.100	125	White, Yellow, Green.	NA	33
Ivö-6-6-12	Profile-6	N 56 08.341 E 14 24.113	425	White, Yellow.	NA	----
Ivö-6-7-12	Profile-6	N 56 08.341 E 14 24.113	475	White, Yellow.	NA	----
Ivö-6-8-12	Profile-6	N 56 08.337 E 14 24.145	775	White, Yellow, Grey.	NA	22
Ivö-6-9-12	Profile-6	N 56 08.337 E 14 24.145	825	White, Yellow, Grey.	NA	26

Appendix 6: Sketch log of profile-6.

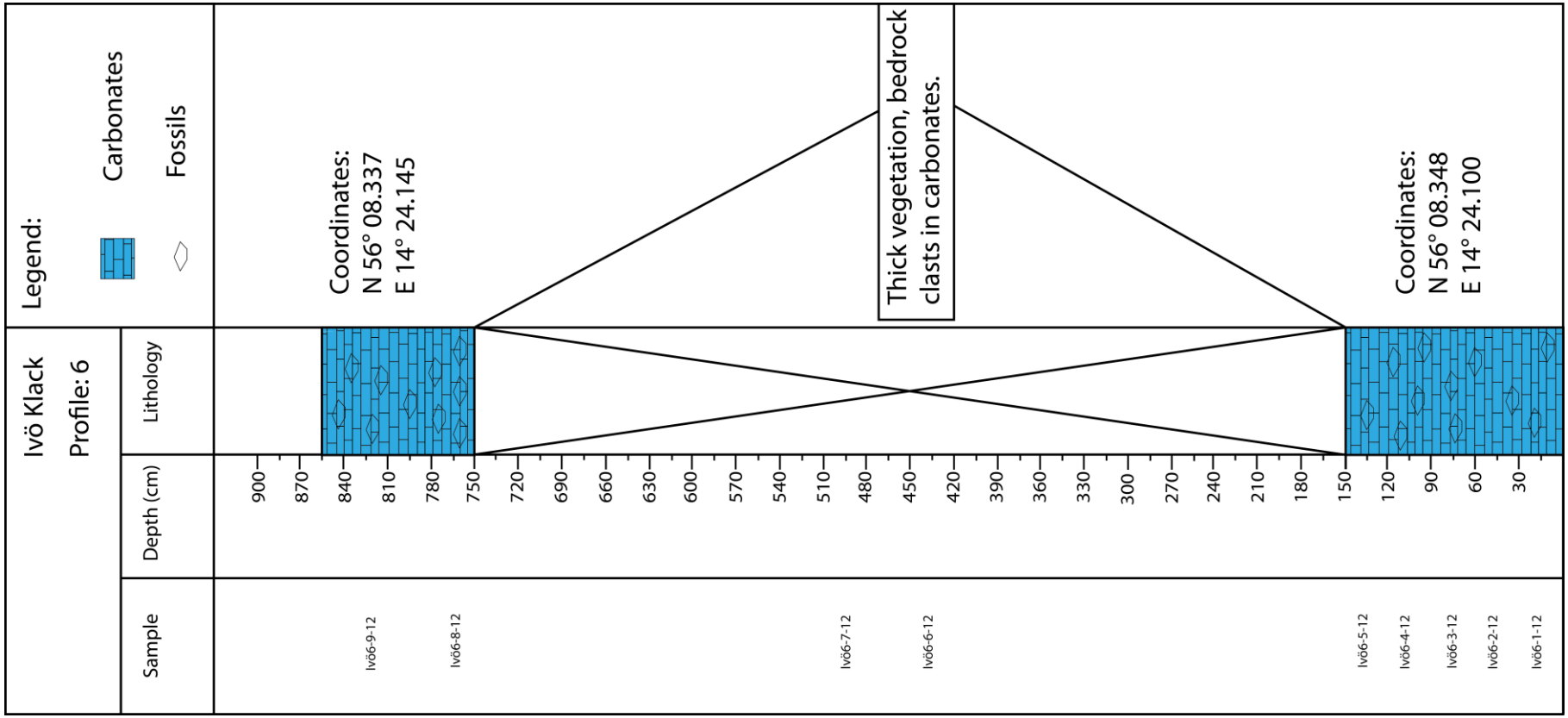

Acknowledgements

First and foremost, I thank Almighty Allah Pak for giving me strength needed during completion of this master thesis. Special praises to Prophet Muhammad WA Aal-E-Muhammad (A.S) who are well-wishers for whole mankind.

I would like to express my gratifications to Professor Henning Dypvik and Lars Riber at the Geosciences Department, University of Oslo. Henning Dypvik deserves big thanks for always being available for support and discussions throughout this master thesis. Friendly attitude and supportive nature of Lars Riber is also appreciated.

Thanks to Nikolas Oberhardt and Kamran Javed for their support and good teamwork during working on Utsira Project. Again thanks to Nikolas Oberhardt for maintaining a friendly and supportive working environment during field trip at Scania and Bornholm. Financial support of Lundin AS during this field trip is highly appreciated.

Berit Løken Berg has been very helpful in making stubs available and her assistance during sessions at scanning electron microscopy. A special thanks to Maarten Aerts for his support during preparation of samples for XRD analysis and afterwards analysing of these samples. Salahalldin Akhavan has been very helpful in the making of thin sections.

I would also like to thank all my classmates and friends for their support and help during course of this study.

Last but not the least, I would like to pay my gratitude to my Family for their love and confidence in me.

P.S. “Allah Pak sab naal changyaan kar c”.